Technische Universität München

Dissertation

General Aspects of Sound Localization through Internally Coupled Ears

Anupam Prasad Vedurmudi

Physik Department T35

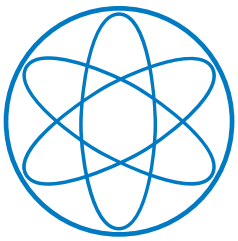

June 2018

Physik Department

Lehrstuhl für theoretische Biophysik T35

General Aspects of Sound Localization through Internally Coupled Ears

Anupam Prasad Vedurmudi

Vollständiger Abdruck der von der Fakultät für Physik der Technischen Universität München zur Erlangung des akademischen Grades eines

Doktors der Naturwissenschaften (Dr. rer. nat.)

genehmigten Dissertation

Vorsitzender:		Prof. Dr. Karl Duderstadt
Prüfer der Dissertation:	1.	Prof. Dr. J. Leo van Hemmen
	2.	Prof. Dr. Martin Zacharias

Die Dissertation wurde am 05.06.2018 bei der Technischen Universität München eingereicht und durch die Fakultät für Physik am 20.06.2018 angenommen.

"*The story so far: In the beginning the Universe was created. This has made a lot of people very angry and been widely regarded as a bad move.*"

Douglas Adams (1952–2001)
The Restaurant at the End of the Universe, 1980

Abstract

Internally coupled ears or ICE for short is an anatomical hearing adaptation found in over half of the extant terrestrial vertebrates. All lizards and most frogs, birds and crocodilians are equipped with some form of internally coupled ears. In its simplest form, ICE corresponds to an acoustic coupling of the eardrums through an air-filled chamber known as the interaural cavity. The vibration of one eardrum in response to an external sound stimulus creates an internal pressure wave that propagates through the interaural cavity and drives the opposite eardrum. In this doctoral dissertation, a mathematical analysis of the eardrums and the connecting passages as well as the direction-dependent cues in the form of time and amplitude differences between the ears, reveal the role played by ICE in sound localization. On the basis of the geometry of the interaural cavity and the elastic properties of the two eardrums confining it at both ends, the mathematical and physical principles underlying hearing through ICE are reviewed and analytical expressions for eardrum vibrations as well as the pressures inside the internal passages in response to an external pressure are derived. Given sound pressure inputs of equal amplitude and a small direction dependent phase (or time) difference at the ears, the emergence of highly directional hearing cues is demonstrated. In the first portion of the thesis, with an emphasis on lizards as ICE archetypes and in conjunction with the novel piston approximation for the eardrum vibrations, the role of the tympanic fundamental frequency in segregating the hearing range into a low- and high-frequency regimes is demonstrated. Moreover, by exploiting the physical properties of the coupling, we describe a concrete method to numerically estimate the eardrum's material properties solely through measurements taken from alive animals. In the second portion, the role played by ICE in underwater hearing in the fully aquatic frog *Xenopus laevis* as well as the implications of an interaural coupling at higher frequencies in the barn owl *Tyto alba* is analyzed. In both animals the interaural cavity is augmented by a secondary air-filled chamber which is modeled as a Helmholtz resonator. It is shown that, while the resonator improves underwater hearing sensitivity and directionality in *Xenopus*, it improves high-frequency directional cues in the barn owl by negating the effects of the interaural cavity resonances. The ICE-like amplitude-difference magnification at low-frequencies in the barn owl is also established.

Table of contents

List of figures

List of tables

Chapter 1

Introduction

The perception of external stimuli, be it sight, smell or sound, is a fundamental trait of all living organisms and one that is essential to their survival. Among these stimuli, the perception of sound has distinct advantages. First, it is omnidirectional, i.e., the listener need not be oriented towards a source in order to be able to hear it. Second, the wavelength of sound is typically much longer than that of visible light and thus, unlike light, is not hindered by small objects. For this reason, one can typically hear a sound source behind an obstacle before being able to see it. For this reason, being able to hear confers the obvious advantage of being able to react to approaching threats without having to be able to see them. To hear the sound emanating from a particular source, an animal first needs at least one appropriate receiver sensitive to sound stimuli propagating through the surrounding medium, be it earth, water or air. Among terrestrial vertebrates that hear in air, the most common organ dedicated to receiving sound is the eardrum or tympanic membrane, which vibrates in response to an external sound stimulus. In humans, the eardrum is a thin flexible membrane located at the end of the external auditory meatus, or ear canal opening at the side of the head, while in animals such as the Tokay gecko, for example, the eardrum is located rather superficially. Figures 1.1a and 1.1b illustrate the position of the eardrum in humans and the Tokay gecko, along with some of the accompanying components relevant to hearing being explicitly shown in the case of the former.

In order to appropriately react to a sound source and thus fully exploit the sense of hearing, it is imperative for an animal to be able to accurately judge the location of the source. In contrast to visual stimuli, the ability to hear a sound source does *not* by itself entail the ability to assess its location or, in other words, the ability to *localize* a sound source. In certain specific cases, the information from one ear provides sufficient directional information. Vertical sound localization, for example, is can be achieved through the use of only one ear. In order to accurately localize in the azimuth, however, the animal would need

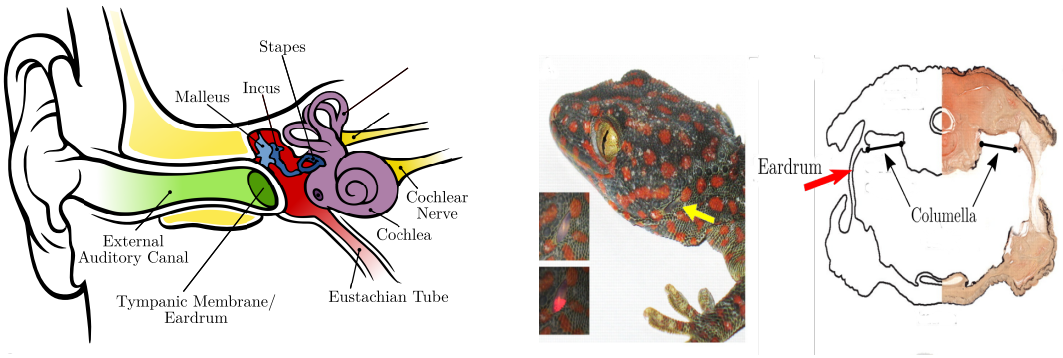

(a) Human (b) Gecko

Fig. 1.1 Figure (a) shows the positions of the human eardrum or tympanic membrane and the main middle- and inner ear components. The eardrum is situated at the end of the external auditory canal and is connected via the ossicles - malleus, incus and stapes - to the cochlea. The cochlea converts the received auditory stimulus to neuronal signals which are transmitted to the brain via the cochlear nerve; figure adapted from Chittka and Brockmann [1]. The gecko eardrum (b) on the other hand is located fairly superficially and can be easily made out on the side of the head (marked by arrows). The vibrations of the eardrum are now transmitted to the cochlea by a single middle-ear bone, the *columella*. Figure adapted from Christensen-Dalsgaard et al. [2].

to simultaneously rely on information from both the ears. The spatial separation of the ears, as well as the differing paths taken by sound waves to reach the opposite ears often result in inherent directional differences between the individual sound inputs at both the ears. In either case, the animal must first convert the mechanical signal of sound into electrochemical signals that can be processed by its nervous system. Directional information can then be extracted from the resulting electrochemical signals via neuronal computations.

The quality of information available in this manner, as well as the strategies to efficiently process it, however, vary greatly among animals. In several animals, the directional information available to the animal via the two eardrums is limited owing either to their small size, or to limited neuronal power and often to both. In this thesis, we study a specific adaptation that overcomes the aforementioned problems – a physical coupling of the eardrums on their internal side through air-filled cavities in the animal's skull – a system referred to as internally coupled ears or ICE. Our goal is a quantitative and qualitative analysis of the role played by the ears, as well as the *interaural* coupling between them in generating and improving the directional information available to the animal. In the present chapter we briefly introduce some concepts relevant to hearing and sound localization in general, and ICE in particular. We begin by briefly reviewing the mechanism of tympanic hearing and its evolution as well as the directional information generated by both ears. Although the goal of the thesis is

an acoustic and mechanical analysis of ICE, we will also give a very brief introduction to the neuronal representation of directional information. We will then provide a concise introduction into the current state of research in ICE. Finally, we will end the chapter with a brief outline of the structure of the present dissertation.

1.1 Tympanic hearing and its evolution

In its essence, a tympanic hearing system consists of two eardrums or tympanic membranes situated on either side of the head, which serve as the primary receivers of auditory stimuli in the form of sound pressure waves. Tympanic membranes are generally very thin, light and flexible, making them especially compliant to sound pressure waves in air, which typically have very small amplitudes. For example, normal conversations between people have an amplitude of 60 dB in decibels, which corresponds to a pressure amplitude of .02 Pa or roughly 2×10^{-7} times atmospheric pressure. In mammals, the vibrations of the tympanic membrane are transmitted via the middle ear bones or ossicles [3] namely, the malleus, incus and stapes (see Fig. 1.1a), to the inner ear, where the cochlea conducts a spectral decomposition of the input into its constituent frequency components. In non-mammalian vertebrates, on the other hand, the vibration of the tympanic membrane is transmitted to the cochlea via a single middle-ear bone – the columella [4]; cf. Fig. 1.1b.

The ancestors of most terrestrial (land-living) vertebrates that survive today including amphibians, turtles, lizards, crocodilians, birds and mammals *independently* developed a tympanic hearing system adapted to sound pressure in air around the early triassic, i.e., ca. 250 million years ago, over a period of tens of millions of years [6, 7]; Fig. 1.2. It has also been suggested that the appearance of hearing organs sensitive to sound in air correlated with the evolution of sound production in insects [8]. In Fig. 1.2, an apparent distinction between the mammalian and non-mammalian terrestrial vertebrates has been emphasized – while in the former, the ears are independent or acoustically isolated from each other, most of the latter seem to be equipped with some form of a connection between the ears or, in other words, with internally coupled ears or ICE; Figs. 1.3a and 1.3b. By acoustic isolation we mean that, sound waves originating on the internal side of one ear cannot travel to the opposite ear. As is often the case, there are exceptions to the rule. A form of interaural coupling has been observed in mammals like the platypus and talpid moles [9], while non-mammals like snakes [10] and turtles [11] have hearing organs that are acoustically isolated. Nonetheless, the species with ICE, estimated to be more than 15,000 [12], are overwhelmingly non-mammalian.

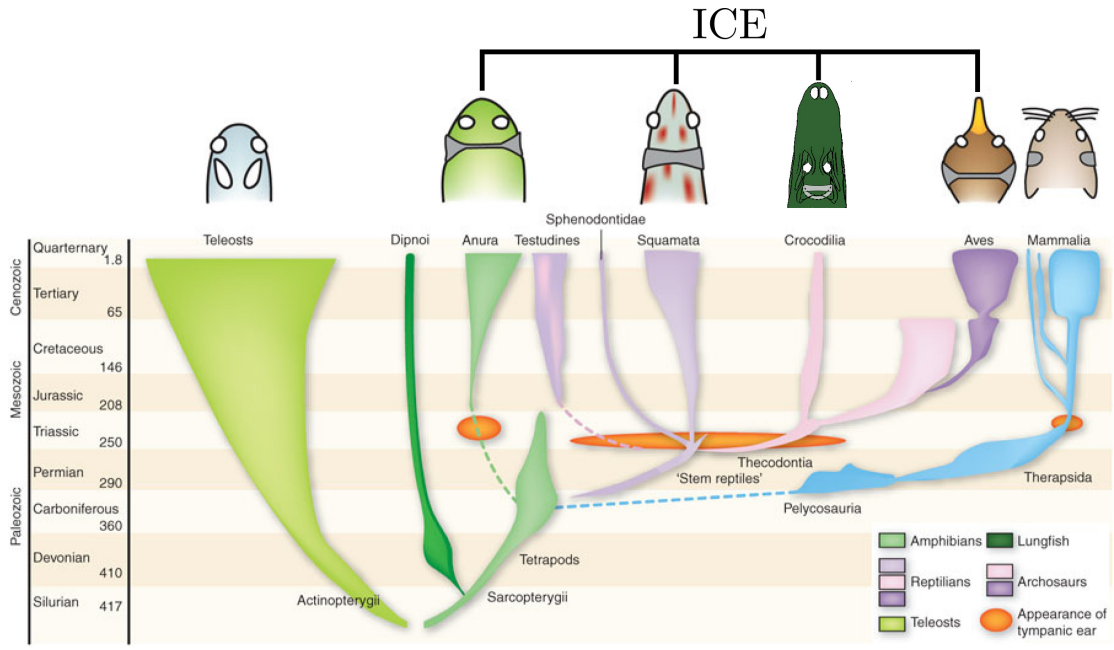

Fig. 1.2 The evolution of tympanic ears in vertebrates. Tympanic ears evolved independently in the major tetrapod groups at least five times in anurans (frogs), lepidosaurs (e.g. lizards), archosaurs (e.g. birds and crocodilia), testudines (turtles) and mammals. In most cases tympanic ears appeared around the Triassic and the approximate origins are indicated by orange blotches. The figures above the evolutionary trees show the heads of the animals along with a cross-section representing the schematic configurations of the respective middle ears. The major groups with internally coupled ears or ICE, i.e, frogs, lizards, crocodilians and birds, have been indicated separately by the overhead black bar. Snakes, turtles and mammals do not fall under the category of animals with coupled ears. Figure adapted from Schnupp and Carr [5]

1.1.1 Azimuthal sound localization and binaural hearing

As mentioned at the start of the chapter, frequency specific modifications to the sound reaching the eardrum are made by the external ear or pinna, as well as the head and torso in humans and other mammals, depending on the direction (elevation and azimuth) of a sound source [13, 14]. Thus, directional information in the form of *monaural* sound localization cues can be extracted from the response of a single ear. Monaural refers to the fact that, the cue is derived from a single ear. In general, the sound input to a single ear does not by itself contain enough directional information to fully localize a source. On the other hand, as the ears of most animals are spatially separated by virtue of being on opposite sides of the head, the inputs they receive differ from each other. Moreover, as the differences in inputs usually depend on the sound source direction, they can also be used as directional hearing cues to localize the source. In contrast to monaural cues, those obtained by simultaneously

(a) Independent ears (b) Coupled ears

Fig. 1.3 Animals utilizing tympanic membranes can be broadly divided into two categories, those with independent ears (a) and those with coupled ears (b). Animals with independent ears typically have very narrow eustachian tubes (compare Fig. 1.1a) coupling the eardrums such that the eardrums are acoustically isolated from each other. In animals with coupled ears, wider eustachian tubes along with opening in to the mouth cavity or pharyngeal cavity allow the propagation of sound waves from one eardrum to the other. As a result of such an *interaural* coupling, sound waves can travel from one ear to the other. Barring a few exceptions, mammals belong to the category of animals with independent ears, whereas non-mammalian vertebrates have coupled ears.

comparing the inputs from both ears are referred to as *binaural* cues. Given sound inputs from a single source presented to two spatially separated ears, two binaural cues are of particular importance with respect to sound localization in the azimuth,

- the phase or, equivalently, the time difference between the inputs known as the interaural time difference (ITD) [15, p. 140] and,
- the amplitude or level difference between the inputs, known as the interaural level difference (ILD) [15, p. 155]

The notion that the position of a sound source can be determined by the interaural time and level differences is known as the duplex theory, first postulated by Lord Rayleigh [16, 17].

Typically, ITDs are reliable sound localization cues at low frequencies, where the amplitude of the sound wave is much longer than the interaural distance; Fig. 1.4a. If the distance between the ears, or the interaural separation is L, the maximal ITD between the ears at low frequencies is approximately L/c, where c is the speed of sound in the medium. For a typical adult human head, the separation between the ears is around $L = 22$ cm, such that the maximum ITD between the ears is around 660 μs for sound with a speed of $c = 340$ m/s in air. When the sound wavelength becomes comparable in length to, or smaller than the distance between the ears, the head becomes a sizable obstacle to the propagation of sound waves, such that an "acoustic shadow" is formed on the side farther away from the source;

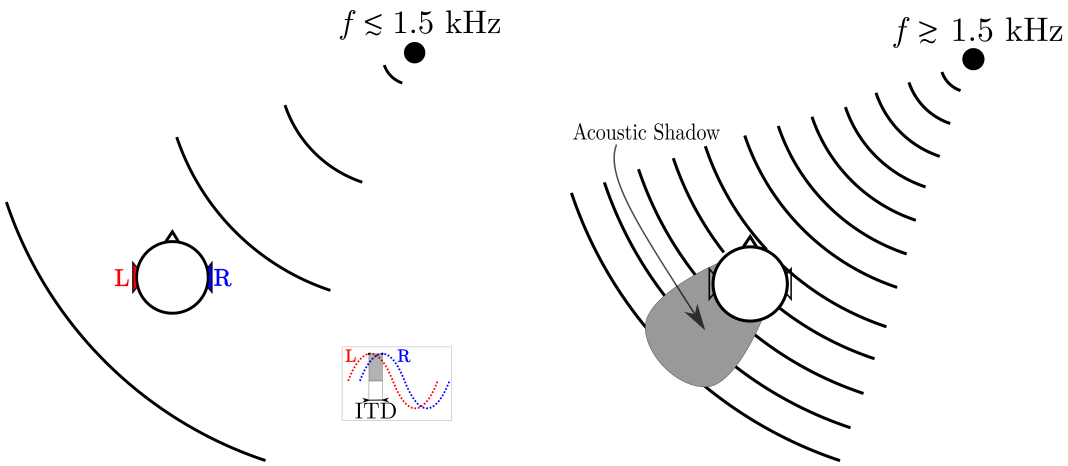

(a) Interaural time difference (b) Interaural level difference

Fig. 1.4 An illustration of the frequencies at which (a) the interaural time difference (ITD) and (b) the interaural level difference (ILD) are reliable cues for sound localization. At low frequencies ($\lesssim$ 1.5 kHz), where the sound wavelength is longer than the separation between the ears, the phase difference or, equivalently, the time difference between the inputs to the ears is a reliable cue for sound localization. The ITD, represented by an equivalent phase difference between sinusoidal sound inputs at the left (L, red) and right (R, blue) ears, is illustrated in the inset. At higher frequencies ($\gtrsim$ 1.5 kHz), the animal's head is a sizable obstacle to the propagation of sound, resulting in an acoustic shadow and amplitude or level differences between the inputs to the ears which, in turn, provide information regarding the location of a source. In nature, however, sounds are complex and contain both high and low frequency components, often requiring the simultaneous utilization of both ITDs and ILDs.

Fig. 1.4b. As a result, the amplitude of the sound input on the side closer to the source would be higher than on the opposite side. At these frequencies, the interaural level difference becomes a more reliable cue for sound localization. Moreover, at frequencies higher than 3 kHz, ambiguities corresponding to phase differences larger than 2π makes the ITD an unreliable cue. The transition between the frequency regimes corresponding to ITDs and ILDs occurs around 1.5 kHz, where the sound wavelength is roughly equal to the head width. In practice, however, the sounds present in nature are often very complex and will have both high and low frequency components. The auditory system would thus need to simultaneously use information from both ITDs and ILDs to localize a sound source [18, p. 177]. Note that the ITDs and ILDs in the form defined so far can only distinguish objects on the left from objects on the right and cannot distinguish sources in the front from those behind.

Neuronal representation of ITDs and ILDs

The present thesis deals primarily with the acoustical aspects of sound localization and a detailed analysis of the subsequent neuronal processing is beyond its scope. Nonetheless, a very brief introduction to the neuronal representation of ITD and ILD cues will help put the results of the following chapters into perspective. The vibrations of the eardrum that are transduced to the oval window of the cochlea via the middle ear bone(s) (cf. Figs. 1.1a and 1.1b), set the fluid in the inner-ear into motion. The cochlea of all vertebrates are equipped with hair cells that convert the mechanical energy of the fluid motion into electrochemical signals appropriate for neuronal processing [19]. The basic building block of neuronal processing is, of course, the neuron. A neuron consists of three parts: dendrites that collect inputs from other neurons, the soma that processes inputs and the axon that transmits output signals to other neurons. For our limited purposes, we can ignore the finer details of neuronal processing and consider the neuron to be a single unit that responds or "fires" based on a pre-defined computation on a specific number of inputs.

The processing of interaural time difference cues is carried out by neurons that are excited by simultaneous inputs originating from both ears, which are referred to as excitatory-excitatory or EE neurons [20]. As the neuron is excited by inputs from both ears, it is referred to as a binaural neuron. The strength of the response of the neuron is determined by the timing of the inputs such that, the response is strongest for the most precisely synchronized inputs. Sound localization using such neurons is conventionally explained by means of the Jeffress model [21], in which the neurons are arranged along two axonal delay lines, such that each neuron receives an input from both ears and is tuned to a particular ITD and consequently, a particular direction; Fig. 1.5. As the neurons are sensitive to synchronized inputs, they are also referred to as coincidence detector neurons. By comparing Figs. 1.4a and 1.5 we can conclude that, as the input is closer to the right ear, the neurons left of center receive synchronized inputs and their resultant excitation leads to a localization of the sound source. Effectively, a Jeffress circuit forms a *map* of ITDs which facilitates a fast localization. Experimental evidence from birds provides strong evidence for the presence of such a delay line arrangement [22, 23].

The neuronal processing of interaural level differences, in contrast, is modeled in terms of a central binaural neuron that is excited by an input originating from one ear and inhibited by an input from the other, in other words, an excitatory-inhibitory or EI-neuron [24]. In essence, a neuron on the left side of the head would be excited by an input from the left ear, while it would be inhibited by an input from the right ear, such that the strength of excitation or inhibition depends on the strength of the corresponding input. Conversely, a neuron on the right side would be excited by an input from the right ear and inhibited by one from the

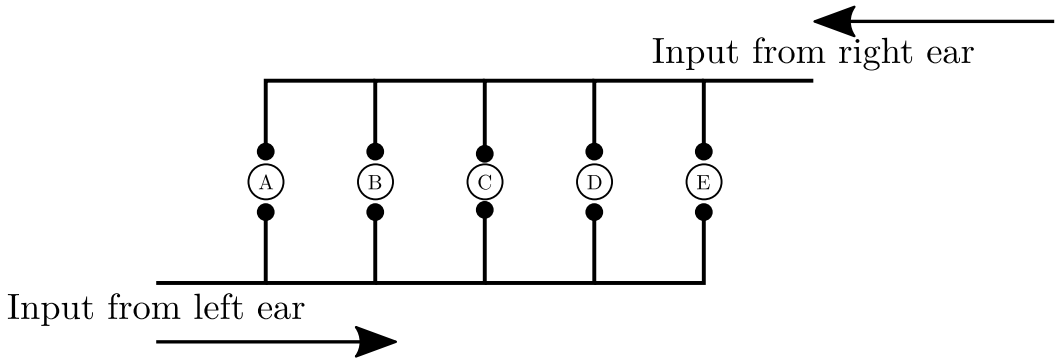

Fig. 1.5 A simplified representation of the Jeffress model. The coincidence detector or EE neurons, represented by the letters A-E, simultaneously receive inputs from both ears. They respond or "fire", when both their inputs are precisely synchronized. For example, when the sound reaches the left ear first, the inputs reaching the rightmost neuron is synchronized due to the input from the left ear being delayed. In contrast, a sound from directly in the front would result in the synchronization of the neuron in the middle.

left ear. Thus, a simple binaural comparison of the response of the left and right neurons would provide an animal with directional information. It has been suggested [25, 26] that the directional response of neurons in the gecko's midbrain can be explained by the response of EI neurons [27]. For the case of Fig. 1.4b, the acoustic shadow would lead to a weaker input to the left ear as compared to the right ear. As a result, the neurons on the right side of the head would receive a stronger excitatory input from the right side than an inhibitory input from the left side, thus enabling a localization of the sound source.

The "small animal" problem

When the wavelength of sound is much larger than the head size, acoustic shadowing effects are negligible and the interaural level difference between the ears all but vanishes. In addition, the interaural time difference is far too small to be a reliable directional cue. For example, the Tokay gecko, with its interaural separation of around 2 cm, would have a maximal ITD of around 64 μs between the inputs to its ears. Small animals lacking a pinna, like the Tokay, would therefore be at a disadvantage as they can neither generate sufficient monaural cues, nor can they rely on the binaural cues available through the external sound inputs at their ears [28]. In addition, smaller non-mammalian vertebrates often lack the sophisticated neuronal hardware of mammals, making them unable to exploit the limited hearing cues available to them solely from the external inputs. Nevertheless, animals like the Tokay gecko and other similarly sized lizards are able to localize sounds at low frequencies [25, 26]. As we will subsequently see, the resolution to the so-called "small animal" problem comes from

connection between the ears or, in other words, the *interaural coupling* between the ears, mentioned earlier in Sec. 1.1.

When the eardrums are solely driven by the external sound pressure from a source, i.e. the ears are independent, the internal time and level differences would be informationally identical to the interaural time and level differences. On the other hand, if one eardrum also feels an internal pressure dependent on the response of the opposite eardrum, i.e. the ears are coupled as in ICE, the internal and interaural differences are no longer identical. Thus, in contrast to the ITD and ILD which can be determined directly from external sound inputs, the actual hearing cues available to the animals with coupled ears, determined from the eardrum vibrations, are the *internal* time and level differences, or **i**TD and **i**LD for short. Thus, for animals with independent ears, the iTD and iLD are equivalent to the interaural time and level differences.

1.2 The ICE model

The resolution to the "small animal" problem comes from the interaural cavity that essentially forms an air-filled connection between the eardrums, that we introduced in Section 1.1. Apart from the lizards, several other terrestrial vertebrates including most frogs [29–31], crocodilians [32–34] and birds (eg. barn owls [35], chickens [36], budgerigars [37] and quails [38]) possess a hearing system where the eardrums or tympanic membranes are functionally coupled by anatomical (usually air-filled) connections through the skull; cf. Fig. 1.2. As a result, a signal arriving at one eardrum can propagate through these connections and influence the vibrations of the opposite eardrum, resulting in an acoustic coupling. The different interaural cavity configurations found in nature are illustrated in Figs. 1.6a to 1.6c for frogs, lizards and birds, respectively. A system conceptually similar to ICE has also been observed in the field cricket *Gryllus bimaculatus* [39], albeit with a more elaborate interaural connection with branches directly receiving acoustic stimuli without a tympanic membrane, or other sound receiving apparatus as an interface. A remarkable exception, in which an interaural connection and, consequently, directional hearing is achieved through a simple mechanical coupling rather than an acoustic coupling of the sound receiving organs has been observed in some parasitic flies [40]. In the present thesis, however, we limit ourselves to the vertebrates with a closed, air-filled interaural connection as the archetypes of ICE.

The theory of internally coupled ears had its origins in the so-called pressure-difference receiver principle, used to explain sound localization in locusts by Autrum [42, 43], which was later expanded upon by Michelsen [44]. Furthermore, the directional behavior of pressure-difference ears was also found to be analogous to the directionality of pressure-gradient

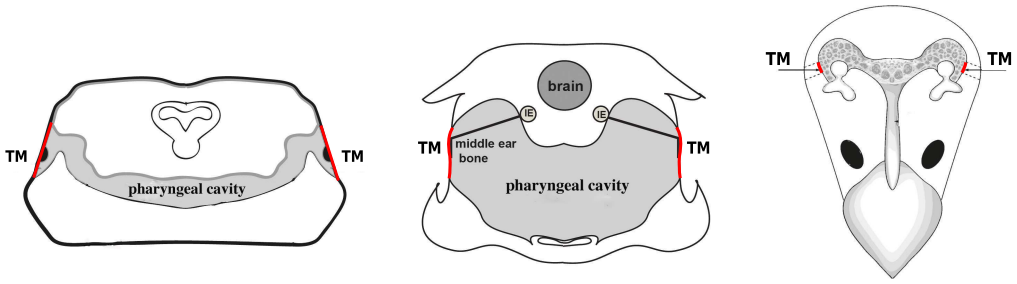

(a) Frog (b) Lizard (c) Bird

Fig. 1.6 Realizations of ICE in different terrestrial vertebrates like (a) frogs, (b) lizards and (c) birds. The interaural cavity for frogs and lizards is illustrated through coronal slices, while the bird is shown in a transverse slice as a dorsal view from above. The tympanic membranes TM (or eardrums) bound the interaural cavity and are indicated by red lines. Also indicated in the lizard diagram are the columellae, which transfer the eardrum vibrations from the eardrum to the inner ear (open circles) situated near the brain, indicated by a large filled circle. Figure taken from van Hemmen et al. [41].

microphones [45]. A review of the evolutionary aspects of ICE can be found in [46] and [47], while that of its mathematical treatment can be found in [48]. A mathematical treatment of internally coupled ears, referred to as the ICE model, was first presented by Vossen [49, 50], where a simple system consisting of circular membranes representing the eardrums, and a cylindrical canal representing the air-filled cavity between them was shown to generate the necessary interaural coupling to explain eardrum vibration data obtained via laser vibrometry in the Tokay gecko, *Gekko gecko* and the common house gecko, *Hemidactylus frenatus*. In the present dissertation, we will extend Vossen's work in order to construct a more general theory of ICE. In particular, we are interested in the directional and frequency behavior of the response of the coupled eardrums, as well as of the iTD and iLD cues generated from them. Moreover, the dependence of the resulting expressions on the system's geometrical and material parameters will also be clarified.

1.2.1 Outline

The present study of internally coupled ears will divided into two conceptual parts. Chapters 2 and 3 will comprise the first portion, where we will first generalize Vossen's [49, 50] treatment of the ICE model and then analyze the response of the system, as well as the hearing cues generated by it. In Chapter 2, we will introduce our generalized version of the mechanical ICE model in a way that will emphasize the role played by the individual components of the model as well as their material and geometrical properties. In Section 2.1, the eardrums, interaural

cavity and the head model for the sound input will be introduced as the main components of ICE and the exact expressions for the direction and frequency dependent vibrations of the eardrums will be derived by means of the piston approximation in Section 2.2. As in Vossen's development of the theory of internally coupled ears, we will also assume that the inputs to the ears have limited inherent directional information in the form of a small phase difference, and thereby stress the role played by the interaural coupling in the enhancement of hearing cues. In addition, we will also provide simplified descriptions of ICE in Section 2.3, based on lumped electrical and mechanical elements. Chapter 3 will deal with the directional hearing cues generated by the system of internally coupled ears and their dependence on the input frequency, as well as on the material and geometrical parameters of the system. In particular, the dependence of the postulated [50] low-high frequency segregation of hearing cues in ICE on the eardrum fundamental frequency f_0 will be established in Section 3.3. The internal time and level differences (iTD & iLD) will be formally defined in Chapter 3. Moreover, in Section 3.6, a numerical procedure to estimate membrane parameters from a live animal, by only using the properties of the directional cues will be presented. These chapters will correspond to a "definitive" description of ICE as a low-frequency terrestrial hearing adaptation for small animals. In order to test our theory against experimental data, we will focus on two lizards – the Tokay gecko and the water monitor *Varanus salvator*.

The second part, comprised of Chapter 4, will extend the definition of ICE to animals that do not fit the mold of the preceding two chapters. In contrast to the lizards of Chapters 2 and 3, which are terrestrial animals that use ICE as a low frequency hearing adaptation, Chapter 4 will focus on the African clawed frog *Xenopus laevis* – a fully aquatic animal, and the barn owl *Tyto alba* – a bird that hears at frequencies far higher than those of typical animals with ICE. Based on the results of Chapter 2, the eardrum and interaural cavity of both animals will be modeled in parallel in Sections 4.1 and 4.2, respectively. In particular, a modified mathematical description accounting for the unique *Xenopus* eardrum will be derived in Section 4.1, while stressing its adaptation to an underwater environment. The common thread tying the two vastly different species together, i.e. an additional air-filled chamber attached to the interaural cavity will be modeled in Section 4.2.2. Finally, in Section 4.5 the directional behavior of both animals' eardrums, as well as the directional internal time and level differences defined in Chapter 3 will be analyzed. In particular, the implications of the additional air-filled chamber will be stressed for underwater hearing in *Xenopus*, as well as for high-frequency hearing in the barn owl. Moreover, in this chapter we will also model the variation of the cavity resonance with volume, which was numerically estimated for arbitrary cavity shapes by Vossen et al. [50]. Thus, in contrast to the two chapters preceding it, Chapter 4 will introduce a modified theory of ICE which will extend its applicability

to underwater, as well as high-frequency hearing, as opposed to terrestrial, low-frequency hearing.

Chapter 2

Mathematical ICE Model

In Chapter 1 we briefly introduced the concept of internally coupled ears, or ICE, as a unique adaptation that facilitates sound localization in animals that hear at frequencies where the wavelength is several times larger than their head size; Section 1.2. The coupling between the ears or, in other words, the interaural coupling serves to enhance sound localization cues in the form of time differences between the eardrum vibrations. Moreover, ICE can also generate directional amplitude differences between the eardrums even in the absence of amplitude differences between the incoming sound inputs. Through ICE, the notion of pressure-difference ears, i.e., ears driven by both an external and internal pressure [42, 44], has been expanded into a general theory describing sound-localization in the Tokay gecko and the common house gecko *Hemidactylus frenatus* [49, 50]. In the present and the following chapters, we will generalize the concept of ICE in order to explain the sound localization ability of a much larger group of animals. Our aim is a quantitative understanding of ICE which first requires a thorough mathematical analysis of the different components involved in the system.

The goal of the present chapter is to first describe the material and geometrical properties of the anatomical components relevant to ICE and, subsequently, to derive expressions for the *coupled* eardrum vibrations in response to an external stimulus. The anatomical system consists of two main parts – the eardrums which serve as the primary sound receivers and an interaural cavity, which is an air-filled chamber that generates the coupling between the eardrum vibrations. Subsequently, we will model the sound input taking into account the size of the head with respect to the incoming sound wavelength. Once the aforementioned biophysical systems have been described, we can proceed with a mathematical analysis of the different components in order to derive explicit expressions for the directional and frequency dependence of the coupled eardrum vibrations, such that the roles played by the different components are immediately apparent. Though the ICE theory to be explained is universal

and far more general, in the present and following chapters we place a special emphasis on lizards, particularly the Tokay gecko and the water monitor *Varanus salvator*, in order to formulate a *definitive* description of ICE. The content of the present chapter has previously appeared in Vedurmudi et al. [12] and, in more detail, in Vedurmudi et al. [48].

2.1 Components of the model

Although the exact form of the anatomical components can vary according to the animal under consideration, a general physical theory can constructed to describe ICE across all species. The ICE system and, hence, our model, has three primary components,

- the middle-ear system which consists of the eardrums, usually in the form of tympanic membranes, including the mechanism to transduce sound to the inner ear,
- the air-filled interaural cavity which is responsible for the coupling that leads to the modification and often enhancement of the hearing cues and, finally,
- the sound source and the animal's head which gives us a mathematical expression for the stimulus at the eardrums.

A clear description of the geometrical and material nature of the above components will allow us to conduct a thorough quantitative analysis of the ICE model later in the chapter. In doing so, we formulate a system that accurately describes how ICE functions across the many species equipped with it.

2.1.1 The middle ear

The middle ear is the primary sound receiving apparatus in vertebrates capable of hearing. As it serves to transmit sound energy from a source to the inner ear and, consequently, the brain for neuronal processing, a consistent mathematical model describing its behavior is an essential first-step in obtaining a quantitative understanding of sound localization using internally coupled ears. As ICE-like systems are mostly restricted to non-mammalian amniotes [41], we need not include the external ear comprising the *pinna* and the external auditory meatus in our model, as it is an exclusively mammalian feature whose purpose is to convey and amplify sound energy to the eardrum.

The main components of the middle ear of lizards are the eardrum, the columella, and the extracolumella. The tympanum, or eardrum, is a thin membrane that separates the outer ear from the middle ear and vibrates in response to external sound waves. The space on the deep

(inner) side of the tympanum is the middle ear cavity; this cavity is linked, by the Eustachian tube, to the larger midline pharyngeal cavity; cf. Fig. 2.2b. The eardrums, usually in the form of tympanic membranes, vibrate in response to a pressure generated by an external sound sources. In addition, they are usually bounded by an air-filled middle-ear cavity on their deep (inner). As a result, the eardrums also feel an internal pressure generated by their own vibrations. The eardrums are typically placed on either side of the head behind the eyes. This can be seen in Figs. 2.1a to 2.1c for the leopard gecko – a typical animal with ICE. The superficial nature of the placement of the eardrums is also directly apparent in the images.

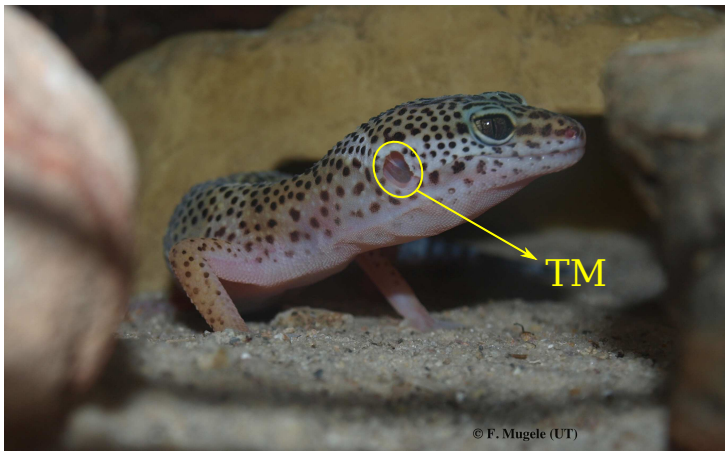

(a) Leopard gecko

(b) Close-up of the Leopard gecko's head

(c) Close-up of the eardrum

Fig. 2.1 Top: The leopard gecko – a typical animal with ICE. The location of the eardrum or tympanic membrane (TM) on the side of its head has been highlighted. Bottom Left: Close-up of its head, where its eardrum as well as the embedded extracolumella (brighter protrusion, top-left), can be discerned clearly. The vibrations of one of the eardrums excites the air inside the cavity, which in turn influences the vibrations of the opposite eardrum and vice versa. Bottom Right: Close-up of the eardrum. The lighter colored protrusion on the top-left of the tympanum is the extracolumella, which transfers the eardrum vibrations, via the columella, to the cochlea; cf. Figs. 2.6b, 2.3a, and 2.3b. Photograph courtesy of Prof. Frieder Mugele (University of Twente).

In effect, the eardrums separate the middle-ear cavity from the outside world. Unlike humans, animals with ICE only possess a single middle ear bone, namely, the *columella*. The columella functions as a transducer for the eardrum vibrations into the cochlea and is attached to the eardrum via a cartilaginous extension known as the *extracolumella* which, together, apply a significant load [51] on the eardrum surface. Moreover, in lizards [51], birds [4] and crocodilians [52, p. 933], the extracolumella attaches asymmetrically to the eardrum resulting in a pronounced deviation from a symmetric vibration pattern. The placement of the extracolumella for the gecko can be seen on the left in Fig. 2.2a. The placement of the eardrums, also known as the tympanic membranes, relative to the middle-ear cavity, the columella and the connection of the latter to the inner-ear through the oval window is shown in in Fig. 2.2b, which is a more detailed version of Fig. 1.1b.

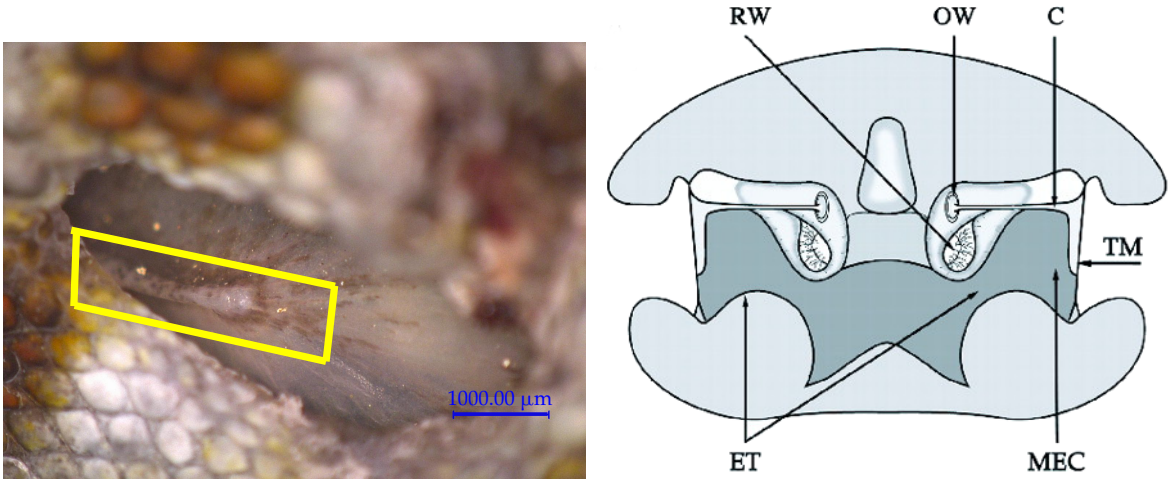

(a) Gecko eardrum (b) Head cross section

Fig. 2.2 Left: Close-up shot of a Tokay gecko illustrating the scale and shape of the eardrum (or tympanic membrane) and the extracolumella (yellow box). As the extracolumella is embedded into the tympanic membrane, it picks up the membrane vibrations and transmits them through the columella – see also Fig. 2.5 – to the cochlea. Courtesy of Prof. Zhendong Dai (NUAA). Right: Cross-section of a lizard's head. The Tympanic Membranes (TM) as well as the air inside the Middle Ear Cavity (MEC) and Eustachian Tubes (ET) are excited by incoming sound waves. Because of the large width of the Eustachian Tubes (ET), the air inside the Pharynx (P) is also excited. The tympanic vibration drives the Columella (C) in such a way that its lever construction transmits the vibrations to the Oval Window (OW), the membrane at the entrance to the cochlea. The OW vibration excites the cochlear fluid, giving rise to a frequency-dependent activation of the underlying auditory nerve fibers. The Round Window (RW) is a membrane that serves to compensate the pressure within the fluid. Figure taken from [25].

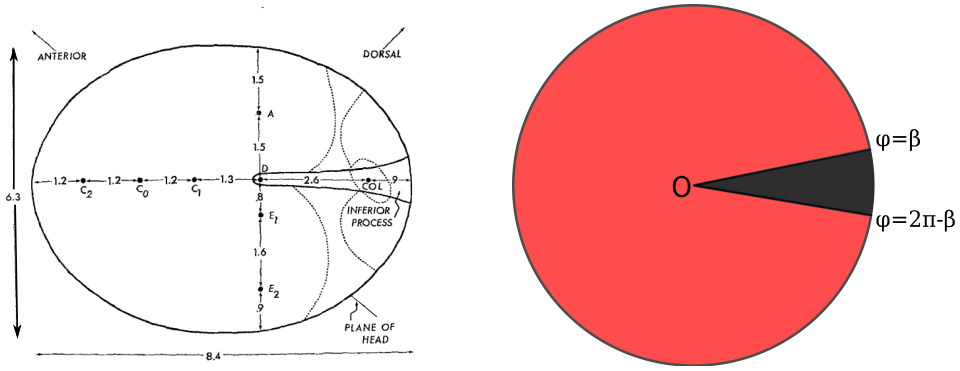

(a) Gecko eardrum (b) ICE eardrum

Fig. 2.3 Left: Sketch of the eardrum of a Tokay gecko, taken from Manley [51]. "COL" is the approximate position of the columella on the extracolumellar footplate. Dimensions in millimeters. Right: The tympanic membrane in ICE. The lightly shaded region is modeled as a linear-elastic membrane whereas the darkly shaded region ($\beta < \phi < 2\pi - \beta$) represents the extracolumella, which together with the masses behind it is taken to be infinitely heavy; see main text. The angle β corresponds to the breadth of the extracolumella and is estimated from anatomical data.

The membrane-extracolumella-columella system functions as a second-order lever where the internal and external pressures drive the membrane, which in turn causes a displacement of the extracolumella. This is illustrated in Figs. 2.4a and 2.4b. This motion is transferred via the columella to the inner ear or, to be more precise, the perilymphatic fluid of the cochlea [53]. The cochlear hair cells transduce this fluid motion into electrochemical impulses, which will be passed on to the brain via the auditory nerve; cf. Fig. 2.2b. . For frequencies that are not too high (say, below 4 kHz), the extracolumella can be taken to move as a completely stiff bar. It has been shown [54] that the extracolumella begins to flex at higher frequencies, which is illustrated in Fig. 2.5. This flection reduces the columellar transfer efficiency and is partly responsible for the poor high-frequency response of gecko middle ears, a feature also observed in other non-mammalian vertebrates. In our current treatment, however, we assume that the extracolumella behaves as a rigid plate as our frequencies of interest to auditory processing are < 4 kHz.

In a previous treatment [50] of ICE, the tympanum was modeled as a clamped circular membrane with asymmetrically attached sectorial load between $-\beta < \phi < \beta$. This manifests itself as an additional boundary condition at $\phi = \beta$ and $\phi = -\beta$ which has to be satisfied via a numerical approximation of keeping the extracolumella straight. In other words, the membrane would be constrained to vibrate with a profile that would best approximate a straight line at the extracolumella boundary. While this method has the advantage of being

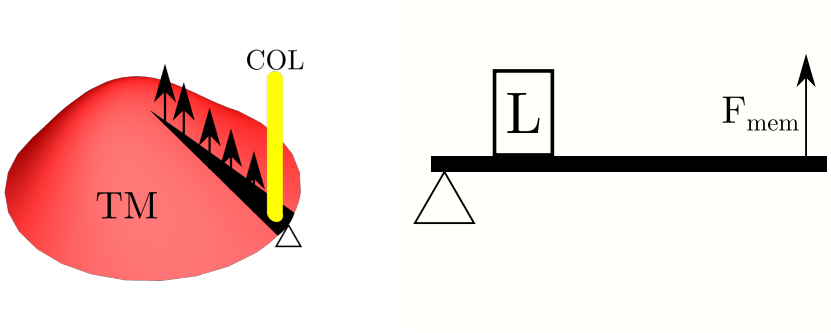

(a) Columella motion (b) Second order lever

Fig. 2.4 Left: Sketch showing an exaggerated displacement of the tympanic membrane and extracolumella driven by a sound pressure, resulting in the displacement of the columella (COL, yellow rod) about the edge of the eardrum; cf. Fig. 2.3b. Right: Equivalent second-order lever construction, where the extracolumella has been replaced by a single bar and the columella by a load (L) close to the fulcrum (triangle). The force exerted by the eardrum motion has been reduced to an cumulative point force at the opposite end of the bar in the simplified lever construction.

able to quite accurately reproduce the complex vibration patterns of the eardrum, it does not lend itself well to an analytical treatment of the coupled system. Furthermore, the constraint applied in the previous analysis is artificial in the sense that it does not take into account the mass of the attached extracolumella and columella.

Instead we take a slightly different path. The tympanic membrane will be modeled as a rigidly clamped sectorial membrane with its vibrating part limited to $\beta < \phi < 2\pi - \beta$ [12, 48]. This means that in addition to the radial boundary at a_{tymp}, we have a new set of boundaries at $\phi = \beta$ and $\phi = 2\pi - \beta = -\beta$ where the membrane vibration is set to zero. This is illustrated in 2.3. The membrane material will be assumed to be linear-elastic. As before, the equations describing the vibrations of the membrane will consequently be linear 2^{nd}-order partial differential equations (PDE's) to be derived in Section 2.2.1. We will effectively be analyzing the average displacement of the membrane surface in order to calculate the hearing cues.

2.1.2 Interaural Cavity

The interaural cavity (IAC) refers to the tympanic or middle-ear cavities and the air-filled connection between them, that generates the acoustic coupling between the eardrums. In general, the nature of the connection shows great variation both in size and shape among animals with ICE. A consistent mathematical description of the qualitative and quantitative

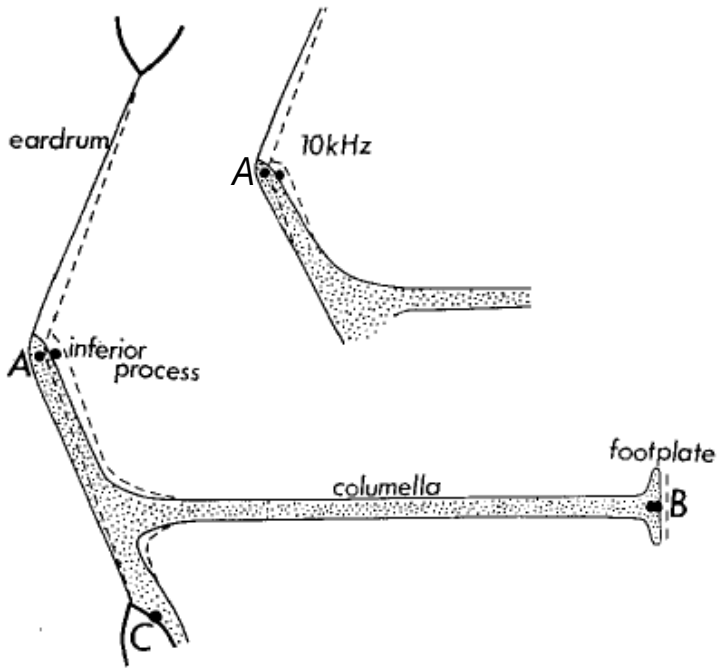

Fig. 2.5 Operation of the middle ear lever in Geckos reproduced from [54]. The inferior process of the extracolumella (AC) hinges at point C. At low frequencies the extracolumella is a stiff bar, but at higher frequencies the inferior process of the extracolumella begins to flex as shown in the inset. The columellar footplate (B) is a piston that fits into the oval window of the cochlea.

properties of ICE can nonetheless be achieved through an air-filled cylinder of length L, commonly termed the interaural distance, obtained through direct measurement.

The single cylindrical canal system describes ICE in the majority of animals possessing the system [12, 50]. Lizards [26] and most frogs [55] fall into this category, in which both tympanic cavities open into wider spaces such as the pharyngeal or the buccal cavity via the Eustachian tubes, resulting in a single continuous connection between the eardrums; cf. Figs. 1.6a and 1.6b. On the other hand, in birds like the barn owl *Tyto alba* [56], and the African clawed frog *Xenopus laevis* [57], the Eustachian tubes extend into a single narrow canal independent of the mouth cavity; cf. Fig. 1.6c. We note, however, that, in spite of the variation in geometry, the general physical principles discussed in this chapter apply to both cases. The special cases of *Xenopus* and the barn owl, will be discussed in more detail in Chap. 4.

In an earlier mathematical treatment of ICE [49, 50], the oral cavity was modeled as a simple cylinder closed at both ends by rigidly clamped (baffled) circular eardrums. In the aforementioned model (cf. Fig. 2.6a), the cylinder length is the interaural distance L and the radius of the cylinder was taken to be equal to that of the eardrum, i.e., $a_{\text{cyl}} = a_{\text{tymp}}$, which

resulted in a cavity volume

$$V_0 = \pi a_{\text{tymp}}^2 L \,, \tag{2.1}$$

which was about an order of magnitude smaller than what is observed in nature. In the present treatment of ICE, we improve upon the model by treating the cavity volume as a variable parameter (see Fig. 2.6b) such that,

$$a_{\text{cyl}} = \sqrt{\frac{V_{\text{cav}}}{\pi L}} \,. \tag{2.2}$$

Thus, the effect of V_{cav} on the internal coupling between the two eardrums and, consequently,

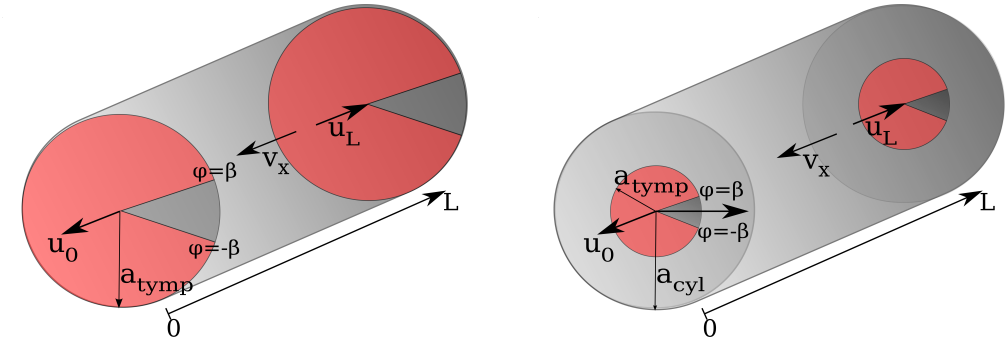

(a) Interaural cavity [50] without volume correction.

(b) Interaural cavity [12] allowing volume correction with $a_{\text{tymp}} < a_{\text{cyl}}$

Fig. 2.6 The first model (a) is represented by a cylinder of radius a_{tymp} and length L closed at both ends by sectorial membranes of radius a_{tymp}. The current model (b) accounts for the volume of the interaural cavity and is instead represented by a cylinder of radius $a_{\text{cyl}} > a_{\text{tymp}}$ and length L. The bold arrows represent the direction conventions along the cylinder's axis. The darkly shaded v-shaped region corresponds to the extracolumella; see Section 2.1.1. The membranes are driven both by an external sound pressure as well as by the internal pressure inside the cavity (lightly shaded region). The membrane motion in turn moves the extracolumella like a second-order lever, i.e. the load is situated between the effort and the fulcrum; Figs. 2.4a and 2.4b. Finally, the extracolumella transduces the membrane vibration via the columella to the cochlea; cf. Fig. 2.5.

its effect on the iTD and iLD can be directly analyzed. As we will see in Chap. 3, the geometrical model illustrated in Fig. 2.6b explains the directionality of eardrum vibrations, as well as the generation of directional hearing cues in the Tokay gecko and the monitor lizard *Varanus* [12, 48] within their hearing ranges, i.e. < 4 kHz and < 2 kHz, respectively.

The exact nature of the internal coupling will be discussed in Sec. 2.2 where we perform a thorough evaluation of the complete system. We will be working in a cylindrical coordinate

system with $x \in (0, L)$ being the direction along the cylindrical axis and (r, ϕ) the polar coordinates in the plane perpendicular to it.

2.1.3 Head model and sound input

In realistic environments the acoustic fields experienced by animals are often very complex. In addition to sound waves radiated directly from one or more sources, they also involve waves reflected from objects in their immediate neighborhood. Most mammals possess the neuronal power required to carry out the sophisticated signal processing needed to derive useful information from these signals, whereas smaller animals with limited neuronal power like geckos respond to simpler cues – usually the direct field from the nearest or strongest source. We will therefore model our incoming input as a simple plane wave (or equivalently, a pure tone) of a given frequency. As the ensuing mathematical description is linear, more complex inputs can be represented as a combination of pure tones. The input is specified in terms of its intensity, frequency, and direction. Such a stimulus can be generated experimentally, for instance in an anechoic chamber using loudspeakers that are placed at a distance from the animal that is large compared to the animal's size and the wavelength of the sound involved [2, 25, 26]. In other experiments, a similar stimulus has also been provided by means of a headphone sealed to the ear [58].

At frequencies within the hearing range of animals with ICE, the sound pressure amplitude on the outer surface of the eardrum can be taken as uniform. The spatial variation can be safely neglected as the typical eardrum is less than 1 cm in diameter, while the sound wavelength in air is around ~ 7 cm at 5 kHz, which, for most animals with ICE, is well outside the hearing range. For instance, the smallest sound wavelengths in the hearing range of an adult water monitor *Varanus* is ~ 170 mm (2 kHz, [59]) and is around ~ 85mm (4000 Hz, [4]) for the smaller Tokay gecko.

In general, as a result of the diffraction of sound around the head and body of an animal, there would be a difference in phase as well as amplitude between the sound at the two ears. The exact variation depends on the size (and shape) of the animal, the direction and the frequency of the incident wave. Nevertheless, because of the small interaural lengths (relative to the stimulus wavelength) of many animals with ICE, certainly lizards and frogs, the amplitude (or level) difference is negligible [60]. The phase difference, although small in animals with ICE, is typically not negligible. In smaller animals, i.e., where the sound wavelength λ is much larger than the interaural distance L, we can neglect diffraction effects resulting in a phase difference which only depends on the distance between the ears. This is illustrated in Fig. 2.7 for an incoming sound wave from a source whose distance from the animal is much larger than the interaural distance. A sound wave has to travel an extra

distance Δ to reach the ear on the opposite side, here referred to as the ”contralateral“ ear, compared to the ear on the same side as the source – the ”ipsilateral“ ear.

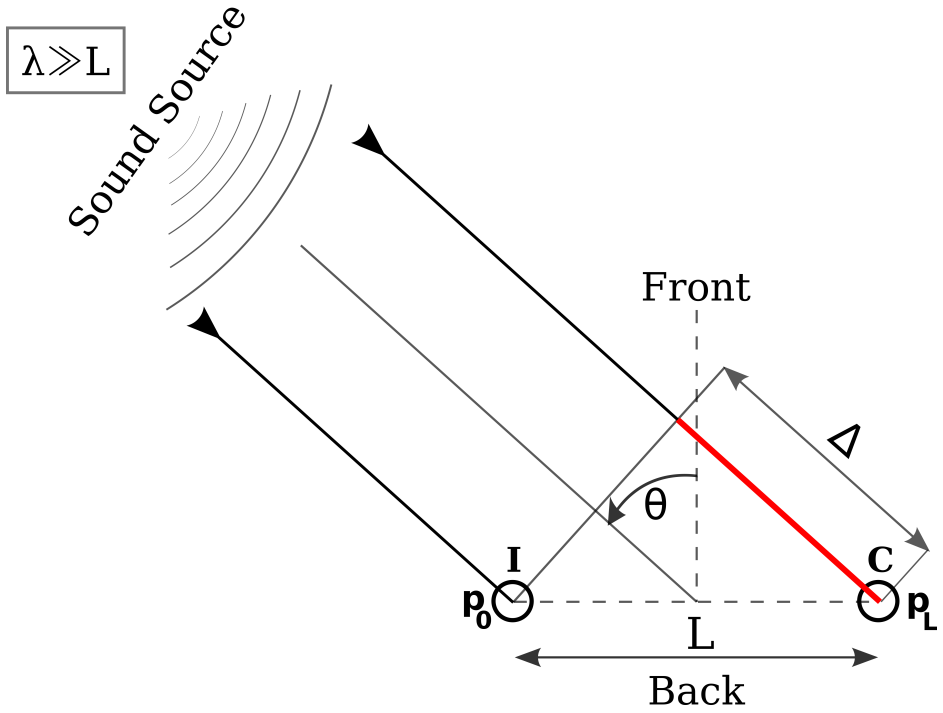

Fig. 2.7 The acoustic head model for ICE for head size (L) much smaller than wavelength λ. Depending on the angle of the sound source θ, the distance between the sound source and the **C**ontralateral ear is longer than its distance from the **I**psilateral ear. The extra distance traveled by the sound wave to reach the contralateral ear is $\Delta = L\sin\theta$, which gives rise to a phase difference $k\Delta$. The small head size of many of these animals lets us safely [60] neglect diffraction effects on the phase and amplitude difference, which would have required us to account for the fact that the sound wave would have to travel *around* the head to reach the contralateral ear.

The sound source direction is quantified by an angle θ such that, positive values correspond to ipsilateral sources and negative ones to contralateral sources. According our convention, $\theta = 0^\circ$ corresponds to sources directly in front of the animal and $\theta = \pm 180^\circ$ to those directly behind. We have therefore chosen a coordinate system relative to the *median-sagittal* plane or the head midline of the animal such that θ gives the angle of incidence of the sound wave relative to this plane. For more complex auditory systems we would require two angles (θ, ϕ) with the second representing the elevation of the source, but this is not needed for our current analysis. The terms ipsi- and contralateral also refer to the stimuli at the respective ears; cf. Fig. 2.7.

We consider as our sound input a pure-tone signal of frequency f and amplitude p emanating from a far-away source at a direction θ. The angular frequency is given by

$\omega = 2\pi f$ and the wavenumber is given by $k = \omega/c$, where c is the speed of sound in the medium. As the sound wave reaching the opposite ear travels an additional distance $\Delta = L\sin\ \theta$, the inputs to the ears have a small frequency and direction dependent phase difference $k\Delta$. The sound inputs to both ears are given by [61, p. 154]

$$p_0^{\text{ex}} = p\exp(i\omega t)\exp(ik\Delta/2), \qquad p_L^{\text{ex}} = p\exp(i\omega t)\exp(-ik\Delta/2) \tag{2.3}$$

$$\text{where,} \quad \Delta = L\sin\theta\ . \tag{2.4}$$

We will later see (cf. Chap. 3) that, through ICE, even animals with small interaural distance L can obtain useful internal time and level differences. As ICE is usually a terrestrial adaptation, c refers to the sound speed in air. As we will also deal with ICE in water in a later chapter (cf. Chap. 4), we note that our definition for the sound inputs to the ear (2.3) is nevertheless valid in both media for small animals.

2.2 Derivation of the mathematical model

We will now use the physical model for internally coupled ears described in the previous section to derive an expression for the vibrations of the eardrum in response to the sound inputs given in Eq.(2.3), as well as an expression for the pressure inside the interaural cavity. Put in more precise terms, we will derive the steady-state response of the system to a pure tone stimulus. In doing so, we will be neglecting transient effects. Our goal is to accurately represent the functions and do so in such a way that the frequency and direction dependence as well as the effects of coupling on the eardrum vibrations are apparent. Thus, we will be able to analyze the resulting hearing cues in the next chapter. While deriving the main functions of interest, we will also discuss the appropriate boundary conditions and approximations that relate the membrane vibrations to the internal pressure. In Table 2.1 the main functions used in the derivation below have been listed, together with their physical interpretation. In order to motivate the derivation below, we start by briefly discussing the final expression that relates the membrane vibrations to the sound inputs. This also serves to clearly see the interplay between the terms corresponding to the membrane and to the internal cavity. Given a pair of internally coupled eardrums of area $S_{\text{tymp}} = (\pi - \beta)a_{\text{tymp}}^2$ driven by the sound pressures given in (2.3), the displacement of its surface at a position (r, ϕ) is given by

$$u_{0/L}(r,\phi;\omega,t) = \frac{1}{2}\left(\frac{p_L^{\text{ex}} + p_0^{\text{ex}}}{1+\Lambda_{\text{tot}}\Gamma_+} \mp \frac{p_L^{\text{ex}} - p_0^{\text{ex}}}{1+\Lambda_{\text{tot}}\Gamma_-}\right)\Lambda\,. \tag{2.5}$$

Table 2.1 Functions and variables used in the ICE Model

θ, ω, k	Sound source direction, angular frequency and wavenumber ($k = \omega/c$) with sound speed $c = 343$ ms^{-1} in air.
$p_{0/L}$, Δ	Sound pressure inputs to the two ears given the direction and the phase difference between them.
$u_{mn}(r,\phi;t)$, ω_{mn}	Tympanic membrane eigenmodes and corresponding eigenfrequencies.
$u_{0/L}(r,\phi;t)$, $u^{\text{ave}}_{0/L}(t)$	Membrane displacement – full and average.
$\Lambda(\omega)$	Membrane frequency response.
ρ_{M}, d_{M}, c_{M}, a_{tymp}	Tympanic membrane density, thickness, wave propagation velocity and eardrum radius.
$\beta < \phi < 2\pi - \beta$	Extent of the vibrating part of the membrane. The remaining sector corresponds to the extracolumella.
f_0, α	Membrane fundamental frequency and damping coefficient.
L, V_{cav}, V_{tymp}	Interaural separation, total cavity volume, tympanic cavity volume.
a_{cyl}, S_{cyl}	Radius and cross section of the cylindrical cavity.
J_q, μ_{qs}, ν_{qs}	Order q Bessel function of the first kind, its s^{th} zero and s^{th} extremum respectively.
$p_{qs}(x,r,\phi)$, ζ_{qs}	Cavity pressure modes and corresponding axial wavenumbers.
$p(x,r,\phi;t)$, $\text{v}_x(x,r,\phi;t)$	Cavity pressure distribution and air velocity.

where

$$\Lambda = \sum_{m,n}^{\infty} \frac{u_{mn}(r,\phi)\int dS\, u_{mn}}{\rho_{\text{M}} d_{\text{M}} \Omega_{mn} \int dS\, u_{mn}^2}\ , \tag{2.6}$$

$$\Lambda_{\text{tot}}(\omega) = \int_{\mathscr{S}_{\text{mem}}} dS\, \Lambda(r,\phi,\omega)\ . \tag{2.7}$$

Here $\Omega_{mn} = \omega^2 - \omega_{mn}^2 - 2i\alpha\omega$ and the $\Gamma_{\pm}$ coefficients quantitatively relate the internal pressures at p_L^{in}, p_0^{in} the eardrums to the eardrum displacement u_L, u_0 such that

$$2\, p_L^{\text{in}} = \Gamma_+ \int_{\mathscr{S}_{\text{mem}}} dS\, (u_L + u_0) + \Gamma_- \int_{\mathscr{S}_{\text{mem}}} dS\, (u_L - u_0) \tag{2.8}$$

$$2\, p_0^{\text{in}} = \Gamma_+ \int_{\mathscr{S}_{\text{mem}}} dS\, (u_L + u_0) - \Gamma_- \int_{\mathscr{S}_{\text{mem}}} dS\, (u_L - u_0) \tag{2.9}$$

The integrals in Eqs.(2.6)&(2.7) are taken over the vibrating part membrane surface,

$$\mathscr{S}_{\text{mem}} = (r,\phi) \in (0, a_{\text{tymp}}) \times (\beta, 2\pi - \beta) \ .$$

The membrane eigenmodes, denoted by u_{mn}, can be explicitly written down as

$$u_{mn}(r,\phi) = \sin\kappa(\phi-\beta) J_\kappa(\mu_{mn} r) \ , \tag{2.10}$$

where $\kappa[m] = \frac{m\pi}{2(\pi-\beta)}$, $m = 1,2,3,\ldots$ and J_κ is the order-κ Bessel function of the first kind with $\mu_{mn} \times a_{\text{tymp}}$ being its n^{th} zero. The remaining quantities are defined in Table 2.1.

For a solitary driving pressure $p\exp(i\omega t)$ on an individual membrane's surface, $\Lambda(r,\phi) = u(r,\phi)/p$ is its frequency response and Λ_{tot} is the integral of Λ over the vibrating part of the membrane surface $\mathscr{S}_{\text{mem}}$. The frequency dependence of both these terms is contained in Ω_{mn} which will be defined later; cf. (2.41). The coefficients $\Gamma_\pm$ effectively correspond to the frequency response of the interaural cavity. In the following, we derive expressions for the eardrum vibrations and cavity pressure in succession and use the results to finally derive expressions for coupled membrane vibrations using appropriate boundary conditions.

2.2.1 Tympanic vibrations

As described in Sec. 2.1.1, the eardrum consists of two parts, namely, the tympanic membrane and the attached extracolumella. The vibrating part of the eardrum or tympanum will be modeled as a damped linear-elastic membrane. In order to be described as a membrane, the membrane radius a_{tymp} should be much larger than its thickness d_{M}. A typical criterion is that, in order to be described as a membrane, the ratio $a_{\text{tymp}}/d_{\text{M}}$ should be greater than 80 [62]. This is certainly true for most animals with tympanic hearing as the tympanic diameter is of the order of a centimeter, while the thickness is of the order of tens of microns. For a Tokay gecko ($a_{\text{tymp}} \approx 2.6$ mm, $d_{\text{M}} \approx .01$ mm), this gives us a ratio $a_{\text{tymp}}/d_{\text{M}} \approx 260$.

As the eardrum is modeled as having a (nearly) circular shape in ICE, we will be working in polar coordinates denoted by a radial distance and angle (r,ϕ). We denote the pressure difference across the eardrum surface by $\Psi(r,\phi;t)$ and the transverse displacement at any point on its surface by $u(r,\phi;t)$, such that, $u \ll a_{\text{tymp}}$. In other words, the membrane only undergoes small deflections. Moreover, we also assume that the deflections are small enough such that the gradients are also much less than unity, i.e., $|\nabla u(r,\phi)| \ll 1$. Finally, in our derivation, we assume that the thickness d_{M} and and density ρ_{M} are uniform over the membrane surface.

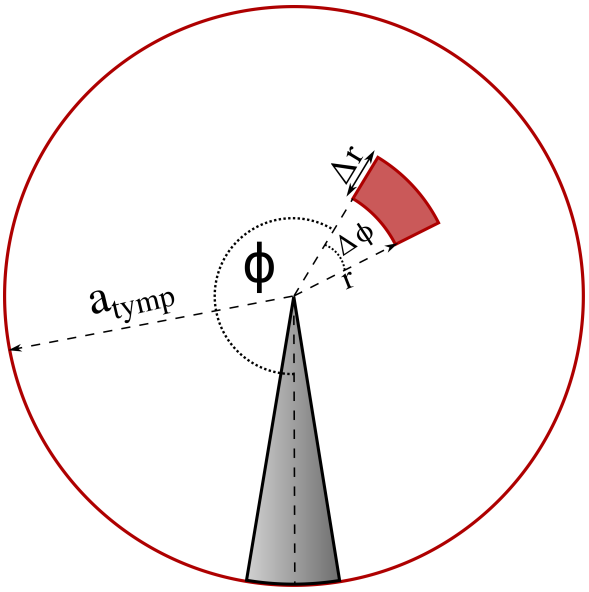

Fig. 2.8 Infinitesimal section of area $r\Delta r\Delta\phi$ on the surface of the vibrating membrane of radius a_{tymp}. The shaded region corresponds to the extracolumella; cf. 2.3b. The element is at a distance r from the center of the eardrum and at an azimuthal angle ϕ, such that $\phi = 0$ corresponds to the midline of the extracolumella. We work in polar coordinates as we have chosen the eardrum to have a nearly circular shape in our model.

The following derivation is based on Kreyszig [63, p. 575]. Let us consider a surface of infinitesimal area $r\Delta r\Delta\phi$ on the membrane surface at a distance r from the center and at an azimuthal angle ϕ; cf. Fig. 2.8. The angle ϕ is chosen such that $\phi = 0$ corresponds to the midline of the extracolumella and the vibrating part of the membrane is limited to $S_{\text{memb}} = \{r < a_{\text{tymp}} \text{ and } \beta < \phi < 2\pi - \beta\}$; cf. Sec. 2.1.1&Fig.2.3b. Given a uniform membrane tension τ, the restoring forces act normal to each edge of the infinitesimal element along the gradient of the membrane displacement u; cf. Fig. 2.9a. As the displacements and gradients are small, the angle made by the gradient with the horizontal plane at any point is also small. As a result the horizontal forces acting on opposite ends of the infinitesimal elements cancel out. Denoting the angles made by the gradient at each edge by $\theta_{r1},\ \theta_{r2},\ \theta_{\phi 1},\ \theta_{\phi 2}$ (see Figs. 2.9a and 2.9b), the vertical component of the net forces at the radial edges are given by

$$\begin{aligned}\tau(r+\Delta r)\Delta\phi\sin\theta_{r2} - \tau r\Delta\phi\sin\theta_{r1} &\approx \tau(r+\Delta r)\Delta\phi\tan\theta_{r2} - \tau r\Delta\phi\tan\theta_{r1}\\ &= \tau(r+\Delta r)\Delta\phi\left.\frac{\partial u}{\partial r}\right|_{r+\Delta r} - \tau r\Delta\phi\left.\frac{\partial u}{\partial r}\right|_{r}. \qquad (2.11)\end{aligned}$$

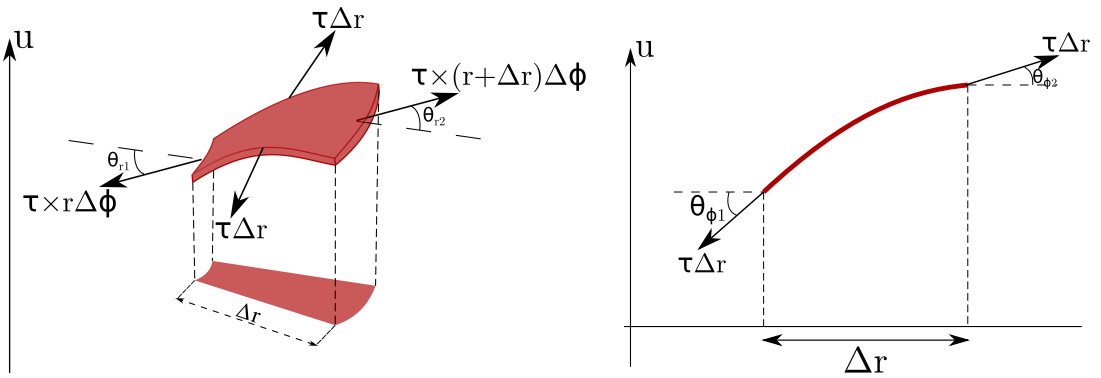

Fig. 2.9 Forces acting on the displaced infinitesimal section from Fig. 2.8 due to the inherent tension τ in the radial direction (b) and azimuthal direction (c).

Similarly, the vertical components due to the azimuthal edges are given by

$$\begin{aligned}\tau\Delta r\Delta\phi\sin\theta_{\phi 2}-\tau\Delta r\sin\theta_{\phi 1}&\approx\tau\Delta r\tan\theta_{\phi 2}-\tau\Delta r\tan\theta_{\phi 1}\\&=\tau\frac{\Delta r}{r}\left.\frac{\partial u}{\partial\phi}\right|_{\phi+\Delta\phi}-\tau\frac{\Delta r}{r}\left.\frac{\partial u}{\partial\phi}\right|_{\phi}.\end{aligned}\tag{2.12}$$

In addition to the restoring force due to the membrane tension, we also add an empirical damping term quantified by a coefficient α. The Newton's equation for the infinitesimal element driven by a pressure $\Psi(r,\phi;t)$ can thus be written as,

$$\begin{aligned}\rho_{\mathrm{M}}d_{\mathrm{M}}r\Delta r\Delta\phi\ddot{u}=\Psi(r,\phi;t)r\Delta r\Delta\phi&+\left(\tau(r+\Delta r)\Delta\phi\left.\frac{\partial u}{\partial r}\right|_{r+\Delta r}-\tau r\Delta\phi\left.\frac{\partial u}{\partial r}\right|_{r}\right)\\&+\left(\tau\frac{\Delta r}{r}\left.\frac{\partial u}{\partial\phi}\right|_{\phi+\Delta\phi}-\tau\frac{\Delta r}{r}\left.\frac{\partial u}{\partial\phi}\right|_{\phi}\right)-2\alpha\rho_{\mathrm{M}}d_{\mathrm{M}}r\Delta r\Delta\phi\dot{u}\,.\end{aligned}\tag{2.13}$$

where, the overhead dot denotes a derivative with respect to time. Dividing through the above equation by the infinitesimal area term $r\Delta r\Delta\phi$ gives us

$$\begin{aligned}\rho_{\mathrm{M}}d_{\mathrm{M}}(\ddot{u}+2\alpha\dot{u})=\Psi(r,\phi;t)&+\frac{\tau}{\Delta r}\left(\left.\frac{\partial u}{\partial r}\right|_{r+\Delta r}-\left.\frac{\partial u}{\partial r}\right|_{r}\right)-\frac{1}{r}\left.\frac{\partial u}{\partial r}\right|_{r+\Delta r}\\&+\frac{\tau}{r\Delta\phi}\left(\left.\frac{\partial u}{\partial\phi}\right|_{\phi+\Delta\phi}-\left.\frac{\partial u}{\partial\phi}\right|_{\phi}\right).\end{aligned}$$

Finally, taking the limits $\Delta r \to 0$ and $\Delta\phi \to 0$ allows us to rewrite the equation of motion for the membrane element as an inhomogeneous wave equation

$$\frac{\partial^2 u}{\partial t^2} + 2\alpha\frac{\partial u}{\partial t} - c_{\mathrm{M}}^2\Delta_{(2)}u = \frac{1}{\rho_{\mathrm{M}} d_{\mathrm{M}}}\Psi(r,\phi;t) \tag{2.14}$$

$$\Delta_{(2)} = \frac{\partial^2}{\partial r^2} + \frac{1}{r}\frac{\partial}{\partial r} + \frac{1}{r^2}\frac{\partial^2}{\partial\phi^2}\,. \tag{2.15}$$

where $\Delta_{(2)}$ is the 2D-Laplacian and c_{M} is the wave-propagation velocity on the membrane surface which is defined as (cf. Table 2.1)

$$c_{\mathrm{M}} = \sqrt{\frac{\tau}{\rho_{\mathrm{M}} d_{\mathrm{M}}}}\,. \tag{2.16}$$

Furthermore, $\Psi(r,\phi;t)$ is the total pressure driving the membrane (on both the inner and the outer surface). The tympanic membrane is fixed at its radial boundary $r = a_{\mathrm{tymp}}$ and, as a consequence of the presence of the extracolumella, at $\phi = \pm\beta$.

As a preliminary exercise, we first derive expressions for the free (i.e., $\Psi = 0$) and force-driven vibrations of a circular membrane. We will then use our results to move on to the sectorial membrane which corresponds to the tympanum loaded by the extracolumella.

Circular membrane

We consider a rigidly clamped circular membrane of radius a_{tymp} and solve for the membrane displacement $u(r,\phi)$ at a point (r,ϕ) with $r < a_{\mathrm{tymp}}$ and $0 \le \phi < 2\pi$. Due to the absence of the extracolumella, the membrane is only subject to the Dirichlet boundary condition

$$u(r,\phi;t)|_{r=a_{\mathrm{tymp}}} = 0\,. \tag{2.17}$$

We first determine the eigenmodes of an undamped circular membrane by solving (2.14) for $\alpha = 0,\ \Psi = 0$. We solve the resulting 2-dimensional Helmholtz equation by using a separation ansatz [64, p. 187]

$$u(r,\phi;t) = f(r)g(\phi)T(t)\,, \tag{2.18}$$

which results in the following set of equations,

$$\frac{d^2g(\phi)}{d\phi^2} + m^2 g(\phi) = 0 \tag{2.19}$$

$$\frac{d^2T(t)}{dt^2} + c_{\mathrm{M}}^2 \mu^2 T(t) = 0 \tag{2.20}$$

$$\frac{\partial^2 f(r)}{\partial r^2} + \frac{1}{r}\frac{\partial f(r)}{\partial r} + \left[\mu^2 - \frac{m^2}{r^2}\right] f(r) = 0 \tag{2.21}$$

with separation constants μ and m. The first two equations are second-order ODEs, representing the dependence on azimuth ϕ and time t, that can be readily solved to give,

$$g(\phi) = M\cos\ m\phi + N\sin\ m\phi \tag{2.22}$$

$$T(t) = E\exp(i\omega t) + Fe^{-i\omega t}\,. \tag{2.23}$$

In general, m can take any positive real value – a fact that will help us solve the sectorial membrane problem. In the case of a full circular membrane, however, requirements of continuity and smoothness in ϕ result in m taking integer values only.

The third equation (2.50) is known as the Bessel differential equation [65, p. 313] and its general solution is given by

$$f(r) = CJ_m(\mu_m r) + D_m Y_m(\mu_m r)\ . \tag{2.24}$$

J_m and Y_m are the order-m Bessel functions of the first and second kind, respectively. We can set the coefficients $D_m = 0$, as the Bessel function of the second kind diverges at $r = 0$ [65] and we are seeking solutions that remain finite on the membrane surface. Imposing the Dirichlet boundary condition (2.17) at the edges of the membrane effectively results in,

$$J_m(\mu a_{\mathrm{tymp}}) = 0.$$

As the Bessel function J_m has a countably infinite number of zeros [66, p. 370], μ is correspondingly constrained to a discrete set of values. In (2.26), the combination of a_{tymp} and μ_{mn} corresponds to the n^{th} zero of J_m and $\omega_{mn} = c_{\mathrm{M}}\mu_{mn}$ is the eigenfrequency of the eigenmode indexed by (m,n). The circular membrane modes can thus be written as

$$u_{mn}^{\mathrm{circ}}(r,\phi;t) = \left(E_{mn}e^{i\omega_{mn}t} + F_{mn}e^{-i\omega_{mn}t}\right) u_{mn}^{\mathrm{circ}}(r,\phi) \tag{2.25}$$

$$u_{mn}^{\mathrm{circ}}(r,\phi) = \left[M_{mn}\cos m\phi + N_{mn}\sin m\phi\right] J_m(\mu_{mn}r)\,. \tag{2.26}$$

As we will later see (cf. Chap. 3, the fundamental frequency f_0^{circ}, given by

$$f_0^{\text{circ}} = c_{\text{M}}\mu_{01}/2\pi \ , \tag{2.27}$$

is of particular relevance to generating hearing cues in ICE.

The spatial parts of the resulting eigenmodes u_{mn} also form an orthogonal set, i.e.,

$$\int_S dS\, u^{\text{circ}}_{m_1n_1} u^{\text{circ}}_{m_2n_2} = 0, \text{ if } m_1 \neq m_2 \text{ or } n_1 \neq n_2 \ , \tag{2.28}$$

where the integral is taken over a disk of radius a_{tymp}. For later convenience we have denoted the spatial part of the modes by omitting the time-dependence from the argument of the function $u^{\text{circ}}_{mn}(r,\phi)$. The first few of these modes have been plotted in Fig. 2.10. This symmetric vibration profile circular membranes does not agree well with that for lizards due to the inherent asymmetry resulting from the embedded extracolumella (cf. Figs. 2.3a and 2.3b), but does agree fairly well for many frogs since the footplate of their columella is attached symmetrically to the middle of the tympanum [67]; see also Fig. 2.11. We also

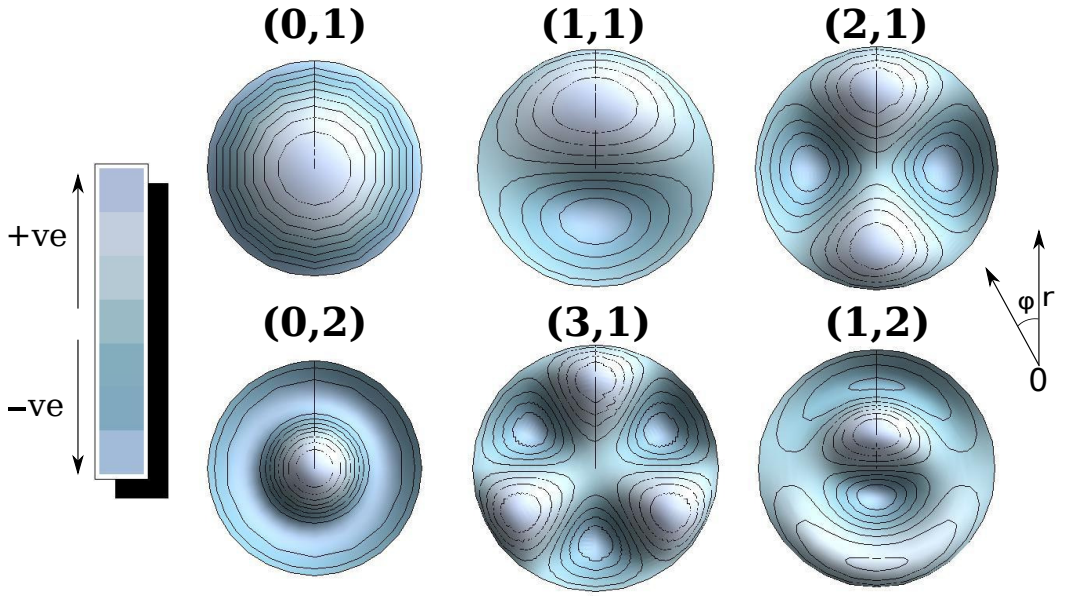

Fig. 2.10 Eigenmodes of a full circular membrane with the characteristic numbers (m,n) of the modes shown above each figure. Displacements into the surface of the paper are darkly shaded while those out are lightly shaded (illustrated in the legend) . The eigenfrequency increases from left to right and top to bottom. This kind of a vibration profile does not agree well with that for lizards due to the asymmetry brought about by the embedded extracolumella, but does agree fairly well for many frogs since the footplate of their columella attaches symmetrically to the middle of the tympanum [67].

note that a freely vibrating membrane can have time-dependent components that are both forward- and backward-moving. The presence of a driving force, however, constrains the time-dependent component in the steady-state.

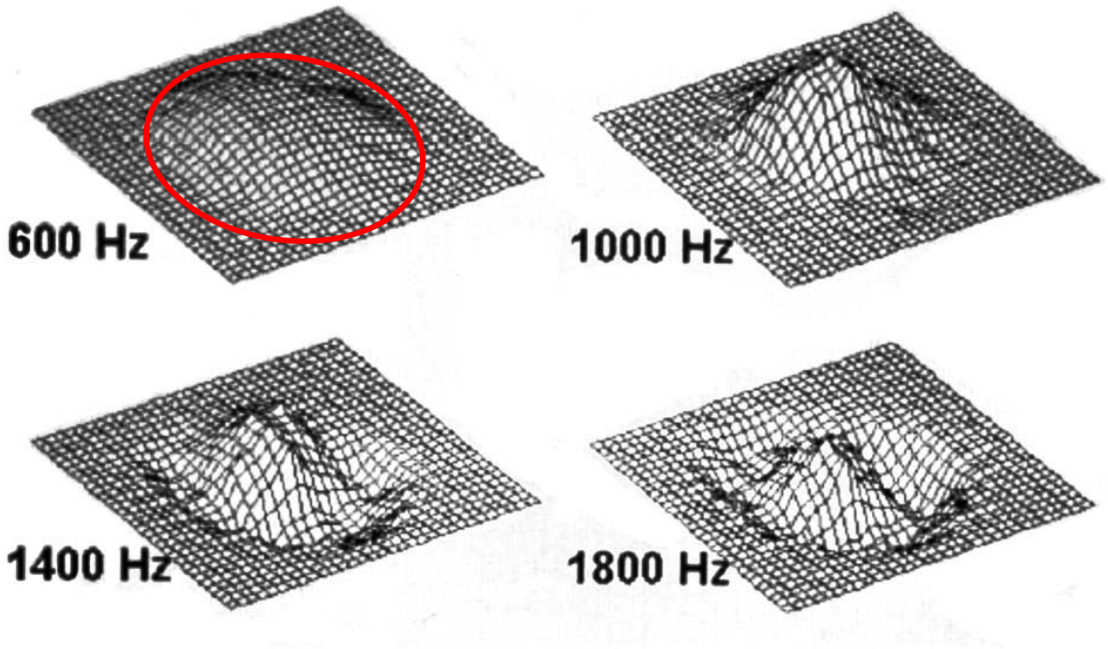

Fig. 2.11 The above plots show the excitation patterns of an anuran (frog) tympanum for different frequencies, as indicated. Unlike lizards, the extracolumella touches the circular eardrum of frogs in the middle, hence not breaking its rotational symmetry. As a result, the vibration patters are nearly rotationally invariant. The fixed, circular, border has been indicated once by a solid (red) circle for 600 Hz. The dominant mode for 600 Hz is the fundamental one (0,1), higher modes mix in as the frequency increases, corresponding nicely to the Bessel function of the mode (0, 2); cf. Fig. 2.10. Plot courtesy of M.B. Jørgensen [67].

Sectorial membrane

In Section 2.1.1, we noted that in vertebrates there is a transducer for the membrane's vibrations in the form of a columella which attaches asymmetrically to the eardrum via the extracolumella; cf. Figs. 2.2b and 2.3a. Consequently, the membrane cannot be modeled as a full circular disk, but rather as a sector of a given angle. For such a membrane, the

equation of motion of the vibrating part remains unchanged. However, as the extracolumella effectively breaks the circular symmetry of the membrane surface, we now have a new set of temporally fixed boundary conditions at the line of contact of the tympanic membrane with the extracolumella (cf. Fig. 2.3a), in addition to the Dirichlet boundary condition at $r = a_{\text{tymp}}$; see Eq. (2.17). In order to calculate the eigenmodes, we proceed from the definition in (2.26) and determine the values that m is constrained to take based on the boundary conditions at *both* edges of the extracolumella.

We also note that, because of the relatively large mass of the extracolumella as well as its attached elements in comparison to the membrane, we can effectively model it as an infinitely heavy sectorial plate of radius a_{tymp} and angle 2β. In other words, the vibrating part of the membrane lies in the region $\beta < \phi < 2\pi - \beta$; see Fig. 2.3b. As a result, we require that the membrane displacement goes to zero at $\phi = \beta$ and $\phi = 2\pi - \beta$ so that the ϕ part of (2.26) takes the form $\sin\kappa(\phi - \beta)$. We therefore obtain the following set of orthogonal eigenmodes,

$$u_{mn}(r,\phi;t) = \left[M_{mn}e^{i\omega_{mn}t} + N_{mn}e^{-i\omega_{mn}t}\right] u_{mn}(r,\phi) \tag{2.29}$$

$$u_{mn}(r,\phi) = \sin\kappa(\phi - \beta) J_\kappa(\mu_{mn} r)\ , \tag{2.30}$$

where, the azimuthal component is indexed by κ which is defined as a discrete function

$$\kappa[m] = 0.5\ (m+1)\pi/(\pi - \beta) \quad m = 0, 1, 2, \ldots . \tag{2.31}$$

We see that the radial – r – part of the modes $u_{mn}(r,\phi)$ is given by the (fractional) order-κ Bessel function of the first kind with $\mu_{mn} \times a_{\text{tymp}}$ being its n^{th} zero. The mode corresponding $m = -1$ represents the trivial "zero" solution to the membrane equation. As in the case of the circular membrane modes (2.28), the sectorial eigenmodes u_{mn} also form an orthogonal set, i.e.,

$$\int_S dS\ u_{m_1 n_1} u_{m_2 n_2} = 0, \text{ if } m_1 \neq m_2 \text{ or } n_1 \neq n_2\ . \tag{2.32}$$

The fundamental frequency f_0 of the sectorial modes follows in a similar way to that of the circular membrane modes (2.27)

$$f_0 = c_{\text{M}}\mu_{01}/2\pi\ . \tag{2.33}$$

It should be apparent from the form of the above modes that, unlike in the case of the circular membrane eigenmodes, these modes are no longer radially symmetric. The sectorial shape of the membrane has important physical consequences and captures the complex vibration patterns of a realistic membrane. For a circular membrane driven by a uniform pressure, the asymmetric modes (with $m \neq 0$) are suppressed. This holds in the case of

frogs [68], where the extracolumella is attached to the middle of the tympanic membrane and its rotational symmetry is not broken; see also Fig. 2.11. On the other hand, for the sectorial membrane as in the case of lizards, the radial symmetry is broken explicitly by the extracolumella. The first few of these modes are shown in Fig. 2.12. The vibrations of a

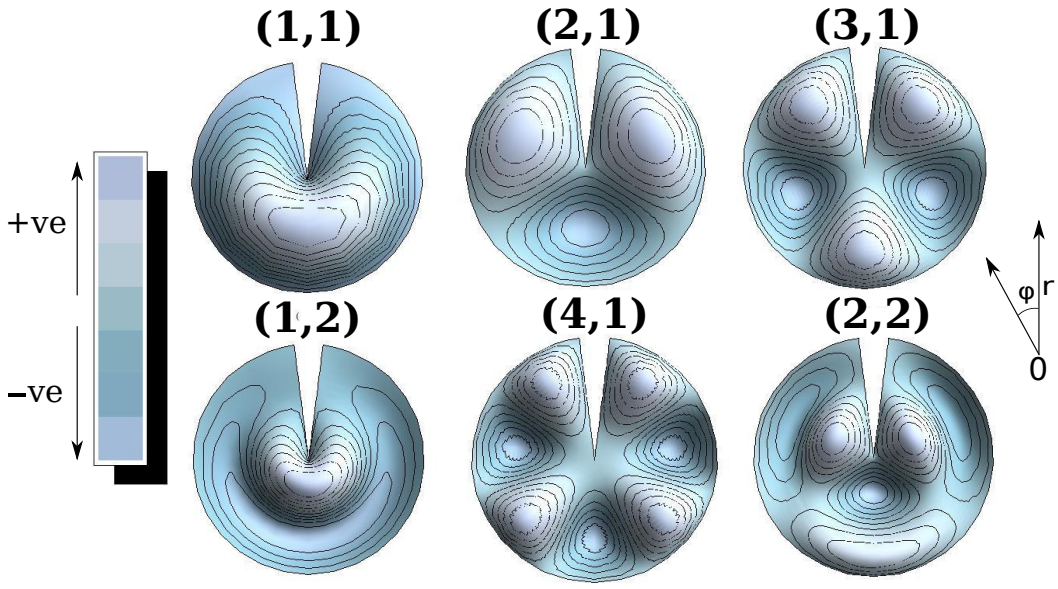

Fig. 2.12 Eigenmodes of a sectorial membrane where the omitted region corresponds to the extracolumella with $\beta = \pi/25$; cf. Fig. 2.3b. The eigennumbers are shown above each figure. As in Fig. 2.10, displacements into the surface of the paper are darkly shaded while those out are lightly shaded. The eigenfrequency increases from left to right and top to bottom.

sectorial membrane are discussed in more detail in [61, p. 87].

Undamped and damped vibrations

For a damped membrane with $\alpha > 0$ in Eq. (2.14), the spatial part of the above eigenmodes remains unchanged. The form of the time-dependent part $T(t)$ as given by (2.18) is obtained from the solution to the following ordinary differential equation,

$$\frac{d^2 h_{mn}(t)}{dt^2} - 2\alpha \frac{dh_{mn}(t)}{dt} - \omega_{mn}^2 h_{mn}(t) = 0 \,. \tag{2.34}$$

The above expression differs from the equation for the time-varying part of the pressure (2.20) only in a first-order damping term. We therefore expect (2.34) to have exponentially decaying solutions in time and look for them.

As an ansatz, we assume h_{mn} to take the form $\exp(i\widetilde{\omega}_{mn})$ where $\widetilde{\omega}_{mn}$ can, in general, be a complex number. This leads to a quadratic equation in $\widetilde{\omega}_{mn}$ with solutions

$$\widetilde{\omega}_{mn}^2 - 2i\alpha\widetilde{\omega}_{mn} - \omega_{mn}^2 = 0 \tag{2.35}$$

$$\widetilde{\omega}_{mn} = i\alpha \pm \omega_{mn}^* \tag{2.36}$$

$$\text{where} \quad \omega_{mn}^* = \sqrt{\alpha^2 + \omega_{mn}^2}\,. \tag{2.37}$$

We see that the new, now damped, eigenmodes possess both an exponential damping term as well as a shift in the original eigenfrequencies. We require the membrane displacement to remain finite as $t \to \infty$. As $exp(-i\widetilde{\omega}_{mn})$ terms lead to vibration amplitudes that increase exponentially as $exp(\alpha t)$ we can safely drop them. This then leads to

$$\widetilde{u}_{mn}(r,\phi;t) = u_{mn}(r,\phi)\left[M_{mn}e^{i\omega_{mn}^* t} + N_{mn}e^{-i\omega_{mn}^* t}\right]e^{-\alpha t}\,. \tag{2.38}$$

The effect of membrane damping is therefore not only an exponentially decreasing damping term, but also a shift in the eigenfrequencies of all the membrane eigenmodes. The general solution is given by a linear combination of u_{mn} with the coefficients that are determined by initial conditions. These could be, for instance, the membrane displacement and velocity at $t = 0$.

Forced vibrations

For a periodically driven membrane, there are two components of the full solution corresponding to forced vibrations. The first of these is the quasi-stationary-state solution which oscillates with the same frequency as the input and does not depend on the initial conditions – u_{ss}. The second of these is the transient solution that depends on the initial conditions but not directly on the driving pressure – u_t.

The quasi-steady-state solution is expressed as a linear combination of the spatial part of the membrane eigenmodes defined in (2.30) with a time-component equal to that of the driving pressure, $\exp(i\omega t)$,

$$u_{ss}(r,\phi;t) = \sum_{m=0}^{\infty}\sum_{n=1}^{\infty} C_{mn}u_{mn}(r,\phi)\exp(i\omega t). \tag{2.39}$$

By substituting (2.39) into (2.14) with $\Psi = p\exp(i\omega t)$ we obtain

$$\sum_{m=0}^{\infty}\sum_{n=1}^{\infty}\rho_{\mathrm{M}}d_{\mathrm{M}}\Omega_{mn}C_{mn}u_{mn}(r,\phi)e^{i\omega t} = p\exp(i\omega t) \tag{2.40}$$

$$\Omega_{mn} = \left[(\omega^2 - \omega_{mn}^2) - 2i\alpha\omega\right]. \tag{2.41}$$

Using the orthogonality of the eigenmodes, we can calculate the coefficients C_{mn},

$$C_{mn} = \frac{p\int dS\, u_{mn}}{\rho_{\mathrm{M}}d_{\mathrm{M}}\Omega_{mn}\int dS(u_{mn})^2} \tag{2.42}$$

with the integral this time being taken over the circular disk of radius a_{tymp} (or equivalently, over the vibrating surface of the tympanum).

The transient solution is found by solving the membrane equation for $\Psi(r,\phi;t) = 0$ which, effectively, is the solution of the free damped membrane, i.e., a linear combination of the eigenmodes given in (2.38),

$$u_t(r,\phi;t) = \sum_{m=0}^{\infty}\sum_{n=1}^{\infty}\widetilde{u}_{mn}(r,\phi;t)\,. \tag{2.43}$$

The complete solution is given by $u = u_t + u_{ss}$ and the coefficients M_{mn} and N_{mn} are determined by the initial conditions (at $t = 0$).

Quasi-Steady-State Approximation

The damping coefficient α is usually given in terms of the membrane fundamental frequency (f_0) and a quality factor Q as $\alpha = 2\pi f_0/2Q$. The eardrums in the animals we are concerned with are generally underdamped, i.e., $Q > 0.5$, which results in damping coefficients that are around $\sim 2700\ \mathrm{s}^{-1}$ for the Gecko lizards and around $\sim 400\ \mathrm{s}^{-1}$ for the larger *Varanus*; see Tab. 3.1 in Chap. 3. As a result, the exponential decay of the transient vibration amplitude allows us to safely assume that within a few time-periods of the input frequency, and even far less for the Geckos, the transient vibrations of the forced membrane are gone. In our subsequent derivations, we can safely neglect the transient parts of the membrane vibration. The transient behavior can be dealt with in a more precise manner, by solving the pressure differential equation with the vibrating membranes serving as time-dependent boundary conditions. A rigorous mathematical treatment of coupled membrane vibrations is beyond the scope of the present work, but has been treated in full elsewhere [69].

2.2.2 Cavity Pressure

Given a cavity of arbitrary shape coupling the two eardrums, understanding the physics of ICE formally reduces to finding an expression for the internal pressure at one eardrum in terms of the internal pressure at the opposite eardrum. To do so, we first need to find an expression for the pressure within the interaural cavity. At our frequencies of interest (< 4 kHz) and given the small interaural sound propagation distances (< 10 cm), viscous acoustic damping in air can be neglected so that we follow common acoustic models (e.g. [70, p. 313], [71, p. 247]) and describe the air inside the cavity by linear acoustics in a cylindrical coordinate system. In this approach, air moves due to a local pressure $p(x,r,\phi;t)$ obeying the 3-dimensional wave equation

$$\frac{1}{c^2}\frac{\partial^2 p(x,r,\phi;t)}{\partial t^2} = \Delta_{(3)} p(x,r,\phi;t) \ , \tag{2.44}$$

$$\text{where } \ \Delta_{(3)} = \frac{1}{r}\frac{\partial}{\partial r} + \frac{\partial^2}{\partial r^2} + \frac{1}{r^2}\frac{\partial^2}{\partial \phi^2} + \frac{\partial^2}{\partial x^2} \tag{2.45}$$

is the 3-dimensional Laplacian in cylindrical coordinates with x denoting the dimension along the cylinder axis, while c is speed of sound. The choice of cylindrical coordinates reflects the circular cross section of the canal(s) comprising the interaural cavity in our treatment of ICE; cf. Sec. 2.1.2. The acoustic wave equation results from a linearization of the Euler equations in terms of small pressure and velocity fluctuations [72, pp. 538–541].

The complete solution must take into account the boundary conditions at and within the cavity walls and the ones at the air-membrane interface. We also note that Eq. (2.44) presumes through its boundary conditions that the animal's mouth is closed, which is typical for a waiting predator or prey.

General solution

In order to solve (2.44) for a particular frequency f with angular frequency $\omega = 2\pi f$, we use the following separation ansatz, similar to the one used in (2.18)

$$p(x,r,\phi,t) = f(x)g(r)h(\phi)\exp(i\omega t) \tag{2.46}$$

which after substitution into (2.44) leads to,

$$\begin{aligned} k^2 f(x)g(r)h(\phi) + f(x)h(\phi)\left[\frac{\partial^2 g(r)}{\partial r^2} + \frac{1}{r}\frac{\partial g(r)}{\partial r}\right] \\ + f(x)g(r)\frac{1}{r^2}\frac{\partial^2 h(\phi)}{\partial \phi^2} + g(r)h(\phi)\frac{\partial^2 f(x)}{\partial x^2} = 0\,. \end{aligned} \tag{2.47}$$

As always, $k := \omega/c$ is the wavelength of the sound wave at the given angular frequency ($\omega = 2\pi f$). Before proceeding we should note that, in general, the time component of the pressure also has a temporally *backward-moving* component, i.e., $\exp(-i\omega t)$. By making the ansatz in (2.46), we have implicitly used the fact that the form of the input as given in (2.3) constrains the pressure to only having a *forward-moving* component, i.e., $\exp(i\omega t)$.

The substitution $\exp(i\omega t)$ in (2.46) actually means that we are looking for the (countable) eigenvalues of $-\Delta$ inside the cavity, in terms of ω^2 with appropriate boundary conditions; see below. Although this might look mathematically contradictory at first, we will soon see that it is not. Making the ansatz of separation of variables and dividing (2.47) by $f(x)g(r)h(\phi)$ gives the following set of separated ordinary differential equations (ODEs),

$$\frac{d^2 f(x)}{dx^2} + \zeta^2 f(x) = 0 \tag{2.48}$$

$$\frac{d^2 h(\phi)}{d\phi^2} + q^2 h(\phi) = 0 \tag{2.49}$$

$$\frac{\partial^2 g(r)}{\partial r^2} + \frac{1}{r}\frac{\partial g(r)}{\partial r} + \left[\underbrace{(k^2 - \zeta^2)}_{=:\nu_q^2} - \frac{q^2}{r^2} \right] g(r) = 0 \tag{2.50}$$

with separation constants q and ζ. The above equations are nearly identical to those in (2.19) – (2.21). As before, the first two equations can be readily solved to give,

$$f(x) = \exp(\pm i\zeta x) \tag{2.51}$$

$$h(\phi) = \exp(\pm iq\phi)\,. \tag{2.52}$$

The third equation (2.50), i.e. the Bessel differential equation can be solved to give (cf. Eq. (2.21))

$$g(r) = C_q J_q(\nu_q r) + D_q Y_q(\nu_q r). \tag{2.53}$$

J_q and Y_q are the order-q Bessel functions of the first and second kind, respectively. We can set the coefficients $D_q = 0$ as the Bessel function of the second kind diverges at $r = 0$ [65, p. 313] and we are seeking solutions that remain finite on within the interaural cavity.

With the above solutions for $f(x)$, $g(r)$, and $h(\phi)$, we can write down a specific solution to (2.44),

$$p_q(x, r, \phi) = \left(A_q \exp(i\zeta_q x) \;+\; B_q \exp(-i\zeta_q x)\right) p_q^{\circ}(r, \phi) \tag{2.54}$$

$$p_q^{\circ}(r, \phi) = J_q(\nu_q r/a_{\text{cyl}}) \left(C_q \cos q\phi + D_q \sin q\phi\right)\,. \tag{2.55}$$

The coefficients A, B, q, ζ and ν will be subsequently determined by the boundary conditions. Through p_q° we denote the components of the eigenfunction in the radial and azimuthal directions.

Pressure boundary conditions

In order to determine the coefficients in (2.55), we have to satisfy three sets of boundary conditions,

- Continuity and smoothness in ϕ or equivalently $h(0) = h(2\pi)$ and $\left.\frac{dh}{d\phi}\right|_{\phi=0} = \left.\frac{dh}{d\phi}\right|_{\phi=2\pi}$
- Vanishing of the normal derivative at the cavity walls – $\left.\frac{dg}{dr}\right|_{r=a_{\text{cyl}}} = 0$.
- Equating the membrane velocity to the air velocity at the inner air-membrane interface.

The first set of requirements, as in the case of a circular membrane, is trivial and constrains q to take integer values. The second and third are a result of the so called "no-penetration" boundary-condition of fluid-mechanics. They arise from the fact that the cavity wall and the eardrum are impermeable boundaries. This translates into the requirement that the normal velocity function should vanish [73, p. 111]. The velocity function ($\mathbf{v}$) is related to the pressure by

$$-\rho\frac{\partial \mathbf{v}}{\partial t} = \nabla p\,, \tag{2.56}$$

where ρ is the density of air. This result emerges directly from the linearization of the Euler equation

$$\frac{\partial \tilde{\mathbf{v}}}{\partial t} + \tilde{\mathbf{v}}.\nabla\tilde{\mathbf{v}} = -\frac{1}{\rho}\nabla P + \mathbf{f}\,. \tag{2.57}$$

Assuming that the acoustic pressure can be described as a fluctuation p around a stationary background (atmospheric) pressure P_0 and that the fluid velocity $\mathbf{v}$, as small fluctuations in a quiescent fluid $\mathbf{v}_0 = 0$, we obtain

$$\begin{aligned}\tilde{\mathbf{v}} &= \mathbf{v}_0 + \mathbf{v} = \mathbf{v}\\ P &= P_0 + p\,.\end{aligned}$$

Neglecting the body forces due to gravity ($\mathbf{f}$) gives us

$$\Rightarrow \frac{\partial \mathbf{v}}{\partial t} + \mathbf{v}.\nabla\mathbf{v} = -\frac{1}{\rho}\nabla p\,. \tag{2.58}$$

We can neglect the convection term $(\mathbf{v}\cdot\nabla\mathbf{v})$ as it is of second order in the extremely small $\mathbf{v}$, and thus arrive at (2.56).

At the cylindrical cavity wall, the normal velocity is in the radial direction, and vanishes. Substituting the expression (2.60) for the pressure into (2.56) leads to a Neumann boundary condition for the pressure,

$$\begin{aligned} \mathrm{v}_r = -\frac{1}{i\rho\omega}\frac{\partial p(x,r,\phi;t)}{\partial r}\bigg|_{r=a_{\mathrm{cyl}}} &= 0 \\ \Rightarrow \frac{\partial J_q(\nu_q r)}{\partial r}\bigg|_{r=a_{\mathrm{cyl}}} &= 0 \end{aligned} \tag{2.59}$$

This constrains ν_q to a discrete set of values which correspond to the local minima and maxima of J_q. This is in contrast to the Dirichlet boundary condition for the corresponding Bessel equation describing the membrane vibrations (2.17). We therefore introduce an additional index s which takes integer values such that $\nu_{qs} \times a_{\mathrm{cyl}}$ corresponds to the s^{th} extremum of the order-q Bessel function of the first kind. This results in (2.54) becoming a set of modes indexed by (q,s) :

$$p_{qs}(x,r,\phi) = \left(A_{qs}\exp(i\zeta_{qs}x) + B_{qs}\exp(-i\zeta_{qs}x)\right) p^{\circ}_{qs} \tag{2.60}$$

$$p^{\circ}_{qs}(r,\phi) = J_{qs}(\nu_{qs}r/a_{\mathrm{cyl}})\left(C_{qs}\cos q\phi + D_{qs}\sin q\phi\right) . \tag{2.61}$$

Effectively, the modes are 3-dimensional waves propagating with wave numbers ζ_{qs} in the x-direction and ν_{qs} in the radial direction. The wavenumber ζ_{qs} of the (q,s) mode is related to the wavenumber k of sound in air as (cf. Eq. (2.50))

$$\zeta_{qs}^2 = k^2 - \nu_{qs}^2 . \tag{2.62}$$

As was the case with the membrane modes (2.32), the pressure modes defined through Eqs. (2.54) and (2.59) form a discrete orthogonal basis inside the cylinder. This means that

$$\int_{\Omega} dV\, p_{q_1 s_1} p_{q_2 s_2} = 0, \text{ if } q_1 \neq q_2 \text{ or } s_1 \neq s_2 \tag{2.63}$$

where the integral is over the volume of the cylinder. This is a consequence of the fact that for different q's the trigonometric parts of the modes are orthogonal, whereas for the same q the Bessel parts are orthogonal for different s's. Expressed mathematically, this requirement gives us

$$\int dS\, f_{q_1 s_1} f_{q_2 s_2} = 0, \; q_1 \neq q_2 \text{ or } s_1 \neq s_2 \tag{2.64}$$

where $dS = rdrd\phi$ with the integral being taken over the disk of radius a_{cyl}. We can therefore write the general solution to Eq. (2.44) as a linear combination of the orthogonal modes given

in (2.60) :

$$p(x,r,\phi;t) = \sum_{q=0}^{\infty}\sum_{s=0}^{\infty} p_{qs}(x,r,\phi)\exp(i\omega t) \tag{2.65}$$

where the individual modes p_{qs} are defined in Eq. (2.54).

The first of these modes (corresponding to $q = 0, s = 0$) is of particular importance. Since the first maximum of J_0 occurs at $r = 0$, we have $\nu_{00} = 0$ and, consequently, $\zeta_{00} = k$. Thus, the first propagating mode in the air-filled cavity is a plane wave that is constant in r and ϕ and only propagates along the axis of the cylinder. Unlike the higher modes, which depend on the radius r and polar angle ϕ, the plane wave mode is the same in all the sections of the interaural cavity. The pressure, particle velocity and volume flow rate for the plane wave mode are given by

$$p(x;t) = (Ae^{ikx} + Be^{-ikx})\exp(i\omega t)\ ,\ , \tag{2.66}$$

$$v(x;t) = -\frac{1}{\rho c}(Ae^{ikx} - Be^{-ikx})\exp(i\omega t) \text{ and} \tag{2.67}$$

$$U(x;t) = -S_{\text{cyl}}\frac{1}{\rho c}(Ae^{ikx} - Be^{-ikx})\exp(i\omega t)\ , \tag{2.68}$$

where, as usual, S_{cyl} is the area of cross section of the cylindrical canal.

The third and final set of boundary conditions at the internal air-membrane interface at either end of the cylinder will be used to determine the remaining coefficients, A_{qs} and B_{qs}. To do so, we first need to use the analytical expression for the membrane vibrations derived in Sec. 2.2.1 as apply them as boundary conditions for the cavity pressure.

2.2.3 Vibration of coupled membranes

We can now move on to the analysis of the vibration of *internally* coupled membranes and derive the expressions defined in (2.5). The analysis in this section is similar to the treatment of the vibration of a circular membrane backed by a cylindrical air cavity closed at the opposite end as given by [74]. The quantities of interest there were the eigenmodes of the circular membrane, but we are primarily interested in the steady state vibration of sectorial membranes that are internally coupled to each other as well as to external stimuli at both ends.

It is convenient to first write down the main equations of the system based on our previously derived expressions. A general expression for the quasi-steady-state vibrations of

the eardrums is given by a linear combination of the sectorial eigenmodes, (2.30),

$$u_{0/L}(r,\phi;t) = \sum_{m=0}^{\infty}\sum_{n=1}^{\infty} C_{mn}^{0/L} u_{mn}(r,\phi)\exp(i\omega t) \tag{2.69}$$

where 0 and L denote the $x=0$ and $x=L$ membranes respectively. Given the cavity pressure distribution $p(x,r,\phi;t)$ as given by Eq. (2.65), the driving pressure on either side of the membrane equals $\Psi^{0/L}(r,\phi;t) = p_{0/L}e^{i\omega t} - p(0/L,r,\phi;t)$. Substituting these expressions into (2.14) gives us the following set of equations,

$$\sum_{m=0}^{\infty}\sum_{n=1}^{\infty} \rho_{\mathrm{M}} d_{\mathrm{M}} \Omega_{mn} C_{mn}^{0/L} u_{mn}(r,\phi)\exp(i\omega t) = \Psi^{0/L}(r,\phi;t)\ . \tag{2.70}$$

The above equation is only valid on the vibrating part of the membrane surface, i.e., for $S_{\mathrm{memb}} = \{r < a_{\mathrm{tymp}} \text{ and } \beta < \phi < 2\pi - \beta\}$.

As discussed in Subsection 2.2.2, the interaural cavity pressure satisfies the no-penetration condition at solid boundaries. This means that at both ends of the cylinder, we equate the velocity profile of air to the velocity profile of the circular surface *including* the membrane; cf. Fig. 2.13a. As the membrane diameter is smaller than the cylinder diameter, we will have to set the air-particle velocity to zero for $r > a_{\mathrm{tymp}}$. Additionally, since the membrane displacement is only in the x-direction, we need only calculate the x-component of the velocity. Using the relation in Eq. (2.56) we get,

$$\mathrm{v}_{qs}(x,r,\phi) = \zeta_{qs}\left(A_{qs}e^{i\zeta_{qs}x} - B_{qs}e^{-i\zeta_{qs}x}\right) p_{qs}(r,\phi) \tag{2.71}$$

$$\mathrm{v}_x(x,r,\phi;t) = \frac{-1}{\rho\omega}\sum_{q=0}^{\infty}\sum_{s=0}^{\infty} \mathrm{v}_{qs}(x,r,\phi)\exp(i\omega t) \tag{2.72}$$

and the exact boundary conditions are given by

$$\mathrm{v}_x(0,r,\phi;t) = \begin{cases} -iu_0,\ (r,\phi)\in S_{\mathrm{memb}} \\ 0,\ \text{otherwise} \end{cases} \tag{2.73}$$

$$\mathrm{v}_x(L,r,\phi;t) = \begin{cases} iu_0,\ (r,\phi)\in S_{\mathrm{memb}} \\ 0,\ \text{otherwise} \end{cases}\ , \tag{2.74}$$

where, according to our convention, membrane displacements outward from the cylinder are taken as positive (in x) and those inward are taken as negative.

Approximate boundary condition

As we have just seen, the exact boundary conditions would require us to set the air velocity to be exactly equal to the membrane velocity. The membrane and cavity modes, while forming orthogonal bases by themselves (2.63), are, however, not orthogonal to each other. In other words, each membrane mode couples with every cavity mode and vice versa. Even in the absence of the extracolumella with full circular membranes on either end of the cylinder, the cavity and membrane modes have different boundary conditions. For the internal pressure, these are Neumann boundary condition, whereas for the membrane, we have Dirichlet boundary conditions (2.17).

Our way around this problem is to approximate the eardrum motion, and thus boundary conditions (2.73) and (2.74). We do this by effectively replacing each sectorial membrane by a circular piston [12] operating on the internal pressure p and moving with the membrane's average velocity $\dot{u}_{0/L}^{\mathrm{ave}}$ so that

$$u_{0/L}^{\mathrm{ave}} = \frac{1}{\pi a_{\mathrm{cyl}}^2} \int \mathrm{d}S\, u_{0/L}\,, \qquad \dot{u}_{0/L}^{ave} = i\omega u_{0/L}^{ave} \tag{2.75}$$

$$\mathrm{v}_x(0,r,\phi;t) = -\dot{u}_0^{\mathrm{ave}}\,, \qquad \mathrm{v}_x(L,r,\phi;t) = \dot{u}_L^{\mathrm{ave}} \tag{2.76}$$

where we have in fact taken the average velocity of the entire cylindrical surface including the eardrum; cf. Fig. 2.13b. Since the bare cylinder surface is solid and nonmoving, the present approximation of averaging over the lateral faces of the cylinder only differs from the average over the membrane surface by a factor. The exact mathematical justification for the current procedure is beyond the scope of the present work and has been presented elsewhere [69]. The *piston approximation* used in our derivation refers to the averaging of the tympanic motion including the non-moving extracolumella non-moving part of the cylinder face and thus, effectively, approximating the Neumann boundary condition for the internal cavity pressure.

Physically, we can assume that air is locally *nearly* incompressible so that in the long-wavelength domain we focus here in a local boundary variation on one or both faces (corresponding to the membrane displacement) has the same effect as the average variation on the left and right face from where it propagates through the cylinder representing the pharyngeal cavity. As said in the caption of Fig. 2.13b, "In effect, it computes the net volume change," as confirmed mathematically [69]

$$\Delta V_{\mathrm{cav}} = \pi a_{\mathrm{cyl}}^2 (u_L^{\mathrm{ave}} + u_0^{\mathrm{ave}})\,.$$

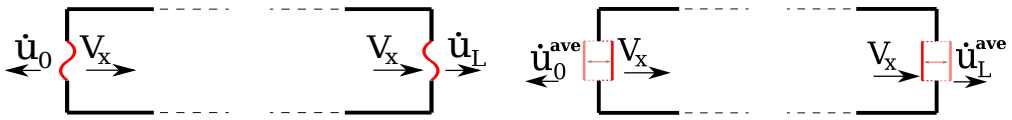

(a) Exact Membranes (b) Piston Approximation

Fig. 2.13 Above: Exact membrane boundary conditions. The velocity of air (v_x) equals that of the membrane ($u_{0/L}$). Below: Piston approximation. The membrane is approximated by a circular piston moving with the membrane's average velocity and with boundary conditions (2.76) applied to (2.44) and (2.56). The piston approximation refers to (2.44) and the boundary condition for the pressure p in the 3-dimensional cavity, not to the motion (2.14) of the eardrum itself. In effect, it computes the net volume change.

Given the modified boundary conditions (2.76), it is straightforward to calculate the coefficients A_{qs} and B_{qs} in terms of $u_{0/L}^{\text{ave}}$. To do this we use the orthogonality of the cavity modes (2.63) and the modal expansion (2.71), (2.72) of the air velocity. By multiplying both sides of the boundary relations in (2.76) by $p_{qs}(r,\phi)$ and integrating over the circular surfaces at the ends of the cylinder, this results in a system of two linear equations for each pair of A_{qs} and B_{qs},

$$A_{qs} - B_{qs} = -L_{qs}\rho\omega^2 u_0^{\text{ave}} \tag{2.77}$$

$$A_{qs}e^{i\zeta_{qs}L} - B_{qs}e^{-i\zeta_{qs}L} = L_{qs}\rho\omega^2 S_L^{\text{ave}} \tag{2.78}$$

$$\text{where} \quad L_{qs} = \frac{\int dS p_{qs}(r,\phi)}{i\zeta_{qs}\int dS p_{qs}^2(r,\phi)}\,. \tag{2.79}$$

We must now make use of the fact that the cavity pressure modes (2.60) integrate to 0 (i.e., $\int dS p_{qs} = 0$) unless $q = 0$ and $s = 0$. For $q = 0$ this is a consequence of the Bessel functions integrating to zero while for $q \geq 1$ this is due to the more obvious fact that the integral of the trigonometric part from 0 to 2π is zero. That is,

$$\int_0^{a_{\text{acyl}}} r J_q(\nu_{qs} r)\,dr = 0\,, \tag{2.80}$$

$$\int_0^{2\pi} \left(A_{qs}\cos q\phi + B_{qs}\sin q\phi\right) d\phi = 0\,. \tag{2.81}$$

As a result we have $A_{qs} = B_{qs} = 0$ for all modes except the $(0,0)$ mode. In other words, as a result of the piston approximation, we only encounter plane wave modes inside the cavity. We will subsequently omit the subscripts "00" for these coefficients. From the above linear

equations, they are given in terms of the total membrane displacement as

$$A = -\frac{\rho\omega^2}{2k\sin kL}\left(u_0^{\text{ave}}e^{-ikL} + u_L^{\text{ave}}\right) , \tag{2.82}$$

$$B = -\frac{\rho\omega^2}{2k\sin kL}\left(u_0^{\text{ave}}e^{ikL} + u_L^{\text{ave}}\right) . \tag{2.83}$$

We have also directly substituted $\zeta_{00} = k$ and simplified the expression for L_{00} in the above expressions. These coefficients can now be substituted in place of the pressure into the right-hand side of (2.70) so as to give

$$\sum_{m=0}^{\infty}\sum_{n=1}^{\infty}\rho_{\text{M}}d_{\text{M}}\Omega_{mn}C_{mn}^{0/L}u_{mn}(r,\phi) = p_{0/L} + \frac{\rho\omega^2}{k}\left(u_{0/L}^{\text{ave}}\cot kL + u_{0/L}^{\text{ave}}\csc kL\right) . \tag{2.84}$$

The time component $\exp(i\omega t)$ cancels on both sides of the equation. We note that the right-hand side of the above equation system is independent of the spatial (r,ϕ) coordinates.

The above coupled system of equations can be considerably simplified by taking their sum and difference to obtain a new set of decoupled equations. After some algebra, we have the following set of "sum and difference" equations,

$$\sum_{m=0}^{\infty}\sum_{n=1}^{\infty}\rho_{\text{M}}d_{\text{M}}\Omega_{mn}C_{mn}^{+}u_{mn}(r,\phi) = p_{+} + \frac{\rho\omega^2}{k}u_{+}^{\text{ave}}\cot\frac{kL}{2} \tag{2.85}$$

$$\sum_{m=0}^{\infty}\sum_{n=1}^{\infty}\rho_{\text{M}}d_{\text{M}}\Omega_{mn}C_{mn}^{-}u_{mn}(r,\phi) = p_{-} - \frac{\rho\omega^2}{k}u_{-}^{\text{ave}}\tan\frac{kL}{2} \tag{2.86}$$

where the "plus" and "minus" have been defined as the sum and difference of the respective "0/L" components. That is,

$$C_{mn}^{+} = C_{mn}^{L} + C_{mn}^{0}, \quad p_{+} = p_L^{\text{ex}} + p_0^{\text{ex}} , \tag{2.87}$$

$$C_{mn}^{-} = C_{mn}^{L} - C_{mn}^{0}, \quad p_{-} = p_L^{\text{ex}} - p_0^{\text{ex}} , \tag{2.88}$$

$$u_{+}^{\text{ave}} = u_L^{\text{ave}} + u_0^{\text{ave}} = \sum_{m=0}^{\infty}\sum_{n=1}^{\infty}C_{mn}^{+}u_{mn}(r,\phi) , \tag{2.89}$$

$$u_{-}^{\text{ave}} = u_L^{\text{ave}} - u_0^{\text{ave}} = \sum_{m=0}^{\infty}\sum_{n=1}^{\infty}C_{mn}^{-}u_{mn}(r,\phi) . \tag{2.90}$$

Thus it is apparent that the above system of equations is decoupled because the $u_{\pm}^{\text{ave}}$ terms can be expressed as a linear expansion of the respective $C_{mn}^{\pm}$ coefficients alone. Analogously to

the calculation of the coefficients for the quasi-steady-state vibration in (2.40) and (2.42) we can now use the orthogonality of the membrane modes u_{mn} to determine the coefficients of the sum and difference vibrations in terms of the pressure and average membrane displacement,

$$C^{+}_{mn}\int dS\, u_{mn} = \left[p_{+} + \frac{\rho\omega^2}{k}u^{\text{ave}}_{+}\cot\frac{kL}{2}\right]\frac{K_{mn}}{\Omega_{mn}} \tag{2.91}$$

$$C^{-}_{mn}\int dS\, u_{mn} = \left[p_{-} - \frac{\rho\omega^2}{k}u^{\text{ave}}_{-}\tan\frac{kL}{2}\right]\frac{K_{mn}}{\Omega_{mn}} \tag{2.92}$$

$$\text{where } K_{mn} = \frac{(\int dS\, u_{mn})^2}{\rho_{\text{M}} d_{\text{M}} \int dS\, u^2_{mn}}\,. \tag{2.93}$$

The integrals are over the vibrating part of the membrane surface $\mathscr{S}_{\text{mem}}$. The substitution K_{mn} will simplify our calculations in the appendix for the estimation of membrane parameters. The next step will be to sum both sides of (2.91) and (2.92) over all the membrane eigenmodes (m,n). The left-hand sides of the equations give us

$$\sum_{m=0}^{\infty}\sum_{n=1}^{\infty} C^{\pm}_{mn}\int dS\, u_{mn} = \pi a^2_{\text{cyl}} u^{\text{ave}}_{\pm}\,. \tag{2.94}$$

Hence we obtain exact expressions for the average membrane displacements,

$$\pi a^2_{\text{cyl}} u^{\text{ave}}_{\pm} = \frac{(p^{\text{ex}}_L \pm p^{\text{ex}}_0)\Lambda_{\text{tot}}}{1+\Lambda_{\text{tot}}\Gamma_{\pm}}\,, \tag{2.95}$$

$$\text{where}\quad \Lambda_{\text{tot}} = \sum_{m=0}^{\infty}\sum_{n=1}^{\infty} K_{mn}\,. \tag{2.96}$$

We have thus shown how the quantities Λ, Λ_{tot} and $\Gamma_{\pm}$ first defined in (2.6), (2.7), (2.8) and (2.9) emerge from our analysis. As stated earlier, the $\Gamma_{\pm}$ terms contain the effect of the coupling through the air cavity and Λ is the frequency response of the membrane to a pure tone of angular frequency ω. Qualitatively we can see that the information about the membrane (a_{tymp}, c_{M}, α) is contained within Λ whereas the properties of the interaural cavity (V_{cav}, a_{cyl}, L) are contained in $\Gamma_{\pm}$. That is, we have obtained the results first motivated in (2.6)-(2.9),

$$\Lambda = \sum_{m,n}^{\infty}\frac{u_{mn}(r,\phi)\int u_{mn}}{\rho_{\text{M}} d_{\text{M}}\Omega_{mn}\int u^2_{mn}}\,,\quad \Lambda_{\text{tot}} = \int_{\mathscr{S}_{\text{mem}}}\Lambda(r,\phi)dS\,, \tag{2.97}$$

$$\Gamma_{+} = -\frac{\rho c^2}{V_{\text{cav}}}kL\cot kL/2\,,\quad \Gamma_{-} = \frac{\rho c^2}{V_{\text{cav}}}kL\tan kL/2\,., \tag{2.98}$$

where, as before, $\Omega_{mn} = \omega^2 - \omega_{mn}^2 - 2i\alpha\omega$. Subsituting the above expressions along with (2.95) into (2.91) and (2.92) gives us the results mentioned at the start of this section,

$$u_{0/L}(r,\phi) = \frac{1}{2}\left(\frac{p_L^{\text{ex}} + p_0^{\text{ex}}}{1+\Lambda_{\text{tot}}\Gamma_+} \mp \frac{p_L^{\text{ex}} - p_0^{\text{ex}}}{1+\Lambda_{\text{tot}}\Gamma_-}\right)\Lambda(r,\phi)\ , \tag{2.99}$$

$$\pi a_{\text{cyl}}^2\, u_{0/L}^{\text{ave}}(r,\phi) = \frac{1}{2}\left(\frac{p_L^{\text{ex}} + p_0^{\text{ex}}}{1+\Lambda_{\text{tot}}\Gamma_+} \mp \frac{p_L^{\text{ex}} - p_0^{\text{ex}}}{1+\Lambda_{\text{tot}}\Gamma_-}\right)\Lambda_{\text{tot}}\ . \tag{2.100}$$

Convergence of Λ

Since the membrane frequency response $\Lambda(r,\phi)$, or equivalently Λ_{tot} in (2.97), is the summation of an infinite number of eigenmodes, in order to proceed with a numerical analysis of our model we first need to ensure that it converges to a finite value. Through the Cauchy-Schwarz inequality we obtain

$$|\Lambda_{\text{tot}}| \leq S_{\text{tymp}} \sum_{m,n} K_{mn}/|\rho_{\text{M}} d_{\text{M}} \Omega_{m,n}| < \infty \tag{2.101}$$

with S_{tymp} as the tympanic area and K_{mn} as the coefficient defined in (2.93). The former inequality is Cauchy-Schwarz, the latter is a general characteristic of the spectrum of the two-dimensional Laplacian associated with the eardrum; cf. (2.14), (2.41), and Table 2.1.

We therefore need to approximate Λ_{tot} by choosing an appropriate mode cutoff based on the hearing range of the animal and the high damping at their corresponding eigenfrequencies. In our analysis we chose a cutoff of $N = 30$ modes. The basic method involves arranging the modes in increasing order of eigenfrequency (or equivalently μ_{mn}). As a result, we can express the summation over a single index. In general, for the frequency ranges of the animals we are interested in, we need not calculate the summation beyond the first 30 eigenmodes. At these frequencies, the damping sufficiently suppresses higher modes with respect to the lower ones.

2.3 Simplified ICE models

Now that we have derived a geometrical ICE model based on the relevant anatomy of animals with coupled ears, wherein the flexible eardrums or tympanic membranes are coupled through a continuous air-filled cavity. With this knowledge at hand, we now present simplified equivalent descriptions of the model by representing the various components through equivalent lumped circuit or mechanical elements. Our goal is to obtain simplified qualitative and quantitative models that mimic the results obtained in the present chapter. In

particular, by presenting the simplified models with appropriate time-varying inputs, we will obtain quantities mathematically similar to those we have derived so far. In doing so we will effectively be exploiting the linearity of the ICE model.

2.3.1 Circuit equivalent

The results of ICE model can, in some cases, be reproduced by representing its components through equivalent circuit elements such as impedances, current sources and voltage sources that quantify the motion of the middle ear components. The method was used to describe the interaural coupling in lizards [25, 26, 75] and was based on methods presented by Fletcher [61, p. 164] and Zwislocki [76]. In such a model, the external sound inputs are represented by voltage sources, while the rest of the system is represented by impedances whose numerical values depend on the material and geometrical properties of the corresponding component. In general, the impedance values thus determined can have both resistive and reactive components. The circuit analog for the ICE model is illustrated in Fig. 2.14. For the eardrum, the higher modes are neglected and the equivalent resistance R_{M}, inductance L_{M} and capacitance C_{M} of the eardrum are given by

$$R_{\mathrm{M}} = \frac{\omega_0 L_{\mathrm{M}}}{Q}, \qquad L_{\mathrm{M}} = \frac{\rho_{\mathrm{M}} d_{\mathrm{M}}}{\pi a_{\mathrm{tymp}}^2} \quad \text{and} \quad C_{\mathrm{M}} = \frac{1}{\omega_0^2 L_{\mathrm{M}}}\,, \tag{2.102}$$

respectively. Recall that $\omega_0 = 2\pi f_0$ is the angular fundamental frequency of the eardrum and Q is its quality factor such that, the membrane damping is given by $\alpha = \omega_0/2Q$; cf. Sec. 2.2.1. For the interaural cavity pressure, its spatial variation between the eardrums is neglected such that it is represented only by a capacitance C_{V} which is defined in terms of the cavity volume V_{cav} as

$$C_{\mathrm{V}} = \frac{V_{\mathrm{cav}}}{\rho c^2}\,. \tag{2.103}$$

The equivalent resistance R_{V} and inductance L_{V} are set to zero for the air-filled cavity. Physically, the air inside the cavity is assumed to be *globally* adiabatic, as opposed to *locally* adiabatic, when deriving the acoustic wave equation. The adiabatic equation of state is thus used to determine the instantaneous pressure change inside the cavity from the instantaneous volume change due to the eardrum motion which, after linearization, results in a uniform pressure inside the cavity. The total impedance Z of both components is given by

$$Z_{\mathrm{M/V}} = R_{\mathrm{M/V}} + j\omega L_{\mathrm{M/V}} + 1/j\omega_0 C_{\mathrm{M/V}}\,. \tag{2.104}$$

The role of the "current" in the circuit is played by the integral vibration velocity of the eardrums, which is defined in terms of the average membrane displacement (2.100) as

$$U_{0/L} = i\omega S_{\text{tymp}} u_{0/L}^{\text{ave}} \,, \tag{2.105}$$

where S_{tymp} is the surface area of the eardrum. The variables $U_{0/L}$ are referred to as the "acoustic flow" and is equivalent to the volume flow rate of air at the eardrum interface, inside the cavity. Requiring a conservation of acoustic flow at the branches, we apply Ohm's law to

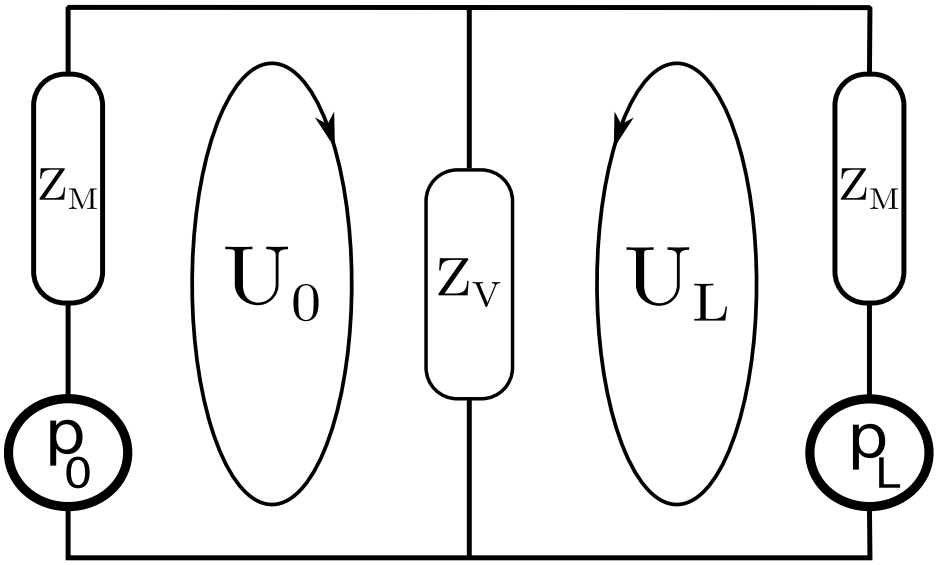

Fig. 2.14 The equivalent circuit model for ICE described using lumped elements. The eardrums are represented by an impedance Z_{M} which depends upon the fundamental frequency f_0 and the damping α. The equivalent impedance Z_{V} represents the interaural cavity and is only a function of its volume, the density of air and the speed of sound. The input pressures p_0^{ex}/L are represented by voltage sources which induce "currents" $U_{0/L}$" in each arm of the circuit.

the circuit in Fig. 2.14 resulting in,

$$p_L^{\text{ex}} = U_L Z_{\text{M}} + (U_L + U_0) Z_{\text{V}} \tag{2.106}$$

$$p_0^{\text{ex}} = U_0 Z_{\text{M}} + (U_L + U_0) Z_{\text{V}} \,. \tag{2.107}$$

Solving the above equations results in

$$2U_{L/0} = \frac{p_L^{\text{ex}} + p_0^{\text{ex}}}{Z_{\text{M}} + 2Z_{\text{V}}} \pm \frac{p_L^{\text{ex}} - p_0^{\text{ex}}}{Z_{\text{M}}} \,. \tag{2.108}$$

The above expressions are, in fact, qualitatively very similar to the expressions for the average membrane displacements $u_{0/L}^{\text{ave}}$ (2.100). The first term in the summation of the membrane frequency response Λ_{tot} (2.97) is equivalent to an "admittance", or the inverse of the impedance Z_{M}

$$\frac{i\omega C_0}{\rho_{\text{M}} d_{\text{M}}(\omega^2 - 2i\alpha\omega - \omega_0^2)} = -\frac{1}{Z_{\text{M}}} \qquad (2.109)$$
$$C_0 = \frac{\int_{\mathscr{S}_{\text{mem}}} dS\, u_{01}^2}{\left(\int_{\mathscr{S}_{\text{mem}}} dS\, u_{01}\right)^2},$$

where u_{01} is the first membrane mode (2.30). The cavity "plus" coefficient Γ_+ (2.98), on the other hand, is equivalent to the impedance Z_{V} in the $f \to 0$ limit, while the cavity "minus" coefficient vanishes, i.e.,

$$\lim_{f\to 0} \Gamma_+ = -Z_{\text{V}} \qquad \text{and} \qquad \lim_{f\to 0} \Gamma_- = 0 \qquad (2.110)$$

The ICE model $\Gamma_\pm$ coefficients are, effectively, corrections to the impedances that account for the spatial variation of pressure inside the cavity.

2.3.2 Mechanical equivalent

A mechanical analog to the ICE model can be similarly constructed by using assumptions similar to those for the electrical equivalent and representing the system by a modified version of a well-known problem, i.e., the coupled vibration of two rigid masses coupled by a massless spring [77, p. 35]. Firstly, the vibrating eardrums can be replaced by rigid objects of mass m_{p}, denoted by $\text{P}_{1/2}$, attached to an infinitely heavy wall by means of springs of stiffness κ_{p} and dashpots with damping coefficient b. As in the circuit analog, we neglect the spatial variation of pressure between the eardrums and represent the effect of the cavity pressure by means of a third spring of stiffness κ_{cav} coupling the rigid masses. The mechanical analog to ICE is illustrated in Fig. 2.15.

The masses are subjected to time varying forces $F_{1/2}(t)$, such that their equations of motions are given by,

$$m_{\text{p}}\ddot{u}_{1/2} = F_{1/2}(t) - \kappa_{\text{p}} u_{1/2} - b\dot{u}_{1/2} - \kappa_{\text{cav}}\,(u_1 + u_2)\,, \qquad (2.111)$$

where $u_{1/2}$ is the displacement of the respective masses and the overhead dot represents the derivative with respect to time. For periodic driving forces differing by a small phase Φ of

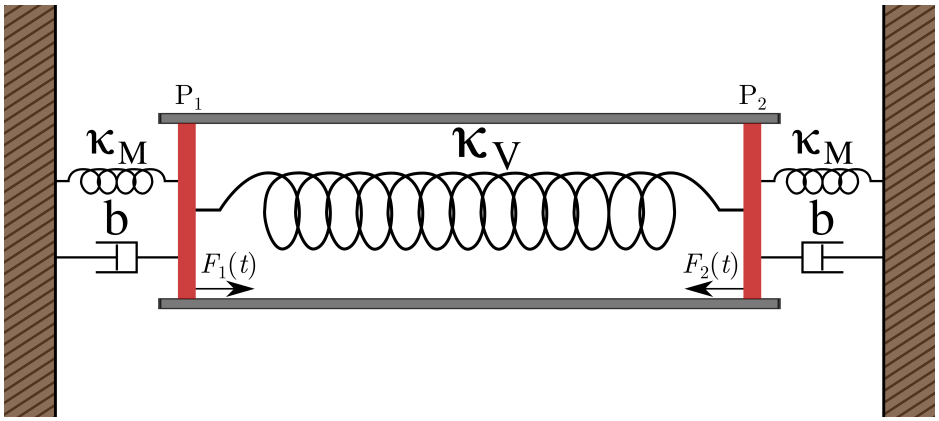

Fig. 2.15 The equivalent mechanical model for ICE described using a coupled mass-spring system. Two rigid objects P_1 and P_2 (red) of mass m_p representing the eardrums and the attached middle-ear components are coupled by a spring of stiffness κ_{cav}, which represents the air inside the interaural cavity. Each mass is also attached to a wall by means of a spring of stiffness κ_p and a dashpot with a damping coefficient b corresponding to the eardrum fundamental frequency and damping respectively. The masses $P_{1/2}$ are driven by time-dependent forces $F_1(t)$ & $F_2(t)$ representing the sound pressure.

the form

$$F_1(t) = Fe^{i(\omega t - \Phi/2)}, \qquad F_2(t) = Fe^{i(\omega t + \Phi/2)}\,, \tag{2.112}$$

the equations of motion can be decoupled by applying the sum-and-difference method used in Sec. 2.2.3 to give

$$m_p \ddot{u}_+ = (F_2(t) + F_1(t)) - \kappa_p u_+ - b\dot{u}_+ - 2\kappa_{cav} u_+ \tag{2.113}$$

$$m_p \ddot{u}_- = (F_2(t) - F_1(t)) - \kappa_p u_- - b\dot{u}_-\,. \tag{2.114}$$

The steady state displacements u^{ss} can be readily obtained from the above equations to give

$$u^{ss}_{1/2}(t) = \underbrace{\frac{\cos\ \omega t}{-m_p\omega^2 + ib\omega + \kappa_p + 2\kappa_{cav}}}_{u^{ss}_+} \mp \underbrace{\frac{i\sin\ \omega t}{-m_p\omega^2 + ib\omega + \kappa_p}}_{u^{ss}_-}\,. \tag{2.115}$$

Moreover, by requiring the initial (at time $t = 0$) displacement and velocity of the masses to be zero, the transient displacements u^{tr} can also be calculated. To do so, we follow the

methods used in Sec. 2.2.1 and solve Eqs. (2.113)&(2.114) independently to give

$$u^{\mathrm{tr}}_{1/2}(t) = \Bigg[\underbrace{\frac{\cos\omega_0^+ t + \alpha t \,\mathrm{sinc}\,\omega_0^+ t}{-m_\mathrm{p}\omega^2 + ib\omega + \kappa_\mathrm{p} + 2\kappa_\mathrm{cav}}}_{u^{\mathrm{tr}}_+} \mp \underbrace{\frac{i\sin\omega_0^- t}{-m_\mathrm{p}\omega^2 + ib\omega + \kappa_\mathrm{p}}}_{u^{\mathrm{tr}}_-} \Bigg] F\, e^{-bt/2m_\mathrm{p}}\,, \tag{2.116}$$

such that, $u_{1/2}(t) = u^{\mathrm{ss}}_{1/2}(t) + u^{\mathrm{tr}}_{1/2}(t)$. Where we have defined

$$\omega_0^+ = \sqrt{-(b/2m_\mathrm{p})^2 + (2\kappa_\mathrm{cav} + \kappa_\mathrm{p})/m_\mathrm{p}}, \qquad \omega_0^- = \sqrt{-(b/2m_\mathrm{p})^2 + \kappa_\mathrm{p}/m_\mathrm{p}} \tag{2.117}$$

as the (angular) resonance frequencies of the "plus" and "minus" components, respectively.

To summarize, in the mechanical analog to ICE, the flexible tympanic membrane is replaced by a rigid mass with a natural frequency and damping provided by an externally attached spring and dashpot, respectively. The parameters for the mechanical equivalent are related to those of the ICE model as (cf. Table 2.1),

$$m_\mathrm{p} = \rho_M d_M S_\mathrm{tymp}, \qquad \kappa_M = m_\mathrm{p}\omega_0^2, \qquad b = 2m_\mathrm{p}\alpha\,, \tag{2.118}$$

$$\kappa_\mathrm{cav} = \frac{\rho c^2 S_\mathrm{cyl}^2}{V_\mathrm{cav}}\,. \tag{2.119}$$

Where, as usual, $S_\mathrm{cyl} = \pi a_\mathrm{cyl}^2$ is the radius of the cylindrical interaural cavity. Thus, as in the circuit equivalent, the mechanical model is an approximation of the full ICE-model which neglects the contribution of higher membrane modes, as well as the variation of pressure within the interaural cavity.

Although the simplified models are analytically tractable, it should be stressed that the ICE model is a more accurate description of the physics of hearing. In comparison to the lumped element and the spring-dashpot method discussed in this section, the ICE model using a cylindrical cavity coupling the eardrums has three main advantages, which are,

- by accounting for the effect of asymmetrically loaded extracolumella, we were able to describe the membrane motion in spatial detail,
- as the model accounts for the spatial variation of pressure within the interaural cavity, it is applicable over a wider frequency range and,
- the source of the external inputs and their nature are not obscured as they are in the simplified models.

2.4 Conclusion

In the present chapter, we have laid the mathematical groundwork for internally coupled ears or, the ICE model. In Sec. 2.1.1, we described the eardrum which serves as the primary receiver of external stimulus in ICE. The presence of a transducer of membrane vibrations in the form of an asymmetrically attached extracolumella was accounted for by requiring the ICE eardrum to have a sectorial shape; see Fig. 2.3b. The extracolumella was represented by a non-moving sector of angle 2β. In Sec. 2.2.1, we derived general expressions for the pressure driven motion of the eardrum, by treating its vibrating part as a linear elastic membrane clamped at its circular boundary and at its point of contact with the extracolumella. Through the use of a sectorial membrane, we also accounted for the asymmetry in its vibration, resulting in markedly different vibration patterns; compare Figs. 2.10 and 2.12. The interaural cavity was modeled in Sec. 2.1.2 as a cylindrical canal connecting the eardrums, with its length equal to the interaural distance L, i.e. the distance between the eardrums in a realistic animal. The cross section or, equivalently, the radius of the cylinder was calculated (2.1) from L and by fixing the volume of the cavity V_{cav}. The radius thus determined was different from the cylinder radius in a previous treatment of ice [50], where it was taken to be equal to the eardrum radius, resulting in a much smaller cavity volume (2.1); compare Figs. 2.6a and 2.6b. Analytical expressions for the pressure were derived in Sec. 2.2.2 by solving the acoustic wave equation inside the cavity. The different nature of the boundary conditions at the circular wall of the cylinder, i.e. Neumann as opposed to Dirichlet for the eardrum, resulted in different modes for the cylindrical cavity; cf. Eqs. (2.60)&(2.61). The vibration of coupled membranes and, consequently, the boundary condition for the pressure at the tympanic membrane interface was dealt with in Sec. 2.2.3. The smallness of the tympanic membrane vibrations relative to the length of the interaural cavity was then exploited to motivate the piston-approximation, where the pressure boundary condition, or, equivalently, the eardrum motion, was approximated by pistons moving with the average velocity of the eardrums. The directional sound inputs defined in Sec. 2.1.3 were then used to derive expressions (see Eqs. (2.99) and (2.100)) for the eardrum vibration driven by an external and internal pressure. We concluded the chapter in Sec. 2.3 by presenting two simplified models for ICE, namely, a lumped circuit model (see Fig. 2.14) with electrical components corresponding to the cavity, eardrum and pressure, and a mechanical model (see Fig. 2.15) which replaced the components with masses, springs and dashpots. The quantities derived in this chapter will be used in the next chapter to analyze the directional and frequency behavior of our system, including the resulting cues for sound localization.

Chapter 3

Hearing and Sound Localization

In the previous chapter, we derived a consistent geometrical model for internally coupled ears. In particular, we now have analytical expressions for the membrane vibration amplitudes u_0 and u_L in terms of the membrane parameters as a function of direction and frequency (2.100). Furthermore, the derived expressions (2.100) will be used to compare the ICE model with experimental results. For the most part, we will be focusing on the Tokay gecko (*Gecko*) and the water monitor (*Varanus*). Using parameters based on standard anatomical data (see Table 3.1) and an extracolumellar angle $\beta=\pi/30(=6^\circ)$, we get a membrane-vibration velocity of $c_\mathrm{M}=5.4\,\mathrm{m/s}$ for *Tokay* and $c_\mathrm{M}=2.0\,\mathrm{m/s}$ for *Varanus*. The data for Tokay are based on values from Christensen-Dalsgaard and Manley [25, 26], while those for *Varanus* are based on data from Bruce Young and can be found in [12]&[48], where the results of the present chapter have previously appeared. This difference in c_M or, equivalently the fundamental frequency f_0 also results in considerable differences in the nature of their hearing cues. Nevertheless, the ICE model adequately explains the generation of hearing cues in both species. In our subsequent computations, we take the speed of sound in air to be $c=343\ \mathrm{ms}^{-1}$ and the density of air as $\rho=1.206\ \mathrm{kgm}^{-3}$.

Table 3.1 System parameters

Parameter	***Gecko***	***Varanus***
Interaural distance L	22 mm	16 mm
Eardrum radius a_tymp	2.6 mm	2.6 mm
Membrane density ρ_M	$1\,\mathrm{mg/mm}^3$	$1.2\,\mathrm{mg/mm}^3$
Eardrum thickness d_M	$10\,\mu$m	$30\,\mu$m
Cavity volume V_cav	3.5 ml	2.0 ml
Cylinder radius a_cav	6.6 mm	6.3 mm
Fundamental frequency f_0	1.05 kHz	0.4 kHz
Damping coefficient α	$\approx 2611\ \mathrm{s}^{-1}$	$\approx 350\ \mathrm{s}^{-1}$

We begin the chapter by analyzing the frequency response of an individual eardrum in the absence of an interaural coupling or, effectively, driven only by an external pressure. In particular, we focus on the membrane frequency response Λ in order to motivate its essential role in our model. We will then proceed to the vibration of coupled membranes, where we will also directly compare calculated values with experimentally determined ones. We will then focus on the directional information available to the animal from the vibration amplitudes by means of *internal* time differences (**i**TD) and *internal* level differences (**i**LD), defined as the time (or, equivalently, phase) and amplitude differences between tympanic membrane vibrations, respectively. These will be contrasted with the *interaural* time and level differences, which correspond to the time and amplitude differences between the external sound inputs to the ears. Thus, by assigning numerical values to the the material properties of the membrane, as well as to the geometry of the interaural cavity, we can analyze the behavior of the hearing cues in greater detail.

Independent eardrum response

Before we compare our model with experimental data, we take a look at the frequency dependence of a single membrane's *independent* vibrations. In other words, we analyze the frequency behavior of the eardrum by means of the eardrum frequency response Λ (2.97), for the fictitious case where it is only subject to an external sound pressure on one side. The frequency response of the real and imaginary parts of Λ are plotted in Figs. 3.1a and 3.1b. In both cases the real part $\Re\{\Lambda_{\text{tot}}\}$ has a low-pass response, i.e., it is more or less frequency independent up to the membrane eigenfrequency f_0 and sharply drops to zero afterwards. The imaginary part $\Im\{\Lambda_{\text{tot}}\}$, on the other hand, has a band-pass response where it peaks close to, but beyond $f = f_0$ and falls off thereafter. The difference in the frequency behavior of Λ in both cases is due to the lower damping of the *Varanus* eardrum. A higher damping coefficient α results in a flatter frequency dependence of the real part $\Re\{\Lambda_{\text{tot}}\}$ and a sharper, narrower peak in the imaginary part $\Im\{\Lambda_{\text{tot}}\}$. The properties of $\Re\{\Lambda_{\text{tot}}\}$ and $\Im\{\Lambda_{\text{tot}}\}$ will be used to estimate membrane parameters in Sec. 3.6. Moreover, as we will see in the subsequent sections, the behavior of the hearing cues (time and level differences) mirrors that of the membrane response.

3.1 Interaural transmission gain

In earlier literature on hearing in animals with internally coupled ears [2, 26], the effect of interaural coupling on eardrum vibration was quantified by means of the so-called interaural

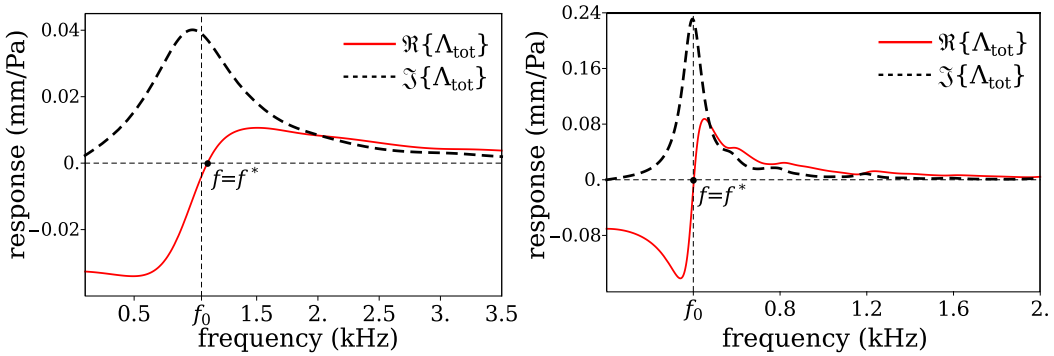

(a) *Gecko* (b) *Varanus*

Fig. 3.1 Real ($\Re$) and imaginary ($\Im$) part of the (integral) membrane-frequency response (2.97) for the ICE Model description of the Tokay gecko (left) and *Varanus* (right). In both cases, the response is dominated by the fundamental frequency f_0 of the tympanic membrane. The presence of local maxima in the response of Varanus is a result of its comparatively low membrane damping. The higher damping coefficient α for the gecko eardrum results in a flatter real part $\Re\{\Lambda_{\rm tot}\}$, while the lower damping in Varanus results in a sharper imaginary part $\Im\{\Lambda_{\rm tot}\}$. The frequency at which the response becomes purely imaginary is denoted by f_* and will be discussed in more detail in Section 3.4. Compare with Figs. 3.6a and 3.6b.

transmission gain. This is defined as the response ratio of eardrum vibrations to unilateral local stimulation. In other words, the ratio of the responses of both eardrums to an external stimulus presented only to a single eardrum is calculated. Such a stimulus is achieved by using, for example, a closely placed headphone at one ear, such that the opposite ear effectively receives *no* external input. The contralateral eardrum is therefore driven solely by the internal pressure set up by the vibrations of the ipsilateral one. A better understanding of ICE could nevertheless be gained by instead studying the responses of both eardrums to simultaneous and, therefore, realistic inputs separated by a small direction-dependent time difference.

Without loss of generality, we can mathematically derive the transmission gain G_T by setting $p_0^{\rm ex} = 0$ and $p_L^{\rm ex} = p\exp(i\omega t)$ in (2.100). The resulting ipsi- and contralateral eardrum vibration amplitudes are then used to calculate G_T,

$$u_{0/L}(r,\phi) = \frac{1}{2}\left(\frac{p\exp(i\omega t)}{1+\Lambda_{\rm tot}\Gamma_+} \mp \frac{p\exp(i\omega t)}{1+\Lambda_{\rm tot}\Gamma_-}\right)\Lambda(r,\phi)\,.$$
$$\Rightarrow G_T^{-1} = \left(\frac{u_0}{u_L}\right)^{-1} = \cos kL + \frac{V_{\rm cav}\sin kL}{\rho c^2 \Lambda_{\rm tot} kL}\,. \tag{3.1}$$

The mathematical expressions for $\Gamma_\pm$ (2.98) allow us to reach the considerably simplified formula of Eq. (3.1).

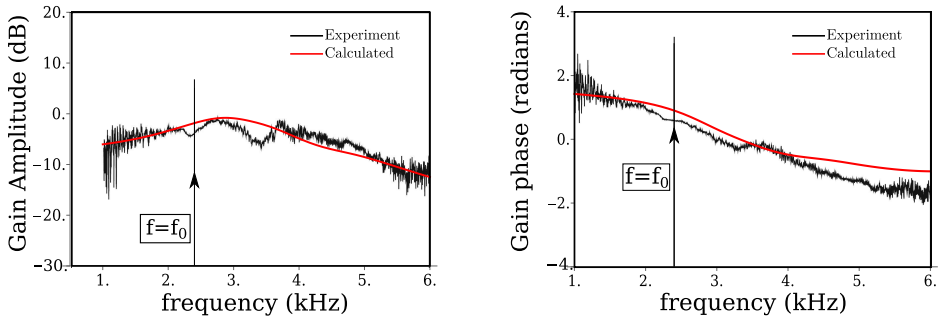

(a) *Hemidactylus*

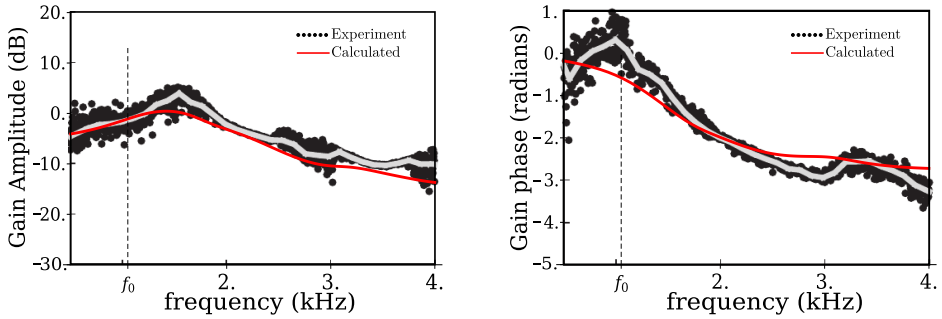

(b) *Tokay*

Fig. 3.2 Top: Experimental and calculated transmission gain for *Hemidactylus* (common house gecko). The transmission gain G_T is defined as the response ratio of contra- and ipsilateral eardrum vibrations under unilateral stimulation; see (3.1). The black lines correspond to values experimentally determined by Christensen-Dalsgaard and Manley [26] and the smooth solid (red) lines to values calculated to the ICE model. Left: Amplitude in decibels and Right: phase in radians. Bottom: Calculated values of transmission gain for *Tokay*. The values were experimentally measured by Christensen-Dalsgaard et al. [2] for five lightly anesthetized specimens. All the presented experimental data have been gathered through laser Doppler vibrometry measurements on the membrane surface.

In Figs. 3.2a and 3.2b the frequency dependence the phase and amplitude of the transmission gain calculated through ICE have been plotted together with the experimentally determined values for (a) *Hemidactylus frenatus*, the common house gecko, and (b) the Tokay gecko. There is a fair agreement between calculated and experimental values. Moreover, the results of our model also agree with the results for *Hemidactylus* from the previous mathematical treatment of ICE [49, 50].

The minor discrepancy in Fig. Fig. 3.2b for Tokay can be explained using the fact that there was a large size and hence weight variation (24–70 g) among the experimental specimens [2]. Variations in size lead to similar variations in the membrane fundamental frequency and can lead to considerable changes in the frequency behavior of the system. In

the following sections we will see examples of this variation across two species when we compare the frequency behavior for an adult gecko with that of a juvenile varanus.

3.2 Membrane vibration velocity

In order to compare our model with experimental results, we define the average vibration velocity in dB re $\mathrm{mms}^{-1}\mathrm{Pa}^{-1}$, meaning the decibel velocity with respect to 1 mm/s for an input pressure amplitude of 1 Pa as $\mathrm{v}_{\mathrm{dB}} = 20\log_{10}|\dot{u}^{\mathrm{ave}}_{0/L}|$. Figs. 3.3a & 3.3b show the respective frequency dependence of the membrane vibrations for ipsilateral $\theta = 90°$ and contralateral $\theta = -90°$ stimuli for both *Gecko* and *Varanus*.

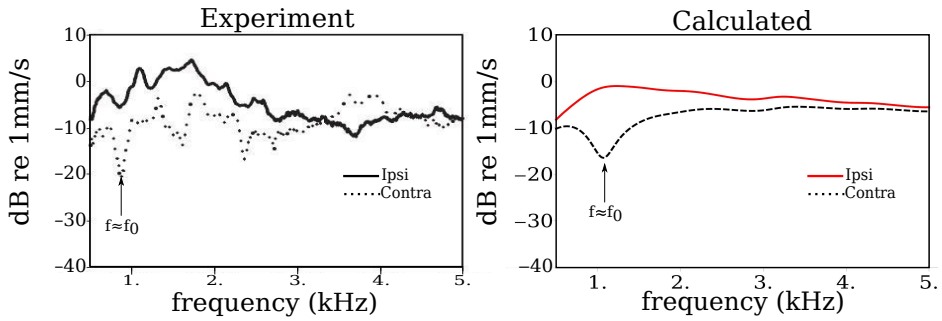

(a) *Gecko*

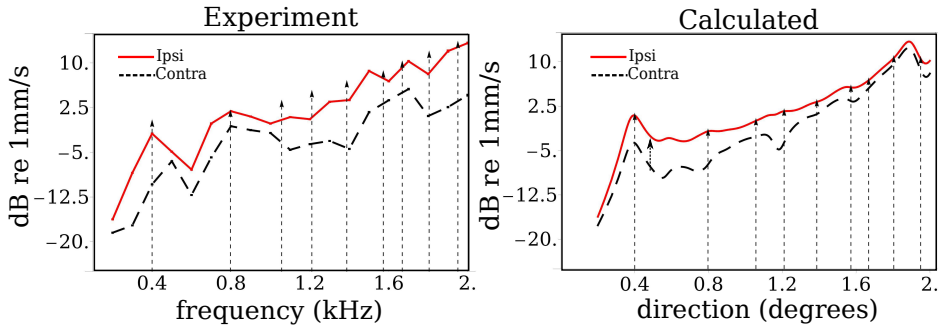

(b) *Varanus*

Fig. 3.3 Top: Experimental and calculated v_{dB} for ipsi- ($\theta = 90°$) and contralateral ($\theta = -90°$) stimuli for *Gecko*. Bottom: Experimental and calculated membrane amplitude for *Varanus* at $\theta = \pm 90°$. The vertical dashed lines in the lower plots correspond to the higher membrane modes for the Varanus. We thus see that not only at f_0 but also at higher membrane resonances does a less taut membrane with low α give peaks; compare Fig. 3.7b. The first resonant peak (or trough) allows a straightforward mathematical specification of the first extremum (max/min) for the iLD or equivalently the tympanic eigenfrequency f_0 in the alive animal. All experimental data presented were gathered through laser Doppler vibrometry.

In the case of *Gecko*, the contralateral response has a minimum near f_0, whereas the spectral response of *Varanus* shows multiple peaks corresponding to higher membrane eigenfrequencies. The occurrence of multiple peaks instead of a single one in the biophysically relevant range of up to 2 kHz is due to the fact that the eardrum of *Varanus* is very underdamped [much smaller α; cf. (2.14)], resulting in higher modes being less suppressed. Nevertheless, the present ICE model explains the frequency behavior in both cases and allows for a determination of the tympanic fundamental frequency in the alive animal.

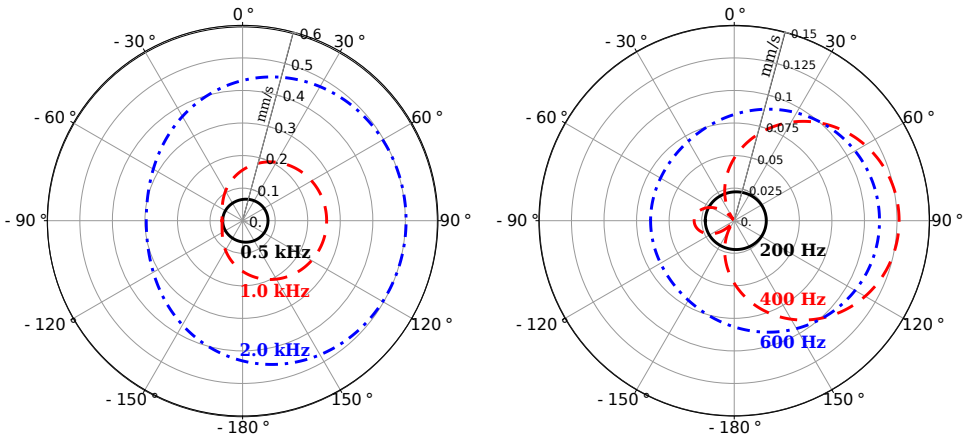

(a) *Gecko* (b) *Varanus*

Fig. 3.4 Polar plots for the membrane vibration velocity in mm $s^{-1}$for different frequencies for *Tokay* (left) and *Varanus* (right). Positive angles correspond to ipsilateral directions and negative angles to contralateral ones. The directionality of the system is immediately apparent from the way in which ipsilateral directions result in higher vibration amplitudes, even though the external inputs to the ears have the same amplitude. The above plots have been generated using the expression given in (2.100) using the parameters from Table 3.1. The input sound pressures have been assumed to have an amplitude of 60 dB SPL.

Figures 3.4a and 3.4b show the variation of the membrane-vibration velocity with direction for different frequencies in *Tokay* and *Varanus*, respectively. For both animals, the ipsilateral ear is on the right-hand side and corresponds to positive values for the angle in degrees with respect to the rostral-caudal axis. In both cases, the eardrum has a markedly higher vibration velocity for sounds coming from an ipsilateral than from a contralateral direction.

3.2.1 Membrane-vibration pattern

The measured vibration patterns [51] are shown on the left in Fig. 3.5a. The amplitudes were measured for eight locations on the membrane to find the pattern seen in the figure. At

around 4kHz, the vibration pattern distinctly develops two maxima – something that would not happen to a centrally loaded tympanum except at frequencies well beyond the hearing range of Geckos (200 Hz to 3 kHz).

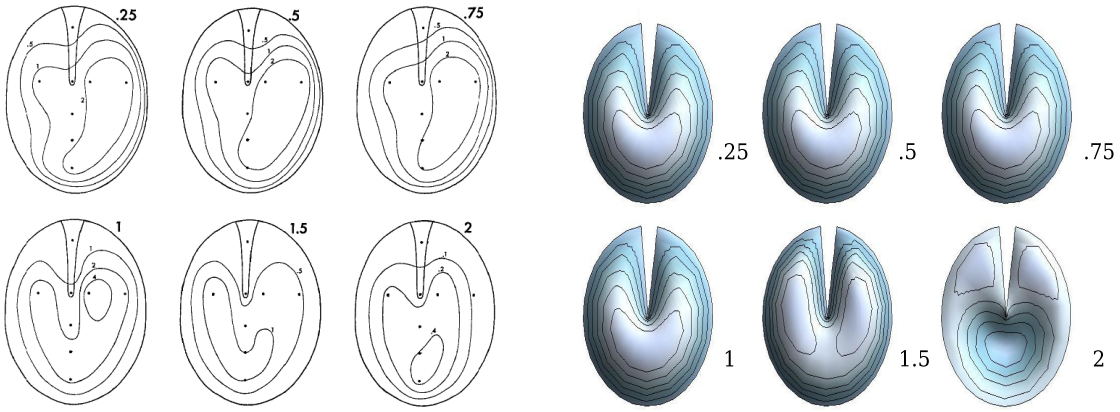

(a) Experiment (b) Calculated

Fig. 3.5 Left: Experimental membrane vibration patterns of the Tokay gecko dependent on sound frequency varying from .25 kHz to 2 kHz, with the corresponding frequencies shown above the membranes [51]. Right: Vibration pattern of one of the membranes in the ICE model for an ipsilateral stimulus. In both cases we see a similar complex vibrational pattern for the membranes, which becomes increasingly *circularly* asymmetric with increasing frequency.

In order to compare our ICE model with the experimental results, we now plot the response of one of the membranes to an ipsilateral stimulus. This is calculated by using (2.100) and is illustrated in Figs. 3.5a and 3.5b (right) for the same frequency range as that of the experimental data.

The asymmetric nature of our membrane vibration pattern is a result of the chosen geometry. Mathematically, it is a result of the fact that a uniform pressure on the surface of a full circular membrane only couples to the circularly symmetric J_0 modes. The extracolumella, however, breaks this symmetry and all the resulting eigenmodes couple with the pressure, which offers a clear contrast to Fig. 2.11. As qualitative and semi-quantitative reproduction, the present model is very strong but for a full quantitative analysis we would need to take into account both the microstructure of the tympanum and the motion of the extracolumella and has been dealt with elsewhere [59].

3.3 Internal time and level differences

As we have seen in the previous section, the membrane vibration amplitudes are directional by themselves. However, we will now show that the difference between the vibrations between the left and right tympanum is more sensitive to the source direction θ. In the following, we focus on three universal aspects of ICE:

1. the internal time difference (**i**TD), which for frequencies $< f_0$ greatly exceeds the interaural time difference (**I**TD) and forms a plateau from $f = 0$ onwards;

2. the internal level difference (**i**LD), which exhibits a pronounced maximum once the iTD has strongly decreased; and

3. the fundamental frequency f_0 of the tympanum segregating the iTD and iLD domain.

Both iTD and iLD also depend on the sound-source direction. Moreover, the directionality of the hearing cues experienced by the animal directly reflect the nature of the stimulus. Finally, it should be constantly borne in mind that what the animal actually "hears" is not the interaural but the internal stimulus and the two may greatly differ; Sections 1.1.1 and 1.2.

It has previously [78] been shown that lizards have two distinct populations of cochlear hair cells – one that responds to amplitude cues and the other to temporal cues. These two hair-cell populations both project bilaterally, i.e., they innervate neurons in both the left and right hemispheres, thus imparting a neuronal template to contrast both the amplitude and temporal patterns [79] arising from the eardrum vibrations. It is well known that certain neurons are sensitive to time differences between eardrum vibrations [5, 2, 46]. We refer to this metric as the internal Time Difference (iTD), in contrast to the Interaural Time Difference (ITD) as measured from the external inputs to the ears. The internal time and level differences are the unique outcome of the interaction between the outside signal and the internal coupling arising from the air-filled interaural cavity; cf. Figs. 1.6a to 1.6c. Furthermore, we follow Jørgensen et al. [31] in postulating an algorithm for determining amplitude (level) differences. More specifically, we assume that this is done by a neuronal subtraction of logarithmic vibration amplitudes of the two membranes. The biological physics is that of hair-cell response being governed by the (Weber-Fechner) logarithm of the amplitude whereas the "subtraction" is that of excitation minus inhibition (E/I), which was briefly discussed in Section 1.1.1. We refer to this subtraction as the internal Level Difference (**i**LD) and contrast it with the Interaural Level Difference (**I**LD), i.e., the logarithmic amplitude difference between the *external* sound inputs to both ears.

3.3.1 Internal time difference - iTD

The internal Time Difference (iTD) corresponds to the actual time difference between left and right membrane vibrations as experienced by the animal and is defined as

$$\text{iTD} = \text{Arg}(u_L^{\text{ave}}/u_0^{\text{ave}})/\omega = \text{Arg}(u_L^{\text{ave}}/u_0^{\text{ave}})/\omega \,, \tag{3.2}$$

$$u_L^{\text{ave}}/u_0^{\text{ave}} = (1+B)/(1-B) \,, \tag{3.3}$$

where

$$B = i\,[(1+\Lambda_{\text{tot}}\Gamma_+)/(1+\Lambda_{\text{tot}}\Gamma_-)]\tan(k\Delta/2) \tag{3.4}$$

is direction-dependent through $\Delta = L\sin\theta$ (2.3). The above expressions can be easily derived by using the expressions for u_0^{ave} and u_L^{ave} from Eq. (2.100),

$$\begin{aligned}
\frac{u_L^{\text{ave}}}{u_0^{\text{ave}}} &= \frac{p_+(1+\Lambda_{\text{tot}}\Gamma_-)+p_-(1+\Lambda_{\text{tot}}\Gamma_+)}{p_+(1+\Lambda_{\text{tot}}\Gamma_-)-p_-(1+\Lambda_{\text{tot}}\Gamma_+)} \\
&= \frac{1+\frac{p_-}{p_+}(1+\Lambda_{\text{tot}}\Gamma_+)/(1+\Lambda_{\text{tot}}\Gamma_-)}{1-\frac{p_-}{p_+}(1+\Lambda_{\text{tot}}\Gamma_+)/(1+\Lambda_{\text{tot}}\Gamma_-)} \\
&= \frac{1+i\tan(k\Delta/2)(1+\Lambda_{\text{tot}}\Gamma_+)/(1+\Lambda_{\text{tot}}\Gamma_-)}{1-i\tan(k\Delta/2)(1+\Lambda_{\text{tot}}\Gamma_+)/(1+\Lambda_{\text{tot}}\Gamma_-)} \,.
\end{aligned} \tag{3.5}$$

The last step follows from the fact that

$$\begin{aligned}
p_+ = p_L^{\text{ex}} + p_0^{\text{ex}} &= p\,(\exp(ik\Delta/2)+\exp(-ik\Delta/2)) \\
&= 2p\cos k\Delta/2 \,, \\
p_- = p_L^{\text{ex}} - p_0^{\text{ex}} &= p\,(\exp(ik\Delta/2)-\exp(-ik\Delta/2)) \\
&= 2ip\sin k\Delta/2 \,.
\end{aligned}$$

In contrast to the iTD, the *interaural* time difference (ITD), calculated from a given sound input (2.3) is

$$\text{ITD} = \text{Arg}\,(p_0^{\text{ex}}/p_L^{\text{ex}})\,/\omega = L\sin\theta/c \,, \tag{3.6}$$

viz., the time difference between the arrival of sound from a given source at both ears; cf. Section 1.1.1. The ITD is independent of frequency and, for the parameters defined in Table 3.1, it is ≈ 64 μs for $\theta = \pm 90^\circ$ for *Gecko* and ≈ 45 μs for a young *Varanus*. Figures 3.6a and 3.6b show the frequency and direction dependence of the internal time

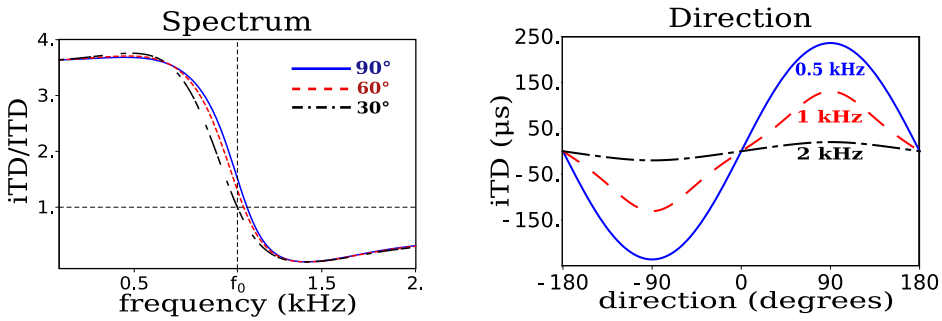

(a) Gecko

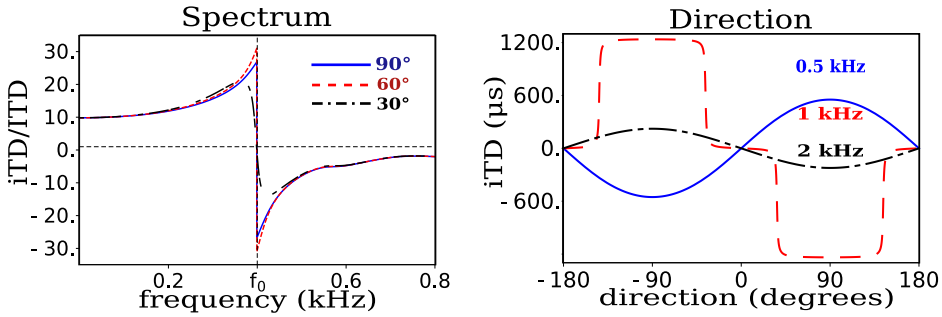

(b) Varanus

Fig. 3.6 Frequency and direction dependence of the iTDs for *Gecko* (top) and *Varanus* (bottom). (a) For *Gecko*, the iTDs exhibit a plateau of iTD ≈ 3.5 ITD, up to about $f = f_0$ and sharply fall thereafter. As indicated, the plateau is uniform, irrespective of the direction θ. Due to the plateau, the iTDs can thus be effective low-frequency cues. (b) For *Varanus*, the iTDs slowly increase up to f_0 and then decrease; the discontinuity is an artefact of 2π which corresponds to a loss of directional information in the iTD. The young animal can therefore only exploit a restricted low-frequency range of iTDs (up to approximately 200 Hz), nevertheless illustrating that the time dilation factor iTD/ITD can differ from 3 appreciably.

difference (**i**TD) for *Gecko* and *Varanus*, respectively. Experimentally, by measuring the phase difference between the eardrum vibrations, one in fact measures the iTD.

In the case of *Gecko*, the iTDs have a low-pass response, i.e., they are more or less constant up to a certain frequency and drop sharply thereafter, with iTD/ITD, $= 1$ at $f \approx f_0$. From a neuronal-processing point of view, this is convenient as it mirrors the behavior of the ITDs, *but strongly increased* by a factor of about 3.5 for $0 \leq f \lesssim \frac{2}{3} f_0$ in *Gecko* and an astounding 15 for $0 \leq f \lesssim 0.2 f_0$ in *Varanus*; cf. Figs. 3.6a and 3.6b (left). The number 3.5 depends on the specific geometry of the internal cavity as found in many lizards, such as *Gecko*, but it is not unique. An increase in the iTD by a factor of 3 has also been observed in some birds [80]. Figure 3.6b illustrates its variation for *Varanus*. We refer to the ratio of internal and interaural time difference as the time dilation factor, or TDF for short.

3.3.2 Internal level difference - iLD

For the input (2.3), the internal Level Difference (iLD) is defined as the logarithmic difference between the left and right (0/L) membrane amplitudes of (2.40), i.e.,

$$\text{iLD} = 20\,\text{Log}_{10}|u_L^{\text{ave}}/u_0^{\text{ave}}| = 20\,\text{Log}_{10}|\dot{u}_L^{\text{ave}}/\dot{u}_0^{\text{ave}}|\,, \tag{3.7}$$

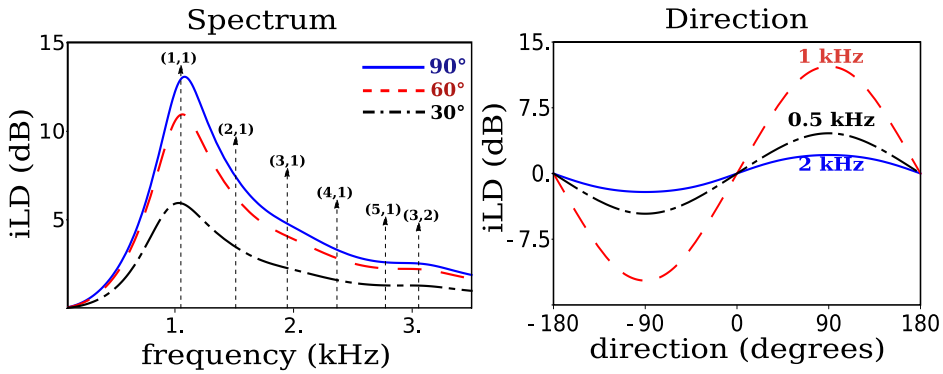

(a) Gecko

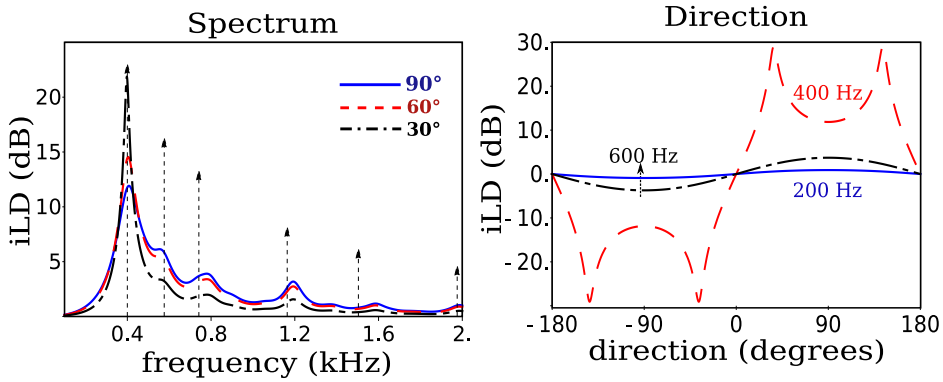

(b) Varanus

Fig. 3.7 Calculated frequency and direction dependence of the iLDs for (a) *Gecko* (top) and (b) *Varanus* (bottom). The location of the eigenfrequencies has been indicated by dashed arrows. For *Gecko*, the iLDs peak close to $f = f_0$ and decrease slowly thereafter. They can therefore serve both as effective high-frequency hearing cues and as an efficient means of determining f_0 in alive animals. Clearly, the higher tympanic eigenmodes play no role for tokay. For juvenile *Varanus* with small α and $f_0 \approx 500$ Hz, however, we see the corresponding peaks of some (at least five) higher membrane eigenmodes.

As the left and right inputs (2.3) effectively have the same amplitude, the interaural level difference (ILD) is identically zero, i.e.,

$$\text{ILD} = 20\,\text{Log}_{10}|p_L^{\text{ex}}/p_0^{\text{ex}}| = 0\,. \tag{3.8}$$

For *Gecko*, the iLD has a band-pass like behavior. It is zero for both very low and high frequencies and peaks close to the membrane eigenfrequency f_0; cf. Fig. 3.7a. The iLDs steeply increase across $\theta = 0°$ and attain a maximum/minimum at $\theta = \pm 90°$. Under normal circumstances, as in *Gecko*, the functional dependence is given by a sine. For *Varanus*, Fig. 3.7b shows an iLD spectrum with multiple peaks near membrane resonances (i.e., eigenfrequencies), corresponding to a much lower damping (smaller α). Moreover, at the fundamental membrane eigenfrequency f_0, the directional response peaks at $\theta = \pm 30°$. A possible explanation of this deviating behavior is that the experiments were performed on juvenile monitor lizards, suggesting that increased membrane damping and cavity volume in adults should give similar results to those shown for the adult *Gecko*.

3.3.3 iTD/iLD transition

From the low-pass behavior of the iTDs and the high-pass behavior of the iLDs we can infer that internal time differences may well work as effective cues at lower frequencies, whereas internal level differences are most effective at higher frequencies. Unlike larger animals where such a transition would rely on the fact that higher-frequency sound waves would have a "shadow" on the contralateral eardrum due to diffraction [61, p .154] and Section 1.1.1, the iTDs and iLDs in ICE are generated solely as a consequence of the internal coupling between the eardrums.

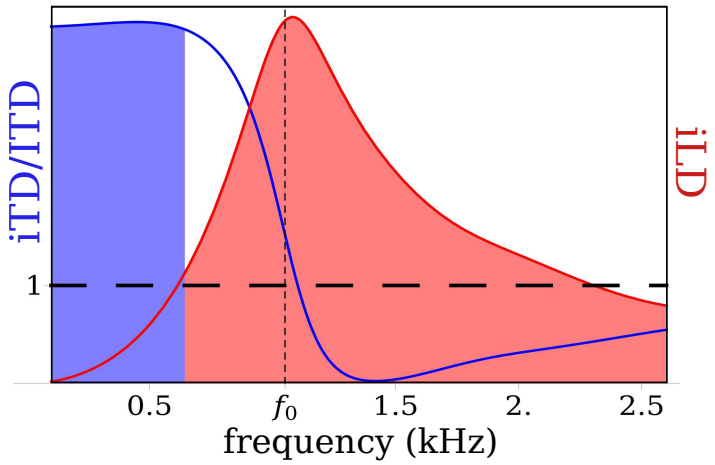

Fig. 3.8 Transition between the iTD and iLD frequency regimes for directions $\theta \neq 0°$. At lower frequencies iTDs work better as directional cues, e.g., with iTD/ITD ≈ 3 for adult lizards, while at higher frequencies the iLDs become pronounced, even though for most lizards the external $ILD \approx 0$. The transition between the two kinds of cues is governed by the eardrum's fundamental eigenfrequency f_0.

In animals with ICE, the transition between the different frequency regimes is governed by the fundamental frequency of the tympanic membrane f_0; see Fig. 3.8. In other words, instead of a segregation of the frequency regimes of hearing cues dictated by the size of the head (see Figs. 1.4a and 1.4b), the transition between the use of hearing cues is dictated by the properties of the eardrum. Despite the lack of an amplitude difference between the inputs, the system uses small phase differences to generate frequency-dependent time (or equivalently phase) and amplitude differences between the eardrums by using the internal coupling and the mechanics of the membrane.

3.4 Role of the membrane-response function Λ

A parallel between the frequency response of the internal time and level differences (iTD and iLD), and the membrane frequency response $\Lambda(r,\phi)$ (2.97) should be immediately apparent; compare Figs.3.1a,3.1b and Figs. 3.6a, 3.6b, 3.7a and 3.7b. This similarity results from the way in which we have defined the ratio of the complex vibration amplitudes (3.3), (3.4). Furthermore, it explains the role of the membrane eigenfrequency as well as the damping α in the generation of interaural cues. Put simply, the flat response of the iTD as well as the magnitude and position of the iLD peak depend on f_0 and α. While a low value of α will result in a strong iLD close to f_0, the TDF (iTD/ITD) will vary strongly with frequency up to f_0, as in the case of the young *Varanus*. Using our definition of B (3.3), the ratio between the membrane vibration amplitudes can therefore be rewritten as,

$$u_L^{\text{ave}}/u_0^{\text{ave}} = \frac{\exp(ik\Delta/2)+\Lambda_{\text{tot}}(\Gamma_-\cos\frac{k\Delta}{2}+i\Gamma_+\sin\frac{k\Delta}{2})}{\exp(-ik\Delta/2)+\Lambda_{\text{tot}}(\Gamma_-\cos\frac{k\Delta}{2}-i\Gamma_+\sin\frac{k\Delta}{2})}\,.$$

We now focus on the case where the sound source is at $\theta=\pi/2(=90^\circ)$ and, subsequently, $\Delta=L$. This means that the sound source is on the same side as the L ear; cf. Fig. 2.7. The ratio between the membrane vibrations can therefore be explicitly written down

$$\begin{aligned} u_L^{\text{ave}}/u_0^{\text{ave}} &= \frac{\exp(ikL/2)+\tilde{\Lambda}_{\text{tot}}(\sin kL/2-i\cos kL/2)}{\exp(-ikL/2)+\tilde{\Lambda}_{\text{tot}}(\sin kL/2+i\cos kL/2)}\,, \\ &= \frac{\exp(ikL/2)-i\tilde{\Lambda}_{\text{tot}}\exp(ikL/2)}{\exp(-ikL/2)+i\tilde{\Lambda}_{\text{tot}}\exp(-ikL/2)}\,, \\ &= \exp(ikL)\frac{1-i\tilde{\Lambda}_{\text{tot}}}{1+i\tilde{\Lambda}_{\text{tot}}}\,. \end{aligned} \tag{3.9}$$

We have used the definitions of $\Gamma_\pm$ from (2.98) and absorbed the factor $\rho c^2 kL/V_{\text{cav}}$ into Λ_{tot} by defining

$$\tilde{\Lambda}_{\text{tot}} = \rho c^2 kL \Lambda_{\text{tot}}/V_{\text{cav}} \,. \tag{3.10}$$

From Figs. 3.1a & 3.1b we can see that there is a frequency f_* where the membrane response becomes purely imaginary. Let us assume that at this point $\tilde{\Lambda}_{\text{tot}} = i\eta$ where η is a positive real number which carries information about both the tympanic membrane as well as the internal cavity. The ratio (3.9) reduces to

$$u_L^{\text{ave}}/u_0^{\text{ave}} = \exp(ikL)\frac{1+\eta}{1-\eta} \,. \tag{3.11}$$

The right-hand side of the above equation is a phase factor multiplied by a real number. The argument of the quantity kL is equal to the phase difference between the inputs to the eardrums and, due to our definition of iTD (3.2), the resultant internal time difference between the ears *equals* the interaural time difference. The corresponding values for f_* can be calculated numerically and are found to be around 1097 Hz for *Gecko* and around 402 Hz for *Varanus*.

For directions other than $\theta = 90°$, a similar result can be obtained, but the exact value of f_* in this case would also depend on the cavity volume. It is only when the source is fully ipsilateral/contralateral to an ear, that f_* can be determined solely from the membrane parameters.

3.5 Volume dependence

In the previous chapter, we defined the interaural cavity of the ICE Model in such a way that the cavity volume V_{cav} can be treated as an independent parameter; see Sec. 2.1.2. Effectively, V_{cav} determines the strength of the internal coupling and is convenient to use in a mathematical analysis. In Figs. 3.9a & 3.9b, we see the frequency dependence of the iTDs and iLDs (at source direction $\theta = 90°$) for different cavity volumes while keeping the other system parameters fixed. The lower limit of possible cavity volumes for a cylindrical interaural cavity is equal to that of a cylinder with a radius equal to that of the membrane, i.e., $a_{\text{cyl}} \geq a_{\text{tymp}}$, leading to a cross-sectional area of $\pi a_{\text{tymp}}^2 L$; cf. Figs. 2.6a and 2.6b and Eq. (2.2).

The volume dependence arises from the coupling parameters $\Gamma_\pm$ defined in (2.98) which decrease with the volume as $1/V_{\text{cav}}$. This means that as we let the volume go to infinity while

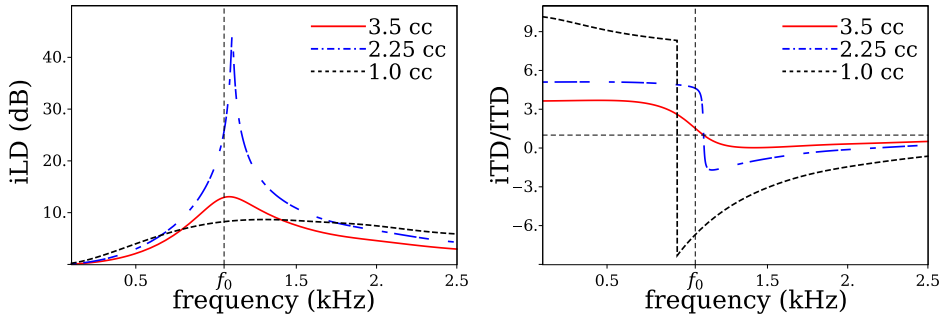

(a) *Gecko*

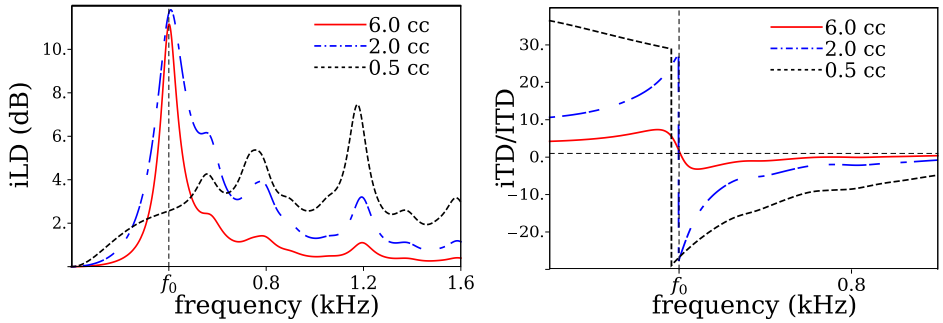

(b) *Varanus*

Fig. 3.9 iTD and iLD frequency response for different cavity volumes for *Gecko* (top) and *Varanus* (bottom). The sound source direction was chosen to be $\theta = 90°$. As we increase V_{cav}, the iLDs become smaller and less sharp around f_0. The iTDs on the other hand increase with decreasing volume, but also result in a phase ambiguity of 2π close to f_0. At an optimal volume of ≈ 2.2 cm^3 for the Tokay gecko and 6 cm^3 for *Varanus*, we have an optimal frequency response for both hearing cues.

keeping the interaural distance L constant ($a_{\text{cyl}} \to \infty$), the eardrums vibrate as uncoupled membranes driven by the sound pressures $p_{0/L}$

$$u_{0/L}(r,\phi;t) = \Lambda(r,\phi)p_{0/L}\,. \tag{3.12}$$

$\Lambda(r,\phi)$ essentially gives us the frequency response of the membrane amplitude at a given point (r,ϕ) on its surface.

For *Gekko* as well as for *Varanus*, the iLD goes to zero for small volumes. The iTD, on the other hand, appears to increase. However, it loses its plateau which is important for auditory information processing for low frequencies using time difference maps of the kind described in Section 1.1.1, and develops a phase ambiguity of 2π close to f_0. This means that the eardrums vibrate with a phase difference of π and can no longer be used to localize sound sources. Thus, both very small and very large volumes effectively break the coupling between the membranes. For the Tokay, we find an optimal response, i.e., flat amplified iTDs

at low frequencies and strong iLDs at higher frequencies for $V_{\text{cav}} \approx 2.2$ cc. This could be due to the fact that the assumed volume of 3.5 cm^3 (cf. Table 3.1) is for an "empty" skull. A live specimen would have a tongue and other organs inside the pharyngeal and mouth cavities which would reduce the effective volume V_{cav}.

Rather more interesting is the fact that, for larger cavity volumes (≈ 6 cc), the frequency response of the iLDs and iTDs of *Varanus* become similar to that of the *Gekko*; cf. Fig. 3.9b, solid (red) lines. The local iLD maxima corresponding to higher membrane modes are suppressed and the iTD has a fairly smooth and flat response at lower frequencies. This implies that the hearing system of an adult *Varanus* would me more effective at localizing sound sources, than a juvenile lizard over a larger frequency range.

3.5.1 Critical volume

In Figs. 3.9a & 3.9b we see that for a certain value of V_{cav} a singularity appears for the iLD close to f_0 for a source direction $\theta = 90^\circ$. A comprehension of what causes this singularity to emerge is essential to a complete understanding of ICE. The physical explanation for this apparent singularity is that at the critical volume the internal pressure at the contralateral membrane cancels the external pressure at the frequency of maximal iLD response. As a result, the contralateral membrane vibration velocity, or equivalently the displacement, vanishes entirely, i.e. $u_0(r,\phi;t) = 0$. Hence by definition the iLD is bound to diverge.

This result can be derived directly from the expression for the membrane displacement (2.5). Rewriting u_0 explicitly in terms of input pressure amplitude and direction gives us

$$u_0(r,\phi) = \frac{1}{2}\left(\frac{2p\cos k\Delta/2}{1+\Lambda_{\text{tot}}\Gamma_+} - \frac{2ip\sin k\Delta/2}{1+\Lambda_{\text{tot}}\Gamma_-}\right)\Lambda(r,\phi)\ .$$

For a sound source closer to the L ear, the opposite 0 ear is on the contralateral side; see Fig. 2.7. We thus have $\Delta = L\sin\theta = L$ for $\theta = \pi/2\ (= 90^\circ)$. The displacement can be rewritten as

$$u_0(r,\phi) = \left(\frac{p\cos kL/2}{1+\Lambda_{\text{tot}}\Gamma_+} - \frac{ip\sin kL/2}{1+\Lambda_{\text{tot}}\Gamma_-}\right)\Lambda(r,\phi)$$

where the $1/2$ has been absorbed into the brackets. As shown in Section 3.4, the frequency where $iTD = ITD$, viz., f_*, is achieved when the membrane frequency response Λ (2.6) becomes purely imaginary. As derived in (3.10) let us suppose that $\tilde{\Lambda}_{\text{tot}}(f = f_*) = i\eta$, where η is a real number and consider the case where $V_{\text{cav}} = \rho c^2 kL\eta$ so that the factor $\frac{\rho c^2 kL\eta}{V_{\text{cav}}}$ in the denominators beside the tan and cos becomes equal to 1. Using the definitions of $\Gamma_\pm$

(2.98) at $f = f_*$ we find

$$\begin{aligned} u_0(r,\phi) &= \left(\frac{p\cos kL/2}{1 - i\cot kL/2} - \frac{ip\sin kL/2}{1 + i\tan kL/2} \right) \Lambda(r,\phi)\,, \\ &= \left(\frac{ip\sin kL/2}{1 + i\tan kL/2} - \frac{ip\sin kL/2}{1 + i\tan kL/2} \right) \Lambda(r,\phi)\,, \\ &= 0\,. \end{aligned}$$

In the second equation we have multiplied and divided the first fraction by $i\tan kL/2$. It is thus clear that for this cavity volume, the membrane displacement on the contralateral side identically vanishes resulting in a singularity of the iLD, actually a trivial one. Nevertheless we can safely use the term "critical" to denote this cavity volume $V_{\text{crit}} = \rho c^2 kL\eta$.

For the animal, V_{crit} is not an optimal cavity volume to fully exploit interaural coupling. This is mainly due to the fact that the iTD response starts to show a phase ambiguity on either side of f_*; cf. Fig. 3.9a (right). The animal would be unable to distinguish between sources on the left and the right and would therefore be better off by operating with a cavity volume slightly above V_{crit}, where a strong iLD is coupled with an unambiguous iTD response.

This is also a possible explanation of the differences observed in the generated hearing cues for the juvenile *Varanus* when we compare it with *Gecko*. Given its other system parameters, i.e., membrane eigenfrequency, damping, interaural separation, the volume of 2.0 cc in *Varanus* is well below its V_{crit} of 6 cc.

3.6 Estimating the eardrum's fundamental frequency and damping coefficient

The fundamental frequency f_0 and the damping coefficient α of the eardrum are important quantities to auditory performance. The former to partitioning the auditory landscape, the latter to determining the duration of transient response of the tympanum. In order to directly measure the material properties of the eardrum, one would, in general need to excise the tissue. The Young's modulus of the *Varanus* eardrum has been measured using such a procedure [59]. The material properties, including viscoelastic damping, were also measured using similar methods for a dissected duck ear [81]. In contrast, we will now propose an experimental and numerical procedure to determine both f_0 and α from the results of the present chapter, thereby only requiring vibrometry data from a live animal.

To determine both, we need two quantities from experimentally measured tympanic vibration and hearing cues. As we see from Figs. 3.6a and 3.6b & Figs. 3.7a and 3.7b,

the maximum of the iLD as well as the frequency f_* at which iTD=iLD, for sound-source directions $\theta = \pm 90^\circ$, the internal iTD equals the external ITD are experimentally accessible and near f_0. We can analytically estimate the location of the iLD maximum and determine f_* in terms of f_0 by using the properties of the membrane frequency response Λ or, more specifically, Λ's integral over the membrane surface Λ_{tot}; cf. (2.97). An experimental recipe follows at the end of this section. Λ_{tot} has been defined as

$$\Lambda_{\text{tot}} = \int_{\mathscr{S}_{\text{mem}}} dS\,\Lambda(r,\phi) = \sum_{m,n}^{\infty} K_{\text{mn}}/\Omega_{\text{mn}} \tag{3.13}$$

where

$$K_{\text{mn}} = \frac{(\int u_{\text{mn}})^2}{\rho_{\text{M}} d_{\text{M}} \int u_{\text{mn}}^2},\ \Omega_{\text{mn}} = (\omega^2 - \omega_{\text{mn}}^2 - 2i\alpha\omega)\ . \tag{3.14}$$

We can now split Λ_{tot} into its real and imaginary parts,

$$\Re\{\Lambda_{\text{tot}}\} = \sum_{m,n}^{\infty} K_{\text{mn}}(\omega^2 - \omega_{\text{mn}}^2)/[(\omega^2 - \omega_{\text{mn}}^2)^2 + 4\alpha^2\omega^2]\ , \tag{3.15}$$

$$\Im\{\Lambda_{\text{tot}}\} = \sum_{m,n}^{\infty} K_{\text{mn}} 2\alpha\omega/[(\omega^2 - \omega_{\text{mn}}^2)^2 + 4\alpha^2\omega^2]\ . \tag{3.16}$$

$\Re\{\Lambda_{\text{tot}}\}$ and $\Im\{\Lambda_{\text{tot}}\}$ have been plotted for *Gekko* and *Varanus* in Figs. 3.1a and 3.1b, respectively. We see that, for a certain frequency f_*, $\Re\{\Lambda_{\text{tot}}\} = 0$. In Sec 3.4 we have also shown that exactly at $f = f_*$ the internal time difference iTD becomes equal to the interaural time difference ITD. Furthermore, it is possible to measure the corresponding iLD at f_*. Using the definition (3.11) of the membrane vibration-amplitude ratio at f_* and recalling that $\rho c^2 k L \Lambda_{\text{tot}}/V_{\text{cav}}\big|_{f=f_*} = i\eta$, we obtain

$$\begin{aligned} \text{iLD}|_{f=f_*} &= 20\log_{10}\left|\frac{u_L^{\text{ave}}}{u_0^{\text{ave}}}\right| = 20\log_{10}\frac{1+\eta}{1-\eta} \\ \Rightarrow \eta &= \frac{10^{\text{iLD}/20}-1}{10^{\text{iLD}/20}+1}\ . \end{aligned} \tag{3.17}$$

Thus, by measuring the iLD at f_*, we can calculate the imaginary part of the membrane frequency response as well. We should also note here that η is a dimensionless quantity. The

resulting *non-linear* equations in α and ω_{mn} are given by

$$\Re\{\Lambda_{\mathrm{tot}}\}|_{f=f_*} = \sum_{m,n}^{\infty} \frac{K_{\mathrm{mn}}(\omega_*^2 - \omega_{\mathrm{mn}}^2)}{(\omega_*^2 - \omega_{\mathrm{mn}}^2)^2 + 4\alpha^2\omega_*^2} = 0 \tag{3.18}$$

$$\Im\{\Lambda_{\mathrm{tot}}\}|_{f=f_*} = \sum_{m,n}^{\infty} \frac{K_{\mathrm{mn}} 2\alpha\omega_*}{(\omega_*^2 - \omega_{\mathrm{mn}}^2)^2 + 4\alpha^2\omega_*^2} = \frac{\eta V_{\mathrm{cav}}}{\rho c L \omega_*} \tag{3.19}$$

where $\omega_* = 2\pi f_*$. We have also used the fact that $k = \omega/c$. Given the above equations, the problem boils down to calculating $f_0 = \omega_{11}/2\pi$ and α as the remaining eigenfrequencies are related to the fundamental eigenfrequency by $f_{\mathrm{mn}}/f_0 = \omega_{\mathrm{mn}}/\omega_{11} = \mu_{\mathrm{mn}}/\mu_{11}$. Here μ_{mn} is the n$^{\mathrm{th}}$ zero of the order κ Bessel function of the first kind J_κ; cf. (2.30).

Having determined f_* as well as η through the corresponding iLD based on membrane vibration amplitudes, it would be possible to use (3.18) and (3.19) to obtain estimates for f_0 and α. This can be done by using standard iterative algorithms to find the roots of functions. A common example is the Newton-Raphson method [82, Ch. 5]. For a real-valued function f, in order to find an approximation for its roots $x : f(x) = 0$ we start with an initial guess of x_0. A better approximation for x is then given by

$$x_1 = x_0 - \frac{f(x_0)}{f'(x_0)}$$
$$x_{n+1} = x_n - \frac{f(x_n)}{f'(x_n)} \, .$$

To find a root for a system of two equations $(x,y) : g_1(x,y) = 0,\ g_2(x,y) = 0$ in two dimensions, we would instead need to calculate the appropriate Jacobian matrix,

$$\mathbb{J} = \begin{pmatrix} \frac{\partial g_1}{\partial x} & \frac{\partial g_1}{\partial y} \\ \frac{\partial g_2}{\partial x} & \frac{\partial g_2}{\partial y} \end{pmatrix} .$$

The corresponding iteration rule is given by

$$\begin{pmatrix} x_{n+1} \\ y_{n+1} \end{pmatrix} = \begin{pmatrix} x_n \\ y_n \end{pmatrix} - \mathbb{J}^{-1} \begin{pmatrix} g_1(x_n, y_n) \\ g_2(x_n, y_n) \end{pmatrix} . \tag{3.20}$$

In dimensions higher than 2, it is more feasible to multiply both sides of (3.20) by $\mathbb{J}$ and to solve the resulting system. Since we only need to estimate two values, the inverse of the Jacobian can be easily calculated. The relevant variables for our numerical problem are

$x = f_0$ and $y = \alpha$ and the corresponding equations are given by

$$g_1(f_0, \alpha) = \Re\{\Lambda_{\text{tot}}\}|_{f=f_*} = 0 \tag{3.21}$$

$$g_2(f_0, \alpha) = \Im\{\Lambda_{\text{tot}}\}|_{f=f_*} - \frac{\eta V_{\text{cav}}}{\rho c L \omega_*} = 0\,. \tag{3.22}$$

Furthermore, the derivatives needed to calculate the Jacobian are given by

$$\frac{\partial \Re\{\Lambda_{\text{tot}}\}}{\partial f_0} = \frac{2}{f_0} \sum_{m,n}^{\infty} \frac{K_{\text{mn}} \omega_{\text{mn}}^2 ((\omega_*^2 - \omega_{\text{mn}}^2)^2 - 4\alpha^2 \omega_*^2)}{|\Omega_{\text{mn}}^*|^4}\,, \tag{3.23}$$

$$\frac{\partial \Re\{\Lambda_{\text{tot}}\}}{\partial \alpha} = 8\alpha\omega_*^2 \sum_{m,n}^{\infty} \frac{K_{\text{mn}} (\omega_*^2 - \omega_{\text{mn}}^2)}{|\Omega_{\text{mn}}^*|^4}\,, \tag{3.24}$$

$$\frac{\partial \Im\{\Lambda_{\text{tot}}\}}{\partial f_0} = \frac{8\alpha\omega_*}{f_0} \sum_{m,n}^{\infty} \frac{K_{\text{mn}} (\omega_*^2 - \omega_{\text{mn}}^2) \omega_{\text{mn}}^2}{|\Omega_{\text{mn}}^*|^4}\,, \tag{3.25}$$

$$\frac{\partial \Im\{\Lambda_{\text{tot}}\}}{\partial \alpha} = 2\omega_* \sum_{m,n}^{\infty} \frac{K_{\text{mn}} ((\omega_*^2 - \omega_{\text{mn}}^2)^2 - 4\alpha^2 \omega_*^2)}{|\Omega_{\text{mn}}^*|^4}\,. \tag{3.26}$$

Where, $\Omega_{\text{mn}}^* = (\omega_*^2 - \omega_{\text{mn}}^2 - 2i\alpha\omega_*)$. The Newton-Raphson method converges quadratically to the correct value of the root.

In order to simplify the estimation of the relevant parameters, it would be more prudent to separate the dependence on the size of the membrane from terms that arise independently in the mathematical analysis. Specifically, we aim to express the coefficients K_{mn} as given by Eq. (3.14) in a way that the dimensional dependence of the membrane parameters is separated from non-dimensional factors arising from the integrals of Bessel functions. Writing the integrals in the numerator and denominator explicitly we obtain

$$\begin{aligned}
\int dS\, u_{\text{mn}} &= \int_{\beta}^{2\pi-\beta} \sin\kappa(\phi-\beta)\, d\phi \int_0^{a_{\text{tymp}}} r J_\kappa(\mu_{\text{mn}} r)\, dr \\
&= \frac{1}{\kappa}\left[1 - \cos m\pi\right] \int_0^{a_{\text{tymp}}} r J_\kappa(\mu_{\text{mn}} r)\, dr \\
&= \frac{a_{\text{tymp}}^2}{\kappa}\left[1 - \cos m\pi\right] \int_0^1 \tilde{r} J_\kappa(a_{\text{tymp}} \mu_{\text{mn}} \tilde{r})\, d\tilde{r}\,, \qquad (3.27) \\
\int dS\, u_{\text{mn}}^2 &= \int_{\beta}^{2\pi-\beta} \sin^2\kappa(\phi-\beta)\, d\phi \int_0^{a_{\text{tymp}}} r J_\kappa^2(\mu_{\text{mn}} r)\, dr \\
&= (\pi-\beta) \int_0^{a_{\text{tymp}}} r J_\kappa^2(\mu_{\text{mn}} r)\, dr \\
&= (\pi-\beta) a_{\text{tymp}}^2 \int_0^1 \tilde{r} J_\kappa^2(a_{\text{tymp}} \mu_{\text{mn}} \tilde{r})\, d\tilde{r} \qquad (3.28)
\end{aligned}$$

where $\tilde{r} = r/a_{\text{tymp}}$. Recall that $a_{\text{tymp}} \times \mu_{\text{mn}}$ corresponds to the n$^{\text{th}}$ zero of J_κ. We have thus separated the geometrical parameter a_{tymp} from the Bessel integrals in (3.27) and (3.28). Furthermore, we see that the integral in (3.27) is non-zero (and equal to 2) only for odd values of m as $\cos m\pi = 1$ for even m.

For $\kappa[m] = 0.5\ m\pi/(\pi-\beta)$, $m = 1,3,5\ldots$, we can rewrite K_{mn}

$$
\begin{aligned}
K_{\text{mn}} &= \frac{16}{\pi^2}\frac{S_{\text{tymp}}}{\rho_{\text{M}} d_{\text{M}}}\widetilde{K}_{\text{mn}}\ , \\
\widetilde{K}_{\text{mn}} &= \frac{\left(\int_0^1 \tilde{r} J_\kappa(a_{\text{tymp}}\mu_{\text{mn}}\tilde{r})\, d\tilde{r}\right)^2}{m^2 \int_0^1 \tilde{r} J_\kappa^2(a_{\text{tymp}}\mu_{\text{mn}}\tilde{r})\, d\tilde{r}}\ .
\end{aligned}
\tag{3.29}
$$

where $S_{\text{tymp}} = (\pi-\beta)a_{\text{tymp}}^2$ is the surface area of the tympanum. The values of $\widetilde{K}_{\text{mn}}$ for 20 modes are given in Table 3.2 and are arranged in a descending order of $K_{\text{mn}}/\mu_{\text{mn}}^2$, which is the value of Λ_{tot} at $f = 0$. The $\widetilde{K}_{\text{mn}}$ are independent of the size of the membrane and depend only on the extracolumellar angle β.

Numerical calculations in experimental practice

In practice we would need to choose an appropriate cutoff for the membrane eigenmodes. Ideally, we have to ensure that the last eigenmode has a frequency well above the hearing range of the animal. In order to test our method for the numerical estimation of f_0 and α, we performed simulations for *Gekko* and *Varanus* while using the first 70 membrane eigenmodes, with the 70^{th} mode corresponding to an eigenfrequency of around 11.7 kHz and 4.45 kHz for *Gekko* and *Varanus*, respectively; - well beyond the hearing range of either species. The estimated values of f_* and η are shown in Table 3.3. In a real-world experimental setup, these values would correspond to those estimated from measured membrane vibration amplitudes and phases.

We seek to test the accuracy of our method by assuming that the values calculated for 70 modes were obtained from a hypothetical experiment. This way we can test the performance of the algorithm in case the experimenter only chooses a limited number of modes. To do so, we would first need initial guesses for f_0 and α. For the fundamental frequency we can take f_* itself as an initial guess for f_0, as eyeballing the iTD plots tells us that the values are fairly close to each other; cf. Figs. 3.6a & 3.6b. Based on the behavior of the membrane response as shown in Figs. 3.3a & 3.3b, one can conclude that the system is overdamped for *Gekko*

Table 3.2 Numerical parameters needed for estimating f_0 and α

m	n	$\mu_{\text{mn}} \times a_{\text{tymp}}$	$\widetilde{K}_{\text{mn}}$
1	1	3.16602	.3833
3	1	4.56064	.04463
5	1	5.87051	.01583
7	2	6.30889	.02812
9	1	7.13348	7.822×10^{-3}
11	2	7.79759	4.13×10^{-4}
13	1	8.36586	4.56×10^{-3}
15	2	9.21062	5.666×10^{-8}
17	3	9.45094	.03299
19	1	9.57637	2.938×10^{-3}
21	2	10.5742	3.541×10^{-5}
23	1	10.7703	2.026×10^{-3}
25	3	10.9788	4.775×10^{-3}
27	2	11.9022	6.028×10^{-5}
29	1	11.9512	1.467×10^{-3}
31	3	12.443	2.01×10^{-3}
33	4	12.5928	8.459×10^{-3}
35	1	13.1214	1.103×10^{-3}
37	2	13.2033	6.768×10^{-5}
39	3	13.8616	1.135×10^{-3}

Table 3.3 Estimated f_* and η

	Gekko	*Varanus*
f_*	1097.78 Hz	402.664 Hz
η	0.666	1.697

and underdamped for *Varanus*. The value of the damping in the former would be $> \omega_*/4$ and $< \omega_*/4$ in the latter, where $\omega_* = 2\pi f_*$.

Given an initial guess, we can calculate the values of $\Re\{\Lambda_{\text{tot}}\}$ and $\Im\{\Lambda_{\text{tot}}\}$ at these values of f_0 and α from Eqs. (3.18) and (3.19). The value of the Jacobian can similarly be calculated by plugging these values into Eqs. (3.23)–(3.26) along with the values of $\widetilde{K}_{\text{mn}}$ given in Table 3.2. Thereafter one can iteratively use the Newton-Raphson method (3.20) until a suitable convergence is reached.

The simulation was performed for $\text{N}_{\text{modes}} = 1,\ 2,\ 5,\ 10,\ 15,\ 20,$ and 25 modes. The results of the simulation are presented in Table 3.4. For both *Gekko* and *Varanus* we see that, with an increasing number of eigenmodes used, the values converge to the quantities defined in Table 3.1. The slower convergence and apparent oscillation in α for *Gekko* is

Table 3.4 Simulation Results

	Gekko		*Varanus*	
N_{modes}	f_0 (Hz)	α (s^{-1})	f_0 (Hz)	α (s^{-1})
1	1097.78	2490.72	402.664	347.637
2	1074.34	2589.08	401.074	349.942
5	1058.12	2611.35	400.333	350.108
10	1052.66	2612.18	400.108	350.046
15	1051.89	2612.09	400.077	350.034
20	1051.02	2611.87	400.041	350.02
25	1050.92	2611.84	400.037	350.018
Exact	1050	2611.45	400	350

due to the higher value of its damping, which causes a greater difference between f_* and f_0. However, we must be careful while choosing initial guesses for *Varanus* as its lower damping results in a larger number of extrema and roots, and a simulation might converge to a point corresponding to a higher eigenmode. In practice, five modes are more than sufficient for good convergence in both f_0 and α. As a side remark, we need to emphasize that the numbers behind the decimal point in Tables 3.3 and 3.4 are experimentally irrelevant, but have been presented in order to demonstrate the accuracy of the numerical procedure.

Focusing on f_0 in particular, as a rule of thumb one can take the location of the minimum of the contralateral eardrum amplitude f_*, which is equivalent to the frequency of maximum iLD, as the fundamental frequency f_0; the error between f_* and f_0 is at most 5% [48]. Determining the damping coefficient α is slightly more involved. The procedure outlined in Eqs. (3.18)–(3.29) gives us a systematic method to approximate α from the membrane vibrations for an arbitrary number of modes. In Table 3.4, we see that assuming f_* to be the fundamental frequency, which is equivalent to assuming $f_0 = f_*$, gives us a value of α with an error of at most 5%. Taking into account the second mode further reduces the error to within 1%. In fact, for the case of a single mode, the expression for α can be written down explicitly by substituting $\omega_0 = \omega_{11} = \omega_*$ in (3.19) giving us

$$\frac{K_{11}}{2\alpha\omega_*} = \frac{\eta V_{\text{cav}}}{\rho c L \omega_*} \,. \tag{3.30}$$

$$\Rightarrow\ \alpha = \frac{\rho c L K_{11}}{2\eta V_{\text{cav}}} = \frac{8\rho c L}{\pi^2 V_{\text{cav}}} \frac{\mathscr{S}_{\text{tymp}}}{\rho_{\text{M}} d_{\text{M}}} \frac{\widetilde{K}_{11}}{\eta} \,. \tag{3.31}$$

We thus have (3.31) as an expression for the membrane damping coefficient α given only the geometrical and material parameters (thickness and density) of the membrane and cavity and η – the iLD measurement at a given frequency. Moreover, apart from the relative ease of

measurement, the above expression would provide a reasonably accurate estimate for α from a realistic eardrum.

3.7 Conclusion

In conclusion, the present chapter dealt with the frequency and directional behavior of the quantities derived in Chap. 2 and the hearing cues generated by them, namely the *internal* time and level differences (iTD & iLD). We began in Sec. 3.1, by comparing the transmission gain, i.e. the relative response at one eardrum to an isolated input at the opposite eardrum, derived using the ICE model to experimentally measured values. The results agreed with values measured for the Tokay gecko and the common house gecko, *Hemidactylus frenatus*; see Figs. 3.2a and 3.2b. In the subsequent analysis we included newer data from the Asian water monitor *Varanus salvator*. The individual membrane vibration velocities of the coupled system were compared to, and showed good agreement with experimentally measured values in Sec. 3.2; cf. Figs. 3.3a and 3.3b. The directionality of the eardrum vibrations was further illustrated through polar plots in Figures 3.4a and 3.4b. Furthermore, the vibration patterns of the eardrum surface showed a characteristic asymmetry, agreeing with values measured using laser vibrometry for the Tokay gecko; see Figs. 3.5a and 3.5b. The frequency and direction dependence of the iTD & iLD, was discussed in Sec. 3.3 and the internal time difference was found to be nearly flat at low frequencies, irrespective of the sound source direction, and thus mirrored the behavior of the interaural time difference (ITD). Close to the membrane fundamental frequency f_0, the iTD sharply drops and thereafter becomes equal to the ITD at higher frequencies, thus showing a low-pass frequency behavior. In other words, at low frequencies, the time dilation factor (TDF), or the ratio of the internal and interaural time difference, is independent of direction and frequency; see Figs. 3.6a and 3.6b. In contrast, the iLD was found to show a band-pass behavior, where it rose sharply from zero at low frequencies, peaking close to f_0, and dropping sharply thereafter; see Figs. 3.7a and 3.7b. Moreover, both the iTD and iLD were shown to be positive for positive values of the direction θ, and vice versa. Thus, the eardrum fundamental frequency f_0 forms a natural segregation of frequencies at which iTDs and iLDs are dominant.

Interestingly, it was also found that the frequency behavior of the hearing cues showed parallels to that of the membrane frequency response Λ, with the iTD corresponding to its real part and the iLD to its imaginary part; cf. Figs. 3.1a and 3.1b & Sec. 3.4. The properties of Λ therefore allowed us to estimate the transition frequency f_* as the frequency at which iTD=ITD. By comparing the results for *Varanus* and Tokay, it was found that the flatness of the iTD response, as well as the peak of the iLD response strongly depend on α. As stated in

Sec. 2.1.2, the cavity volume V_{cav} can be treated as an independent parameter in ICE. This fact was used in Sec. 3.5 to analyze the dependence of the hearing cues, i.e. iTD and iLD, on V_{cav}. It was found that, reducing V_{cav} "strengthened" the interaural coupling by increasing the iTD and iLD, while simultaneously sharpening the latter's peak until a critical volume V_{crit} was reached. It was thus shown that an animal with ICE would need a cavity volume bigger than V_{crit} to optimally exploit its interaural coupling. Finally, in Sec. 3.6, by using the aforementioned properties of Λ, we devised an experimental and numerical procedure to directly estimate f_0 and the membrane damping α from the measured hearing cues in a living animal with ICE. Finally, for the damping α a simple estimate, requiring only measured values of membrane material and geometrical parameters, was also derived (3.31).

Chapter 4

ICE-like Systems

The theory of ICE was initially [49, 50] developed to explain the enhancement of sound localization cues in terrestrial animals hearing at typically low frequencies. The previous two chapters and Vedurmudi et al. [12, 48] dealt with constructing a mathematical and geometrical model for internally coupled ears based on data from two extant lizards, the Tokay gecko and the water monitor *Varanus*; cf. Chapters 2 and 3. In the present chapter, we focus on animals equipped with ICE that utilize the interaural coupling in ways considerably different from those of the lizards. In particular, we will focus on the fully aquatic African clawed frog *Xenopus laevis* [57] and the barn owl *Tyto alba* [56] with its remarkably high range of hearing frequencies. The "small-animal problem" associated with lizards in air would be further exacerbated underwater, where the sound velocity (and thus the wavelength) is approximately four times greater than in air, causing both ITD and ILD cues to be further diminished. However, despite its small size, *Xenopus* communicates by underwater sound and has a rich vocal repertoire [83–85]. Receptive females approach calling males [86] and special adaptations for underwater hearing and sound localization would thus be of utmost importance. Barn owls, which also possess an interaural coupling [56], use frequencies between 3 and 9 kHz to locate prey [87] with a remarkably low localization error of less than 2° in azimuth [88]. Communication calls of adult barn owls, on the other hand, are limited to frequencies below 3 kHz [89]. Although the barn owl interaural cavity was initially thought to play no role in sound localization [90], it has since been shown that for a narrow band at lower frequencies (1.5 to 3 kHz) there is sound transmission through the interaural canal that induces considerable directionality in the eardrums [56]. Thus, while the barn owl can utilize ICE for interspecific communication at lower frequencies, their high range of hearing frequencies suggests that the resonances of their interaural cavity can play a significant role in their hearing.

The present chapter deals with the very different auditory problems faced by *Xenopus* and the barn owl, albeit with remarkably similar solutions. In spite of serving very different purposes with regards to sound localization, the interaural cavities of both animals share geometric similarities and, as a result, can be described using similar physical principles. A key similarity in the cavity geometry for both animals is the presence of a third air-filled chamber medially connected to the interaural cavity. In the barn owl, the cavity of the sphenoid bone [91] plays this role, whereas in *Xenopus*, the lungs themselves are directly connected to the interaural cavity [57]. In this chapter, the medially connected cavity will be treated as a Helmholtz resonator driven by the motion of air in the interaural cavity. The acoustics of a Helmholtz resonator has previously been used [29, 92] to describe the middle ear and mouth cavity of frogs with respect to *terrestrial* hearing. In the present chapter, however, we will see how the *Xenopus* eardrum, as well as the medial connection to its lungs are adaptations to its *underwater* environment. The central role played by the lung volume in generating underwater iLD cues, as well as in improving hearing sensitivity at frequencies relevant to the mating behavior of *Xenopus* will be demonstrated. Furthermore, the interaural cavities of both animals are too narrow to be described using the cylindrical model of Section 2.1.2. As a result, a modified description of the interaural cavity will also be introduced. In the case of *Xenopus*, we will also introduce a different model to account for the special construction of its eardrum. In contrast, the barn owl interaural cavity, along with attached Helmholtz resonator will be shown to generate iLDs in the lower frequency region of its hearing, while also improving iTDs for its higher hearing frequencies – in stark contrast to the lizards. We will also see the importance of "tuning" the volume of the resonator with respect to hearing and sound localization, in both *Xenopus* and the barn owl.

4.1 Eardrum

We will now describe the middle-ear systems of *Xenopus* and the barn owl. The majority of the present section deals with *Xenopus*'s plate-like eardrum and its mechanical properties, while accounting for the surrounding medium, i.e. water. As the barn owl eardrum is geared to hearing in air, and is thus anatomically similar to those of most reptiles and birds, we will limit ourselves to a brief recap of the eardrum vibrations derived in Section 2.2.1.

4.1.1 *Xenopus*

The *Xenopus* eardrum is unusual compared to those of other animals with ICE as well as to those of other frogs [93]. Instead of a flexible tympanic membrane, they possess a

cartilaginous tympanic plate behind the eye covered by skin and fatty tissue [94]. The plate is suspended around its periphery in a cartilaginous annular membrane [95]; cf. Figs. 4.1a and 4.1b. Rather than being deformed by an external sound stimulus like typical eardrums, the tympanic plate moves as a whole within the thin annular cartilaginous ring [57]. The *pars media*, or the shaft of the stapes is attached centrally to the tympanic plate and transmits the vibrations of the tympanic plate to the inner ear via the columella; cf. Fig. 4.1b.

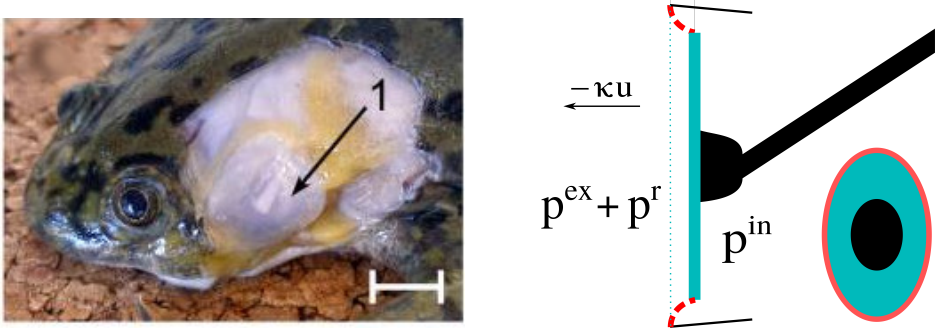

(a) Xenopus tympanic plate (b) Schematic model

Fig. 4.1 (a) Tympanic plate of *Xenopus laevis* after removal of the skin and fat layer. The pars media of the stapes can be discerned through the cartilaginous disc. Scale bar denotes 5 mm; adapted from Mason et al. [95]. (b) Schematic (see inset) and motion of the tympanic plate (thick/blue) driven by an external (p^{ex}) and internal (p^{in}) pressure and displaced from its resting position (dotted/blue). The tympanic plate also experiences a pressure (p^{r}) due to acoustic radiation into the water surrounding *Xenopus*. The restoring force, which is provided by the tympanic annulus (dashed/red) has been quantified as a stiffness κ and is a function of its Young's modulus E and the geometry. The inertial mass of the system includes that of the attached stapes and columella which are represented here in black.

We model the system of tympanic plate and annulus as a composite structure where the tympanic plate plays the role of a pressure receiver whereas the cartilaginous annulus provides a restoring force and thus, a natural vibration frequency to the system. Physically, this entails calculating the force exerted by the annulus given a deflection u of its inner radius. As we will see later in the present chapter, evolution has replaced the thin and decently flexible tympanic membrane by a rather massive plate as an adaptation for underwater hearing. In contrast to our earlier treatment (Sec. 2.1.1 and [12]) of eardrums as thin membranes, we therefore model the motion of the annulus as the bending of a thin annular plate subject to a small uniform deflection at its inner periphery. The deflection w of the surface of a circular *homogeneous* Kirchoff-Love plate with a load $q(r,\phi)$ (Force/Area) acting on its surface is

given by [96, p. 283]

$$D_m \Delta_{(2)}^2 w = q(r,\phi) \tag{4.1}$$

$$\Delta_{(2)} = \frac{1}{r}\frac{\partial}{\partial r} + \frac{\partial^2}{\partial r^2} + \frac{1}{r^2}\frac{\partial^2}{\partial \phi^2}\,, \tag{4.2}$$

where $\Delta_{(2)}$ is the two-dimensional Laplace operator, here taken in polar coordinates. For a plate of thickness h with Young's modulus E and Poisson ratio ν, $D_m = Eh^3/12(1-\nu^2)$ is its flexural rigidity. In our model, the cartilaginous ring is loaded only by the tympanic plate along its inner edge. Moreover, as the loading is uniform and the annulus is modeled as homogeneous, we can neglect the dependence of w on the angle ϕ.

The solution to (4.1) in the absence of a load on the surface of the annulus or, $q(r,\phi) = 0$, is given by

$$w(r) = C_1 \frac{r^2}{4}(2\log r - 1) + C_2 \log r + C_3 \frac{r^2}{2} + C_4\,. \tag{4.3}$$

The coefficients C_{1-4} are to be determined by the boundary conditions at the inner and outer radius, which we denote by a_1 and a_2, respectively. We first require the tympanic annulus to be rigidly clamped at its outer edge, resulting in a deflection with vanishing rotation about the horizontal edge. At the inner edge, the deflection of the ring w is fixed by the displacement of the tympanic plate u. Furthermore, at the inner edge, the bending moment M_{rr} vanishes. This gives us

$$w(r = a_2) = 0 \quad \& \qquad \left.\frac{\partial w}{\partial r}\right|_{r=a_2} = 0\,. \tag{4.4}$$

$$w(r = a_1) = u \quad \& \qquad M_{rr} = \left.\left(\frac{\partial^2 w}{\partial r^2} + \frac{\nu}{r}\frac{\partial w}{\partial r}\right)\right|_{r=a_1} = 0\,. \tag{4.5}$$

Applying the boundary conditions to (4.3) we obtain a set of linear equations for the coefficients C_{1-4}, with solutions

$$C_1 = \frac{4u\,\left[a_1^2(1+\nu) + a_2^2(1-\nu)\right]}{(a_2^2 - a_1^2)\left(a_1^2(3+\nu) + a_2^2(1-\nu)\right) - 4a_1^2 a_2^2 (\log a_2/a_1)(2-(1+\nu)\log a_2/a_1)} \tag{4.6}$$

$$C_2 = \frac{4u\,a_1^2 a_2^2\,[1-(1+\nu)\log a_2/a_1]}{(a_2^2 - a_1^2)\left(a_1^2(3+\nu) + a_2^2(1-\nu)\right) - 4a_1^2 a_2^2 (\log a_2/a_1)(2-(1+\nu)\log a_2/a_1)} \tag{4.7}$$

$$C_3 = \frac{4u\,\left[a_1^2 + a_1^2(1+\nu)\log a_1 + a_2^2(1-\nu)\log a_2\right]}{(a_2^2 - a_1^2)\left(a_1^2(3+\nu) + a_2^2(1-\nu)\right) - 4a_1^2 a_2^2 (\log a_2/a_1)(2-(1+\nu)\log a_2/a_1)} \tag{4.8}$$

$$C_4 = -C_1 \frac{a_2^2}{4}(2\log a_2 - 1) - C_2 \log a_2 - C_3 \frac{a_2^2}{2} \tag{4.9}$$

As the equation of motion is essentially linear, the above coefficients C_{1-4} are proportional to the deflection u at the inner edge.

The restoring force F at the edge in response to the deflection or, equivalently, the shear force [96, p. 53] of the annulus is given by

$$\frac{-F}{2\pi a_1} = D_m \frac{\partial}{\partial r}\left[\frac{1}{r}\frac{\partial}{\partial r}\left(r\frac{\partial w}{\partial r}\right)\right]\Bigg|_{r=a_1} \tag{4.10}$$

$$= \frac{2D_m C_1}{a_1}\,. \tag{4.11}$$

Comparing the above result with the expression for the coefficient C_1 in (4.6), we see that the restoring force F is linearly related to the deflection u through a coefficient of the form

$$\kappa = \frac{16\pi D_m\left[a_1^2(1+\nu)+(1-\nu)a_2^2\right]}{(a_2^2-a_1^2)\left[a_1^2(3+\nu)+a_2^2(1-\nu)\right]-4a_1^2a_2^2\left[2-(1+\nu)\log a_2/a_1\right]\log a_2/a_1}\,, \tag{4.12}$$

so that $F=-\kappa u$. In our model, the tympanic plate and annulus system therefore behaves as a harmonic oscillator with a spring constant κ. For a plate of mass m_p the resonant (angular) frequency is given by $\omega_0 = 2\pi f_0 = \sqrt{\kappa/m_\mathrm{p}}$. The inner radius a_1 is equal to the radius of the tympanic plate a_p, while the width of the tympanic annulus a_ann can be used to set the outer radius equal to $a_2 = a_\mathrm{p} + a_\mathrm{ann}$.

Let us take a tympanic plate of mass m_p and area S_p driven by an external pressure p^ex from the sound source and an internal pressure p^in due to the interaural coupling; see Fig. 4.1b. As a result of its vibrations, the tympanic plate also experiences a force f_r due to acoustic radiation into the medium – namely, water. The restoring force provided by the cartilaginous ring is equivalent to that of a spring of stiffness κ. Let $u_{0/L}(t)$ be the displacement of the tympanic plate from its mean position, with the subscripts $0/L$ denoting the eardrums at $x=0$ and $x=L$, respectively. The equation of motion of the plate is thus given by

$$m_\mathrm{p}\frac{d^2u_{0/L}}{dt^2} = S_\mathrm{p}\left(p^\mathrm{ex}-p^\mathrm{in}\right) + f_r - \kappa u_{0/L} - b\dot{u}_{0/L} \tag{4.13}$$

where b is an empirical damping coefficient and, as usual, we look for quasi-steady-state solutions of the form $u_{0/L}\exp(i\omega t)$. To do so, we now need to determine the radiative force f_r and internal pressure p^in in terms of the displacement $u_{0/L}$. Finally, after defining the acoustic head model, we will obtain sound inputs in the form of an external pressure p^ex which will be used to determine $u_{0/L}$. Eq. (4.13) is structurally similar to equation for the mechanical equivalent of the ICE model from Eq. (2.111); cf. Section 2.3.2. In the present

derivation however, the origin of the spring constant from the tympanic annulus (4.12) has been explicitly derived.

Acoustic radiation from the eardrum

As the external surface of the vibrating eardrum is continuously in contact with a fluid, i.e. water, we must account for the influence of the latter on the eardrum vibrations. The pressure field at a point $\mathbf{r}$ due to an arbitrary acoustic radiator vibrating with an angular frequency $\omega = 2\pi f$ can be computed by treating each infinitesimal area element of the radiator as a point source and integrating over the surface to give [97, p. 179]

$$p_r(\mathbf{r}) = \frac{i\rho_0\omega}{2\pi}\int_S \frac{v(\mathbf{r}')e^{-ik_wR}}{R}dS\,, \tag{4.14}$$

where ρ_0 is the density of the fluid and R is the distance between the point $\mathbf{r}$ and the area element dS at a point $\mathbf{r}'$ on the acoustic radiator, while $v(\mathbf{r}')$ is the vibrational velocity of the radiator surface at $\mathbf{r}'$. The wavelength $k_w = \omega/c_w$ is for sound waves in water with propagation speed c_w.

Let us now consider a circular piston of radius a vibrating harmonically with an angular frequency $\omega = 2\pi f$, while bounded on one side by a fluid of density ρ_0 and sound speed c_0. Let the piston's vibration amplitude in complex notation be $u\exp(i\omega t)$ so that its velocity is $v = i\omega u\,\exp(i\omega t)$. As we are interested in the pressure on the surface of the piston itself, R is the distance between dS and another element on the piston's surface dS'; see Fig. 4.2. The force on the element dS' is given by

$$df_r = -\frac{\rho_0\omega^2 u\,dS'}{2\pi}\int_S \frac{e^{-ik_wR}}{R}\,dS\,. \tag{4.15}$$

The net force is calculated by integrating the above equation over dS'. The integral can greatly simplified by using the acoustic reciprocity principle [97, p. 172], which states that the pressure created at dS' by a vibration at dS is equal to the pressure created at dS by a vibration at dS'. We define the infinitesimal elements as

$$dS = Rd\varphi dR, \quad dS' = r'd\psi dr'$$

and integrate dS over the circle of radius r', i.e. R from 0 to $2r'\cos\varphi$ and φ from $-\pi/2$ to $\pi/2$. Thus the interactions within the circle of radius r' have been accounted for. We then integrate dS' over the area of the piston, i.e., r' from 0 to a and ψ from 0 to π; cf. Fig. 4.2. Having calculated the interelement interaction once, we apply the reciprocity principle by

multiplying the result by two and rewrite the integral (4.15) in the form

$$f_r = -\frac{2\rho_0\omega^2 u}{2\pi}\int_{\psi=0}^{2\pi}\int_{r'=0}^{a}\int_{\varphi=-\pi/2}^{\pi/2}\int_{R=0}^{2r'\cos\varphi}\frac{e^{-ik_wR}}{R}\,(RdRd\varphi)(r'dr'd\psi)\;. \tag{4.16}$$

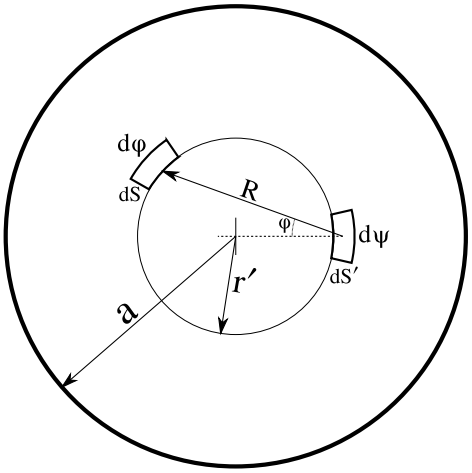

Fig. 4.2 Surface of a vibrating circular piston of radius a. As the piston is bounded by a fluid medium on one side, it behaves as an acoustic source with a characteristic pressure field in the half-space corresponding to the medium, including its own surface. Consequently, each piston surface element dS creates a pressure dp at the surface element dS'. The total force on the piston can be calculated by integrating over both elements using the acoustic reciprocity principle.

As the eardrum radius is of the order of 5 mm and typical hearing frequencies are below 3 kHz, we can reasonably assume that $k_w a \ll 1$ and, as a consequence, $\exp(ik_wR) \approx 1 + ik_wR$. In the low-frequency limit f_r then simplifies to the form

$$f_r \approx \omega\Gamma_r u \qquad \text{with} \qquad \Gamma_r = \rho_0 c_0 S_\mathrm{p}\left(\frac{8k_wa}{3\pi} - i\frac{(k_wa)^2}{2}\right)\;. \tag{4.17}$$

The above derivation is equivalent to a low frequency approximation for the acoustic radiation from a baffled circular piston [71, pp. 301–305]. The force exerted by the medium on the piston is thus proportional to the density ρ_0 and the sound speed c_0 in the medium, as well as to the amplitude u of vibrations. For low frequencies, the real part of Γ_r scales linearly with frequency and is equivalent to an added mass of $m_0 = 8\rho_0 S_\mathrm{p} a/3\pi$ on the surface of the piston. Taking a thickness d_p and density ρ_p for the piston, we find that the relative added mass is given by

$$\frac{m_0}{m_\mathrm{p}} = \frac{8}{3\pi}\frac{\rho_0 a}{\rho_\mathrm{p} d_\mathrm{p}} \tag{4.18}$$

where m_p is the piston mass. The density of air ($\rho_\mathrm{air} \approx 1.2\times10^{-3}$ g/cc) is small relative to that of living tissue, which has a density comparable to that of water. For example, the density of the tympanic membrane and the cartilaginous tympanic annulus in humans was found to be ≈ 1.2 g/cm^3 [98]. As a result, at low frequencies and for small piston radii, we can neglect f_r relative to the force exerted by a sound wave in air. A piston vibrating in water,

however, will be subjected to significant forces even at low frequencies. These forces will be accounted for in our subsequent treatment of underwater eardrum vibrations.

4.1.2 Barn owl

In general, both reptiles and birds show significant variation in anatomical structure of their middle-ears [4]. Nonetheless, they can functionally still both be described using the second-order lever system (see Figs. 2.4a&2.4b) consisting of a tympanic membrane, extracolumella and columella [27]; cf. Fig. 4.3. The barn owl eardrums are geared to terrestrial hearing and will be described, as in the case of the lizards (see Fig. 2.3b and Section 2.2.1), as a circular membrane asymmetrically loaded by the extracolumella; ref. Fig. 4.5b. Analogously to

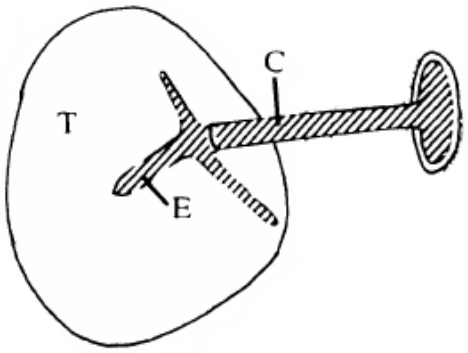

Fig. 4.3 Schematic diagram of a typical avian middle ear. The various processes of the extracolumella (E) are attached asymmetrically to the tympanic membrane (T). The motion of the tympanic membrane in response to a sound stimulus is transmitted via the columella (C) to the inner ear (not shown). Figure adapted from Manley and Gleich [99]. Compare with the gecko ear Fig. 2.3a.

the lizard eardrum, the vibration of the barn owl eardrum is also best described by means of a membrane frequency response Λ (2.97) such that for an input pressure $p\exp(i\omega t)$, the membrane displacement of an independent eardrum is given by $\Lambda p\exp(i\omega t)$. Recall that the membrane frequency response is defined in terms of the membrane modes u_{mn} as

$$\Lambda = \sum_{m,n}^{\infty} \frac{u_{mn}(r,\phi)\int u_{mn}}{\rho_{\mathrm{M}} d_{\mathrm{M}} \Omega_{mn} \int u_{mn}^2}\,, \quad \Lambda_{\mathrm{tot}} = \int_{\mathscr{S}_{\mathrm{mem}}} \Lambda(r,\phi)\,dS\,, \tag{4.19}$$

where $\Omega_{mn} = \omega^2 - \omega_{mn}^2 - 2i\alpha\omega$. As usual, ρ_{M} and d_{M} denote the membrane density and thickness, while ω_{mn} and α denote the eigenfrequency of the (m,n) mode and damping, respectively; cf. Table 2.1.

4.2 Interaural cavity

The cylindrical interaural cavity described in Sec. 2.1.2 allowed us, essentially, to express the cavity pressure as a single plane wave between the eardrums (2.66). While a general theory of ICE can be developed this way, a cylindrical interaural cavity does not provide an accurate

description of interaural coupling in all animals with ICE. Thus far, in our description of ICE, although the volume of the interaural cavity V_{cav} was analyzed as an independent parameter in Section 3.5, it cannot take arbitrary positive values and is bounded from below by the volume of the cylinder V_0 with radius a_{tymp} (2.1) and length L, where a_{tymp} is the radius of the eardrum and L is the interaural distance. In other words,

$$V_{\text{cav}} \geq V_0 \,, \tag{4.20}$$

$$V_0 = \pi a_{\text{tymp}}^2 L \,. \tag{4.21}$$

However, in animals like the African clawed frog *Xenopus laevis* and the barn owl *Tyto alba*, the interaural cavity volumes are far too small to be described by such a cylinder. In both cases, the interaural cavity becomes significantly narrower as one moves inwards from the eardrum [56, 57]; cf. Figs. 4.4a and 4.4b.

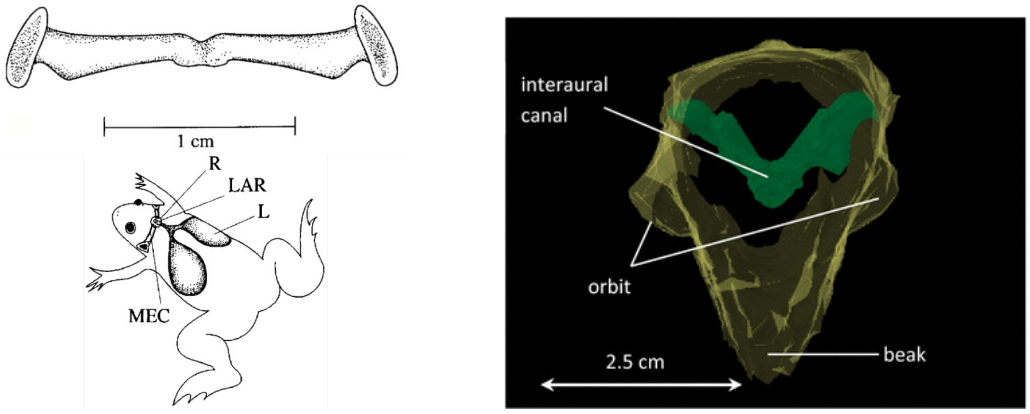

(a) *Xenopus* (b) Barn owl

Fig. 4.4 (a) Dental cement cast of the middle ear cavities in *Xenopus* (above) and schematic diagram of air filled cavities in a submerged *Xenopus* (below). The middle ear cavity (MEC) consists of two tympanic cavities that taper into a shared Eustachian tube which is medially connected to the lungs (L) through a recess (R) in the roof of the mouth. LAR denotes the larynx and is not relevant to our present discussion. Adapted from Christensen-Dalsgaard and Elepfandt [57]. In (a) we see a barn owl's skull from below generated by using CT scans. The interaural canal is the V-shaped structure (illustrated in green). The resulting length of the interaural canal is longer than the physical distance between the eardrums. The opening at the tip of the V-shaped structure into the mouth cavity is not shown. (adapted from Kettler et al. [56], courtesy K. L. Willis and C. E. Carr, University of Maryland).

In order to account for this discrepancy, we now propose a modified description of the interaural cavity. Instead of a single continuous cylinder, we separate the interaural cavity into two tympanic cavities (TC) coupled by means of a narrow "internal" canal (InC). Effectively,

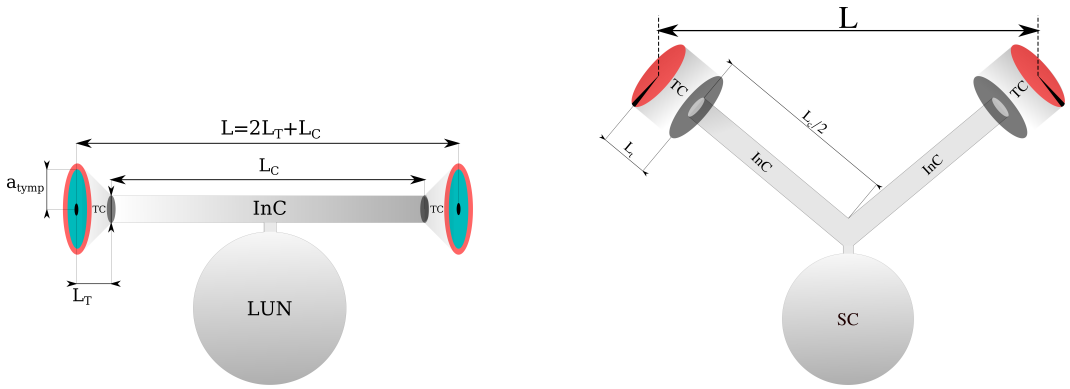

(a) *Xenopus* (b) Barn owl

Fig. 4.5 (a) ICE model schematic for the air-filled cavities in *Xenopus* based on Fig. 4.4a. The rigid cartilaginous tympanic plates (blue) are suspended in a flexible annular outer membrane (red); cf. Figs. 4.1a and 4.1b. The precise mechanics of the eardrums will be discussed in Section 4.1. The shallow tympanic cavities (TC) have a distinct taper in a direction away from the tympanic plates and are connected through a narrow *internal* canal (InC). In (b), we see the schematic interaural canal for the ICE model based on the three dimensional reconstruction of Fig. 4.4b. The circular tympanic membranes are illustrated in red, with the black sectors representing the extracolumella; cf. Fig. 2.3b. The cylindrical tympanic cavity TC has a larger cross section than the internal canal (InC). The barn owl interaural cavity length is greater than the interaural distance, $L > 2L_\mathrm{T} + L_\mathrm{C}$, while in *Xenopus*, they are equal. In both cases the two "arms" of the internal canal join in the middle and open into the lungs (LUN) for *Xenopus* and the sphenoid cavity (SC) for the barn owl, will be both be modeled as a single Helmholtz resonator. Compare with the "regular" ICE interaural cavity of Chapter 2; see Fig. 2.6b.

two *shallow* tympanic cavities of length L_T are coupled by a narrow canal with a circular cross section of radius a_C and total length L_C; see Figs. 4.5a and 4.5b. From the figures, we can see that there are two main distinctions between the interaural cavities of the two animals. Firstly, whereas for the Barn owl it suffices to model the tympanic cavity as a cylinder as well, Xenopus' tympanic cavity tapers sharply to join the interaural cavity and will thus be modeled as a truncated cone. The geometrical model of the tympanic cavities for the barn owl and *Xenopus* are illustrated in Figs. 4.6a to 4.6d. The second difference has to do with the length of the internal canal. In *Xenopus*, the two branches or arms of the internal canal can be assumed to be more-or-less horizontal, such that the total length of the interaural cavity (internal canal + tympanic cavities) between the eardrums is equal to the interaural distance, i.e., $L = L_\mathrm{C} + 2L_\mathrm{T}$; cf. Figs. 4.4a and 4.5a. On the other hand, the barn owl internal canal has a distinct V-shape (see Fig. 4.4b), such that the interaural distance is shorter than the total length of the interaural cavity, i.e., $L < L_\mathrm{C} + 2L_\mathrm{T}$; cf. Fig. 4.5b.

In both animals, the internal canal is separated into two "arms" or branches (0/L) by a medially attached air-filled cavity, although the anatomical origins of the cavities in both species are different. In *Xenopus*, the air-filled cavity represents the lungs that are attached to the canal at a recess in the roof of the mouth [57], whereas in the barn owl, the cavity represented is that of the sphenoid bone [91]. In both cases, we will be treating the cavity as a Helmholtz resonator [71, 100] medially attached to the internal canal. We distinguish the internal canal (InC) from the interaural cavity, such that the former represents the narrow air-filled connection between the tympanic cavities, whereas the latter denotes the entire air-filled connection between the eardrums. Note that, in our model, the medially attached cavity is treated separately from both the internal canal as well as the interaural cavity. The presence of the Helmholtz resonator precludes the treatment of the internal canal as a a single continuous cylinder. As we will see in Sec. 4.2.2, the presence of the medially connected cavity will necessitate the introduction of appropriate junction requirements at the connection. Thus, in our extension of ICE to *Xenopus* and the barn owl, the pressure in the two arms of the internal canal will be treated independently.

Cavity volume: Given the cavity volume V_{cav}, the interaural separation L, the tympanic cavity length L_{T} and the radius of the tympanic membrane or eardrum a_{tymp}, we can determine the length and L_{C}, and radius of the cylindrical canal a_{C} as dependent parameters, such that

$$a_{\text{C}} = \sqrt{\frac{V_{\text{cav}} - 2V_{\text{T}}}{\pi L_{\text{C}}}}, \qquad \text{where} \quad L_{\text{C}} = L - 2L_{\text{T}} \tag{4.22}$$

is the total length of the two arms of the internal canal and V_{T} is the volume of the tympanic cavity. In this way, the volume of the ICE model interaural cavity can be varied to conform to realistic cavity volumes as they occur in nature. Thus, in contrast to the cavity model described in Chapter 2 (cf. Fig. 2.6b), the present treatment of ICE accounts for the case when $V_{\text{cav}} < V_0 = \pi a_{\text{tymp}}^2 L$ by making the connecting canal narrower than the tympanic radius. As we will subsequently see in Sec. 4.5.2, we will also provide a physical explanation for the variance of the cavity acoustic resonances with volume, which was numerically estimated by Vossen [49] in the first mathematical treatment of ICE. In Sec. 2.2.2, the pressure and fluid velocity at the junctions will be subject to continuity requirements. Note that V_{cav} refers to the volume of the interaural cavity *excluding* the lungs/sphenoid cavity.

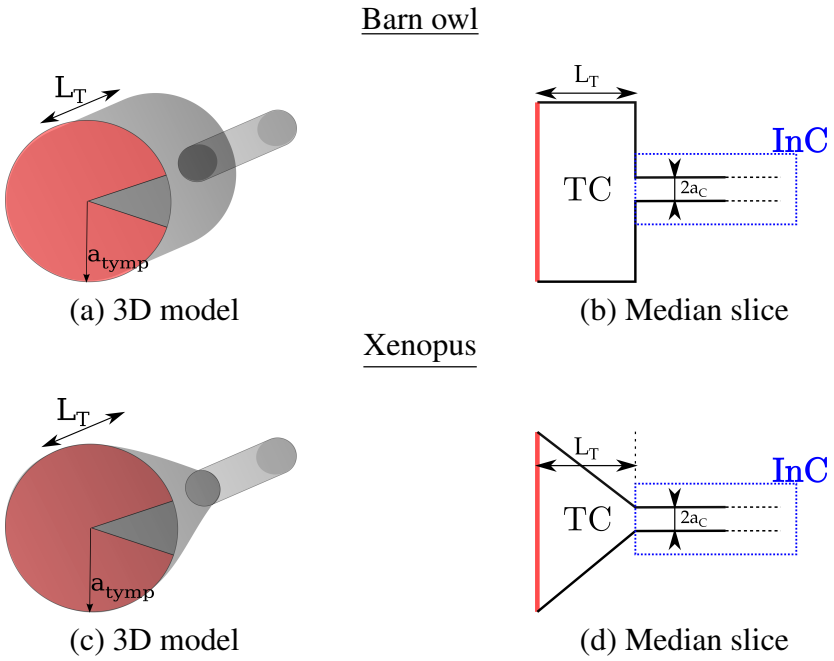

(a) 3D model (b) Median slice

(c) 3D model (d) Median slice

Fig. 4.6 3D view and median slice of the modified ICE tympanic cavity (TC) model for the barn owl (a)&(b) and *Xenopus* (c)&(b). As the total interaural cavity volume is "small", i.e. $V_{\text{cav}} < V_0$, where $V_0 = \pi a_{\text{tymp}}^2 L$ is the volume of the cavity corresponding to the first mathematical model for ICE [49, 50]; cf. Fig. 2.6a, the tympanic cavity is treated separately from the rest of the interaural cavity. For the barn owl the tympanic cavities are modeled as cylindrical in shape, whereas the shape of the *Xenopus* tympanic cavity model is conical. In both cases, the cavities of length L_{T} transition into a narrow "internal" canal (InC) of circular cross section with radius a_{C}. Compare Figures 2.6a and 2.6b

4.2.1 Cavity pressure

In the present section we will show that, as in the case of the lizard, the pressure in the interaural cavity can expressed in terms of coefficients $\Gamma_{\pm}$ (2.98) that relate the vibration velocity of the eardrum derived in Section 4.1 to the pressure on its internal surface for *Xenopus*, as well as for the barn owl. In order to derive $\Gamma_{\pm}$, we therefore need expressions for the internal pressures at the eardrum surfaces or, in terms of the tympanic cavity pressures, $p_{\text{T}}^0(x=0;t)$ and $p_{\text{T}}^L(x=L;t)$. As stated in the preceding section, the modified description of the interaural cavity requires us to treat the pressure in the different components independently of each another. For the barn owl, the cylindrical shape of both the tympanic cavity and the internal canals allows us to use the expressions derived in Sec. Section 2.2.2 to describe the internal sound pressure. Moreover, at our frequencies of interest, the variation in the radial and azimuthal directions can be neglected. As a result, at a given frequency $f = \omega/2\pi$, the

pressure p and particle velocity v in the internal can be described by plane waves,

$$p^{0/L}_{\mathrm{C/T}}(x;t) = (A^{0/L}_{\mathrm{C/T}} e^{ikx} + B^{0/L}_{\mathrm{C/T}} e^{-ikx}) \exp(i\omega t) \,, \tag{4.23}$$

$$v^{0/L}_{\mathrm{C/T}}(x;t) = \frac{-1}{\rho c}(A^{0/L}_{\mathrm{C/T}} e^{ikx} - B^{0/L}_{\mathrm{C/T}} e^{-ikx}) \exp(i\omega t) \,. \tag{4.24}$$

Recall that the pressure and particle velocity are related to each other via the linearization of the Euler equation (2.58). The subscripts C/T refer to the internal canal and the tympanic cavity, while the superscripts 0/L refer to the left and right halves of the system, respectively. The expressions en Eqs. (4.23) and (4.24) are also valid for both the branches of the *Xenopus* internal canal, as they are also cylindrical in shape. However, the conical geometry of the *Xenopus* tympanic cavity, necessitates the calculation of a different expression for its internal pressure.

Conical tympanic cavity

The propagation of acoustic waves in the conical tympanic cavity is modeled using Webster's horn equation [101, 102]. Here, as in the internal canal, the low frequencies allow us to assume that the wave only propagates along the axis in the x-direction as a plane wave with its wavefront perpendicular to the horn axis which represents the tympanic cavity (TC) in Figures 4.6c and 4.6d. For a horn whose cross section varies with the axis as $\chi(x)$, the 3D wave equation reduces to a 1D problem of the form [102]

$$\frac{1}{\chi(x)} \frac{d}{dx} \left(\chi(x) \frac{dp}{dx} \right) - \frac{1}{c^2} \frac{d^2 p}{dt^2} = 0 \,. \tag{4.25}$$

The acoustic wave equation is identical to the horn equation for a constant cross section. As in the case of the interaural canal, we seek pure tone solutions of the form $p(x)\exp(i\omega t)$.

Let the larger cross section of the tympanic cavity and that of the connecting canal be S_{p} and S_{C} , respectively. In a conical horn, the radius varies linearly along its axis or, equivalently, the cross section varies quadratically. The relative variation of the horn cross section with respect to the distance along the axis in the left and right tympanic cavities is given by

$$\frac{\chi_0}{S_{\mathrm{C}}} = \frac{(L_{\mathrm{T}} + l_{\mathrm{T}} - x)^2}{l_{\mathrm{T}}^2} \qquad \text{and} \qquad \frac{\chi_{\mathrm{L}}}{S_{\mathrm{C}}} = \frac{(l_{\mathrm{T}} + x - L_{\mathrm{C}} - L_{\mathrm{T}})^2}{l_{\mathrm{T}}^2} \,, \tag{4.26}$$

respectively. In the above equations we have defined $l_{\mathrm{T}} = L_{\mathrm{T}}\sqrt{S_{\mathrm{C}}}/(\sqrt{S_{\mathrm{p}}} - \sqrt{S_{\mathrm{C}}})$, where L_{T} and L_{C} are the lengths of the tympanic cavity and interaural canal, respectively; see also Fig. 4.5a.

For a pure tone of frequency $f = \omega/2\pi$, the spatial part of the solution to the horn equation (4.25) in the left and right tympanic cavities is given by,

$$p_{\mathrm{T}}^{0}(x) = \frac{A_{\mathrm{T}}^{0} e^{ikx}}{2ik(L_{\mathrm{T}} + l_{\mathrm{T}} - x)} + \frac{B_{\mathrm{T}}^{0} e^{-ikx}}{2ik(L_{\mathrm{T}} + l_{\mathrm{T}} - x)} \quad \text{and} \tag{4.27}$$

$$p_{\mathrm{T}}^{L}(x) = \frac{A_{\mathrm{T}}^{L} e^{ikx}}{2ik(l_{\mathrm{T}} + x - L_{\mathrm{T}} - L_{\mathrm{C}})} + \frac{B_{\mathrm{T}}^{L} e^{-ikx}}{2ik(l_{\mathrm{T}} + x - L_{\mathrm{T}} - L_{\mathrm{C}})}\,, \tag{4.28}$$

respectively. Finally, by using the pressure velocity relation obtained from the linearization of the Euler equation (cf. Eqs. (2.56)&(2.57)), we can also find the particle velocity in the left and right tympanic cavities,

$$v_{\mathrm{T}}^{0}(x) = \frac{A_{\mathrm{T}}^{0} e^{ikx}\left[1 + ikl_{\mathrm{T}}\sqrt{\frac{\chi_0}{S_{\mathrm{C}}}}\right]}{2\rho ck^2(L_{\mathrm{T}} + l_{\mathrm{T}} - x)^2} + \frac{B_{\mathrm{T}}^{0} e^{-ikx}\left[1 - ikl_{\mathrm{T}}\sqrt{\frac{\chi_0}{S_{\mathrm{C}}}}\right]}{2\rho ck^2(L_{\mathrm{T}} + l_{\mathrm{T}} - x)^2}, \tag{4.29}$$

$$v_{\mathrm{T}}^{L}(x) = \frac{A_{\mathrm{T}}^{L} e^{ikx}\left[-1 + ikl_{\mathrm{T}}\sqrt{\frac{\chi_L}{S_{\mathrm{C}}}}\right]}{2\rho ck^2(l_{\mathrm{T}} + x - L_{\mathrm{T}} - L_{\mathrm{C}})^2} - \frac{B_{\mathrm{T}}^{L} e^{-ikx}\left[1 + ikl_{\mathrm{T}}\sqrt{\frac{\chi_L}{S_{\mathrm{C}}}}\right]}{2\rho ck^2(l_{\mathrm{T}} + x - L_{\mathrm{T}} - L_{\mathrm{C}})^2}. \tag{4.30}$$

Flow across junctions

The expressions derived in Eqs. (4.23), (4.24) and (4.27) to (4.30) give us complete expressions for the internal pressure and particle velocity in the tympanic cavities and internal canal for both *Xenopus* and the barn owl. Thus, the problem of calculating the internal cavity pressure is reduced to finding expressions for the coefficients $A_{\mathrm{T/C}}^{0/L}$ and $B_{\mathrm{T/C}}^{0/L}$. As stated, in the start of the present section, we aim to derive coefficients $\Gamma_{\pm}$ that relate the internal pressure at the eardrum surface to eardrum vibration velocity. The procedure can be greatly simplified by expressing the tympanic cavity pressure coefficients on the left side, i.e., A_{T}^{0} and B_{T}^{L} in terms of those on the right side, i.e., A_{T}^{L} and B_{T}^{L}. To do so, we will first need to account the pressure and fluid particle velocity at the "junctions", which are essentially discontinuities in the cavity geometry –

1. The transitions between the tympanic cavity (TC) to the internal canal (InC), and
2. The three-way junction between the two arms of the internal canal and the Helmholtz resonator representing the lungs.

In general, the flow of air across a tube with an abrupt change in cross section results in a region of flow-separation and recirculation in the in the vicinity of such a junction and, as a

result, mechanical energy losses [103]. In case of fluid flow across a junction with an abrupt increase in cross section, the flow separates and a turbulent recirculating flow develops in the region immediately after the expansion as the flow cannot immediately follow the sharp bend in the pipe. see Fig. 4.7b. Similarly, in case of a sudden reduction in cross section, there are regions of flow separation and recirculation at the entrance of the narrower pipe. see Fig. 4.7a. The energy loss ΔE can be expressed in terms of the velocities $v_{1/2}$ at the denoted points in the flow using the Borda-carnot equation [103]

$$\Delta E = \xi \frac{1}{2} \rho (v_1^2 - v_1^2) \ . \tag{4.31}$$

ξ is an empirical loss coefficient and has a value between zero and one. Through numerical

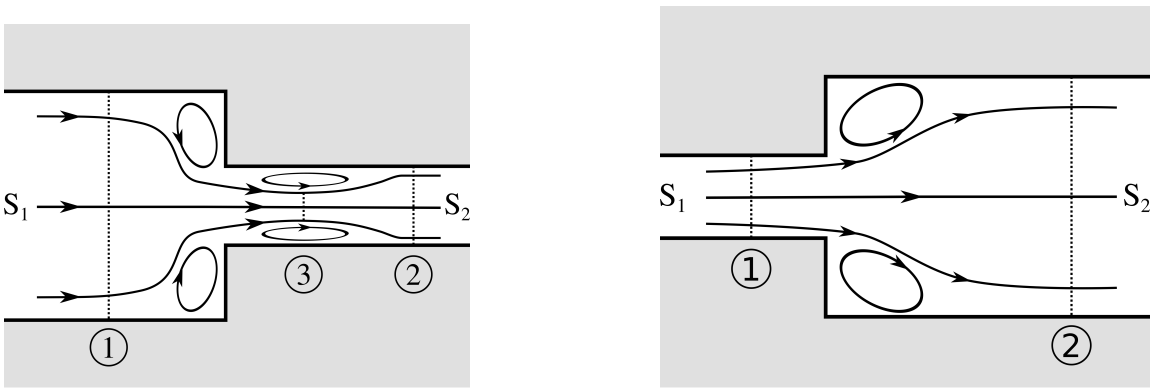

(a) Abrupt contraction (b) Abrupt expansion

Fig. 4.7 Flow through a canal across an (a) abrupt contraction and (b) abrupt expansion in cross section. The case of an abrupt expansion results in a recirculating flow in the vicinity of the change in cross section in the wider canal, while the case of an abrupt contraction results in recirculating flows being generated in both canals. The above behavior is, however, only significant at relatively high velocities. At typical flow velocities of linear acoustics (.02 Pa & .1 mm/s at 60 dB SPL), the region in which the recirculating flow takes place is small compared to the dimensions of the canal. In such a case, it suffices to equate the flow rates at points (1) and (2) in both (a) and (b).

simulations it is possible to show the emergence of vortices in the neighborhood of a sudden change in the cross section [104].

However, realistic flows generated by sound sources in nature are associated with low pressures and particle velocities (.02 Pa & 0.1 mm/s at 60 dB SPL). At these pressure amplitudes, the region in which the recirculating flow that takes place is extremely small compared to the size of the cavity. Moreover, the corresponding fluid flow velocities are of the order of 0.1 mm/s resulting in negligible losses across the junction. We therefore proceed

by requiring the pressure to be continuous across the junction and that the volume flow rate is conserved [101, chap. 8]. Recall that, for a canal of cross section S, the volume flow rate is given by $S \times v(x;t)$ (2.68).

Using the plane wave expressions for the pressure and velocity, we therefore can proceed with the solution for the coefficients by equating the pressure and conserving the volume flow at both the TC-InC junctions. Equating the pressure (cf. Eqs. (4.23), (4.27) and (4.28)) gives us

$$\frac{A_{\mathrm{T}}^0 e^{ikL_{\mathrm{T}}}}{2ik\, l_{\mathrm{T}}} + \frac{B_{\mathrm{T}}^0 e^{-ikL_{\mathrm{T}}}}{2ik\, l_{\mathrm{T}}} = A_{\mathrm{C}}^0 e^{ikL_{\mathrm{T}}} + B_{\mathrm{C}}^0 e^{-ikL_{\mathrm{T}}} \,, \tag{4.32}$$

$$A_{\mathrm{C}}^L e^{ik(L_{\mathrm{T}}+L_{\mathrm{C}})} + B_{\mathrm{C}}^L e^{-ik(L_{\mathrm{T}}+L_{\mathrm{C}})} = \frac{A_{\mathrm{T}}^0 e^{ik(L_{\mathrm{T}}+L_{\mathrm{C}})}}{2ik\, l_{\mathrm{T}}} + \frac{B_{\mathrm{T}}^0 e^{-ik(L_{\mathrm{T}}+L_{\mathrm{C}})}}{2ik\, l_{\mathrm{T}}} \,. \tag{4.33}$$

For *Xenopus*, the tympanic cavity tapers continuously to join the internal canal, such that the area of cross sections at the transition are equal. Therefore, equating the volume flow rate is equivalent to requiring the particle velocity (cf. Eqs. (4.24), (4.29) and (4.30)) be continuous such that,

$$\frac{A_{\mathrm{T}}^0 e^{ikL_{\mathrm{T}}}\,[1-ikl_{\mathrm{T}}]}{2k^2 l_{\mathrm{T}}^2} + \frac{B_{\mathrm{T}}^0 e^{-ikL_{\mathrm{T}}}\,[1+ikl_{\mathrm{T}}]}{2k^2 l_{\mathrm{T}}^2} = A_C^0 e^{ikL_{\mathrm{T}}} - B_C^0 e^{-ikL_{\mathrm{T}}} \,, \tag{4.34}$$

$$A_C^{\mathrm{L}} e^{ik(L_{\mathrm{T}}+L_{\mathrm{C}})} - B_C^0 e^{-ik(L_{\mathrm{T}}+L_{\mathrm{C}})} = \frac{A_{\mathrm{T}}^L e^{ik(L_{\mathrm{T}}+L_{\mathrm{C}})}\,[1-ikl_{\mathrm{T}}]}{2k^2 l_{\mathrm{T}}^2} + \frac{B_{\mathrm{T}}^L e^{-ik(L_{\mathrm{T}}+L_{\mathrm{C}})}\,[1+ikl_{\mathrm{T}}]}{2k^2 l_{\mathrm{T}}^2} \,, \tag{4.35}$$

where, we have used a single axis for the entire length of the interaural cavity, such that the junctions are present at $x = L_{\mathrm{T}}$ and $x = L_{\mathrm{T}} + L_{\mathrm{C}}$ along the axis.

For the barn owl, equating the pressure at the junctions gives us

$$A_{\mathrm{T}}^0 e^{ikL_{\mathrm{T}}} + B_{\mathrm{T}}^0 e^{-ikL_{\mathrm{T}}} = A_{\mathrm{C}}^0 e^{ikL_{\mathrm{T}}} + B_{\mathrm{C}}^0 e^{-ikL_{\mathrm{T}}} \,, \tag{4.36}$$

$$A_{\mathrm{C}}^L e^{ik(L_{\mathrm{T}}+L_{\mathrm{C}})} + B_{\mathrm{C}}^L e^{-ik(L_{\mathrm{T}}+L_{\mathrm{C}})} = A_{\mathrm{T}}^L e^{ik(L_{\mathrm{T}}+L_{\mathrm{C}})} + B_{\mathrm{T}}^L e^{-ik(L_{\mathrm{T}}+L_{\mathrm{C}})} \,. \tag{4.37}$$

As the transition between the tympanic canal (TC) and the connecting internal canal (InC) has an abrupt change in cross section, we need to equate the volume flow rate (2.68) the junctions and not the velocities as in the case of *Xenopus*, which results in,

$$S_{\mathrm{T}} \left(A_{\mathrm{T}}^0 e^{ikL_{\mathrm{T}}} - B_{\mathrm{T}}^0 e^{-ikL_{\mathrm{T}}} \right) = S_{\mathrm{C}} \left(A_{\mathrm{C}}^0 e^{ikL_{\mathrm{T}}} - B_{\mathrm{C}}^0 e^{-ikL_{\mathrm{T}}} \right) \,, \tag{4.38}$$

$$S_{\mathrm{C}} \left(A_{\mathrm{C}}^L e^{ik(L_{\mathrm{T}}+L_{\mathrm{C}})} - B_{\mathrm{C}}^L e^{-ik(L_{\mathrm{T}}+L_{\mathrm{C}})} \right) = S_{\mathrm{T}} \left(A_{\mathrm{T}}^L e^{ik(L_{\mathrm{T}}+L_{\mathrm{C}})} - B_{\mathrm{T}}^L e^{-ik(L_{\mathrm{T}}+L_{\mathrm{C}})} \right) \,, \tag{4.39}$$

where, as usual, the subscript "T" refers to the tympanic cavities and "C" refers to the connecting internal canal; cf. Figs. 4.6a to 4.6d. The direction convention introduced in Chapter 2 (cf. Fig. 2.6b) holds here as well such that directions outward from the interaural cavity are taken as positive. The axis of the interaural cavity is defined such that, $x = 0$ corresponds to the left eardrum and $x = L$ to the right eardrum. Thus, Equations (4.32) to (4.35) relate the coefficients of the tympanic cavity pressure to the internal cavity pressure for *Xenopus*, whereas Equations (4.36) to (4.39) do the same for the barn owl. Effectively, we now have four equations for the six coefficients $A_{\mathrm{C}}^{0/L}$, $B_{\mathrm{C}}^{0/L}$, A_{T}^{L} and B_{T}^{L} in terms of A_{T}^{0} and B_{T}^{0}. In order to eliminate the four cavity pressure coefficients $A_{\mathrm{C}}^{0/L}$, $B_{\mathrm{C}}^{0/L}$, we now need to account for the second junction in our model, i.e., the medially attached air-filled cavity.

4.2.2 The Helmholtz resonator

By analyzing the behavior of the medially attached lungs in the case of *Xenopus* and the sphenoid cavity in the case of the barn owl, we will be able to find a relation between the pressure in the left and right halves of the internal canal. In both cases, we treat the system of air-filled cavity coupled to the interaural canal (cf. Figs. 4.5a and 4.5b) as a Helmholtz resonator [105, p. 103]. In its essence, a Helmholtz resonator is an air-filled cavity of a given volume with an opening in the form of a short and narrow neck; Fig. 4.8. At wavelengths that are large compared to the dimensions of the resonator, the air inside the cavity essentially behaves as a spring with a characteristic resonance frequency f_{H}, which decreases with its volume; the exact relation will be derived in the following. As we will see later in the present chapter, this property of f_{H}, which was initially used to identify the frequency components in musical instruments [106, p. 44], plays a fundamental role in the sound localization ability of both *Xenopus* and the barn owl; cf. Sec. 4.5 .

In our treatment of the attached cavity, we require the resonator to have a volume V_{H}, which joins the two arms of the internal canal through a cylindrical neck of length L_{H} and cross section S_{H} (Fig. 4.8). The pressure and particle velocity at the mouth of the neck determine the appropriate requirements at the junction with the internal canal. Analogous to the junctions between the tympanic cavities and internal canals (Eqs. (4.32), (4.33), (4.36) and (4.37)), we require the continuity of the pressure at the junction of the internal canal and the Helmholtz resonator. Denoting the pressure at the mouth of the resonator by $p_{\mathrm{H}}^{\mathrm{out}}$, we have

$$p_{\mathrm{H}}^{\mathrm{out}} = p_{\mathrm{C}}^{0}(L_{\mathrm{T}} + L_{\mathrm{C}}/2) = p_{\mathrm{C}}^{L}(L_{\mathrm{T}} + L_{\mathrm{C}}/2) \; . \tag{4.40}$$

Moreover, analogously to Eqs. (4.34), (4.35), (4.38) and (4.39), the particle velocity v_{H} of air entering the neck of the Helmholtz resonator can be calculated by the conservation of the

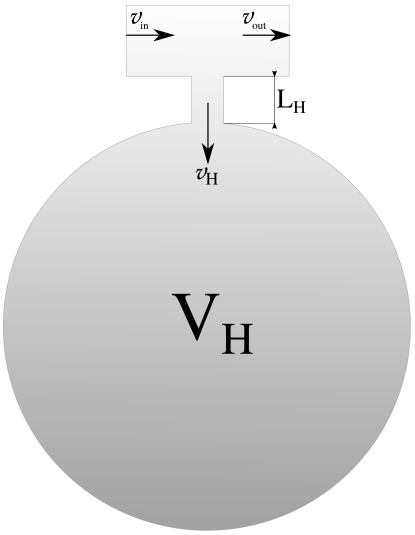

Fig. 4.8 Schematic for the Helmholtz resonator [105]. The resonating volume V_H is connected to a narrow neck of length L_H and cross section S_H. The velocity of air in the neck of the resonator v_H is given by the difference of the flow velocities in the outgoing (v_{out}) and incoming (v_{in}) canals. The resonating volume resists the movement of air in the neck akin to a mass-spring system and can be used to determine the pressure p_H at the mouth of the neck.

volume flow rate at the junction. The volume velocity of the air entering the resonator is thus given by the difference between the incoming and outgoing flow velocities of the internal canal (4.24) at the junction,

$$S_H v_H = S_C (v_{in} - v_{out}) = S_C \left(v_C^0 (L_T + L_C/2) - v_C^L (L_T + L_C/2) \right) \tag{4.41}$$

where S_H is the area of cross section of the neck of the resonator; cf. Fig. 4.8. The flow through the narrow and short neck can be assumed to be incompressible. Following Hirschberg and Rienstra [105] the Bernoulli equation for incompressible flow through the neck of the resonator gives us

$$\rho \frac{d\varphi}{dt} + p_H^{out} = p_H^{in} , \tag{4.42}$$

where $\varphi = \int_{in}^{out} v \, dx$ is the flow potential and p_H^{in} is the pressure at the base of the resonator. As we can neglect the variation of the flow velocity across the short neck length L_H, we can approximate the potential by $\varphi \approx v_H L_H$. Assuming a uniform change in density ρ^{in} inside the resonator, a linearization of the adiabatic equation of state (PV^γ =constant) gives $\rho^{in} = p_H^{in}/c^2$, where c is the speed of sound. The application of an integral mass conservation law to a cavity volume of V_H gives us

$$\frac{V_H}{c^2} \frac{dp_H^{in}}{dt} = -\rho S_H v_H . \tag{4.43}$$

After eliminating $p_{\mathrm{H}}^{\mathrm{in}}$ from Eqs. (4.42) and (4.43), we can relate velocity of air flow through the neck to and the pressure at the mouth of the neck $p_{\mathrm{H}}^{\mathrm{out}}$ through

$$\frac{V_{\mathrm{H}}L_{\mathrm{H}}}{c^2 S_{\mathrm{H}}}\frac{d^2 v_{\mathrm{H}}}{dt^2} + v_{\mathrm{H}} = \frac{-V_{\mathrm{H}}}{\rho c^2 S_{\mathrm{H}}}\frac{dp_{\mathrm{H}}^{\mathrm{out}}}{dt} \,. \tag{4.44}$$

For a quasi-steady-state flow the time dependence can be expressed as a factor of $\exp(i\omega t)$ and the above equations reduce to

$$\left(-\frac{k^2 V_{\mathrm{H}}L_{\mathrm{H}}}{S_{\mathrm{H}}} + 1\right) v_{\mathrm{H}} = \frac{-ikV_{\mathrm{H}}}{\rho c S_{\mathrm{H}}} p_{\mathrm{H}}^{\mathrm{out}} \,, \tag{4.45}$$

where, as usual, $k = \omega/c$ is the wave number. Finally, we equate the pressure at the ends of the outgoing and incoming canals to p_{H} and substitute the expressions for v_{H} from (4.41) and the pressure from (2.66) into (4.45) to relate pressure and velocity on the left and right halves of the interaural canal, which leads to the relation

$$\rho c \left(v_{\mathrm{C}}^0(L_{\mathrm{T}} + L_{\mathrm{C}}/2) - v_{\mathrm{C}}^L(L_{\mathrm{T}} + L_{\mathrm{C}}/2)\right) = \frac{-ikV_{\mathrm{H}}S_{\mathrm{C}}^{-1}}{1 - f^2/f_{\mathrm{H}}^2} p_{\mathrm{C}}^{0/L}(L_{\mathrm{T}} + L_{\mathrm{C}}/2) \,. \tag{4.46}$$

The right-hand-side of the above equation follows from Eq. (4.40). We have also defined

$$f_{\mathrm{H}} = c/2\pi\sqrt{S_{\mathrm{H}}/(L_{\mathrm{H}}V_{\mathrm{H}})} \,, \tag{4.47}$$

as the resonant frequency of the Helmholtz resonator. At f_{H} the connection between the left and right halves of the interaural canal is effectively broken. From the above equation, it should be clear that the resonance frequency f_{H} is inversely proportional to the square root of the resonator volume, such that in the absence of a resonator we have, $V_{\mathrm{H}} \to 0$ and, consequently, $f_{\mathrm{H}} \to \infty$.

4.2.3 $\Gamma_{\pm}$ coefficients

Using the expressions at the junction with the Helmholtz resonator (4.40),(4.40) with the pressure (Eqs. (4.32), (4.33), (4.36) and (4.37)) and velocity (Eqs. (4.34), (4.35), (4.38) and (4.39) continuity relations for *Xenopus* and the barn owl, we obtain six linear equations for both animals, such that six of the eight coefficients $A_{\mathrm{C}}^{0/L}$, $B_{\mathrm{C}}^{0/L}$ and $A_{\mathrm{T}}^{0/L}$, $B_{\mathrm{T}}^{0/L}$ can be expressed in terms of the remaining two. Accordingly, the pressure coefficients of the right tympanic cavity can be expressed in terms of the coefficients of the left tympanic cavity. This

can be compactly written as

$$\begin{pmatrix} A_{\mathrm{T}}^{L} e^{ikL} \\ B_{\mathrm{T}}^{L} e^{-ikL} \end{pmatrix} = M^{\mathrm{xen/owl}} \begin{pmatrix} A_{\mathrm{T}}^{0} \\ B_{\mathrm{T}}^{0} \end{pmatrix} \tag{4.48}$$

where $M^{\mathrm{xen/owl}}$ is a 2×2 matrix which depends on the geometry of the interaural cavity. The superscripts "xen" and "owl" denote *Xenopus* and the barn owl respectively. For *Xenopus*, the coefficients M_{ij}^{xen} of the matrix are given by

$$M_{11}^{\mathrm{xen}} = \frac{e^{ik2L_{\mathrm{T}}} \left[(1+\chi_{\mathrm{H}}) (1+\varsigma_{\mathrm{xen}})^2 e^{ikL_{\mathrm{C}}} - 2\chi_H (1+\varsigma_{\mathrm{xen}}) - (1-\chi_H) e^{-ikL_{\mathrm{C}}} \right]}{\varsigma_{\mathrm{xen}}^2} , \tag{4.49}$$

$$M_{22}^{\mathrm{xen}} = \frac{e^{-ik2L_{\mathrm{T}}} \left[(1-\chi_H) (1-\varsigma_{\mathrm{xen}})^2 e^{-ikL_{\mathrm{C}}} + 2\chi_H (1-\varsigma_{\mathrm{xen}}) - (1+\chi_H) e^{ikL_{\mathrm{C}}} \right]}{\varsigma_{\mathrm{xen}}^2} , \tag{4.50}$$

$$M_{12}^{\mathrm{xen}} = -M_{21}^{\mathrm{xen}} = \frac{\mathfrak{Q}}{\varsigma_{\mathrm{xen}}^2} , \tag{4.51}$$

where, $\mathfrak{Q} = (1-\chi_H)(1-\varsigma_{\mathrm{xen}}) e^{-ikL_{\mathrm{C}}} + \chi_H \left(2-\varsigma_{\mathrm{xen}}^2\right) - (1+\chi_H)(1+\varsigma_{\mathrm{xen}}) e^{ikL_{\mathrm{C}}}$

where, for an input frequency f, we have defined

$$\varsigma_{\mathrm{xen}} = 2ikl_{\mathrm{T}} \qquad \& \qquad \chi_{\mathrm{H}} = \frac{1}{2} \frac{ikV_{\mathrm{H}} S_{\mathrm{C}}^{-1}}{1 - f^2/f_{\mathrm{H}}^2} , \tag{4.52}$$

where f_{H} is the characteristic frequency (4.47) of the Helmholtz resonator of volume V_{H}. With some algebra, it can also be shown that the matrix M has a determinant equal to one, i.e. Det $M^{\mathrm{xen}} = M_{11}^{\mathrm{xen}} M_{22}^{\mathrm{xen}} + (M_{12}^{\mathrm{xen}})^2 = 1$. The corresponding matrix coefficients for the barn owl are given by expressions similar to those for *Xenopus*, which read

$$M_{11}^{\mathrm{owl}} = \frac{e^{ik2L_{\mathrm{T}}} \left[(1+\chi_{\mathrm{H}}) e^{ikL_{\mathrm{C}}} - 2\chi_H \varsigma_{\mathrm{owl}} - (1-\chi_H) \varsigma_{\mathrm{owl}}^2 e^{-ikL_{\mathrm{C}}} \right]}{(1-\varsigma_{\mathrm{owl}}^2)} , \tag{4.53}$$

$$M_{22}^{\mathrm{owl}} = \frac{e^{-ik2L_{\mathrm{T}}} \left[(1-\chi_H) e^{ikL_{\mathrm{C}}} + 2\chi_H \varsigma_{\mathrm{owl}} - (1+\chi_{\mathrm{H}}) \varsigma_{\mathrm{owl}}^2 e^{-ikL_{\mathrm{C}}} \right]}{(1-\varsigma_{\mathrm{owl}}^2)} , \tag{4.54}$$

$$M_{12}^{\mathrm{owl}} = -M_{21}^{\mathrm{owl}} = \frac{-\varsigma_{\mathrm{owl}} (1+\chi_H) e^{ikL_{\mathrm{C}}} + 2\chi_H (1+\varsigma_{\mathrm{owl}}^2) + (1-\chi_{\mathrm{H}}) \varsigma_{\mathrm{owl}} e^{-ikL_{\mathrm{C}}}}{(1-\varsigma_{\mathrm{owl}}^2)} , \tag{4.55}$$

where

$$\varsigma_{\mathrm{owl}} = \frac{S_{\mathrm{T}} - S_{\mathrm{C}}}{S_{\mathrm{T}} + S_{\mathrm{C}}} . \tag{4.56}$$

As in the case of *Xenopus*, Det $M^{\text{owl}} = M_{11}^{\text{owl}} M_{22}^{\text{owl}} + (M_{12}^{\text{owl}})^2 = 1$. Setting $\varsigma_{\text{ex}} \to \infty$ for *Xenopus* and $\varsigma_{\text{owl}} \to 0$ for the barn owl is equivalent to requiring the tympanic and internal canal cross sections to be equal, i.e., $S_{\text{C}} = S_{\text{T}}$. Furthermore, requiring the volume V_{H} of the Helmholtz resonator to vanish results in $\chi_{\text{H}} = 0$ in both cases, which results in the matrix for a cylindrical cavity

$$M^{\text{cyl}} = \begin{pmatrix} e^{ik(2L_{\text{T}}+L_{\text{C}})} & 0 \\ 0 & e^{-ik(2L_{\text{T}}+L_{\text{C}})} \end{pmatrix} . \tag{4.57}$$

The above transformation matrix is equivalent to the plane wave expressions of Eqs. (2.66) and (2.67) for a cylindrical volume of length $2L_{\text{T}} + L_{\text{C}}$.

Using the matrix M we can now obtain the internal pressure p^{in} at the left and right eardrums. For *Xenopus*, this gives us

$$p_0^{\text{in}} = p_{\text{T}}^0(0) = \frac{A_{\text{T}}^0}{2ik(L_{\text{T}}+l_{\text{T}})} + \frac{B_{\text{T}}^0}{2ik(L_{\text{T}}+l_{\text{T}})}, \tag{4.58}$$

$$p_L^{\text{in}} = p_{\text{T}}^L(L_{\text{T}}) = \frac{A_{\text{T}}^L e^{ikL}}{2ik(L_{\text{T}}+l_{\text{T}})} + \frac{B_{\text{T}}^L e^{-ikL}}{2ik(L_{\text{T}}+l_{\text{T}})} \tag{4.59}$$

$$= \frac{1}{2ik(L_{\text{T}}+l_{\text{T}})} (1 \quad 1) M^{\text{xen}} \begin{pmatrix} A_{\text{T}}^0 \\ B_{\text{T}}^0 \end{pmatrix} , \tag{4.60}$$

whereas for the barn owl we have

$$p_0^{\text{in}} = p_{\text{T}}^0(0) = A_{\text{T}}^0 + B_{\text{T}}^0, \tag{4.61}$$

$$p_L^{\text{in}} = p_{\text{T}}^L(L_{\text{T}}) = A_{\text{T}}^L e^{ikL} + B_{\text{T}}^L e^{-ikL} \tag{4.62}$$

$$= (1 \quad 1) M^{\text{owl}} \begin{pmatrix} A_{\text{T}}^0 \\ B_{\text{T}}^0 \end{pmatrix} . \tag{4.63}$$

The coefficients A_{T}^0 and B_{T}^0 are to be determined by the boundary conditions at the eardrums.

Boundary conditions at the eardrums

At the boundary between the eardrums and the internal cavities, the boundary conditions can once again be approximated through the piston approximation from Section 2.2.3 (cf. Eq. (2.75)), where instead of equating the air particle velocity to the membrane vibration velocity at every point on the membrane surface, we approximate the membrane by an integral average. For *Xenopus*, the procedure is simplified further, as its eardrum moves as a piston by definition; cf. Eq. (4.13). At the boundary with the eardrums moving with velocity

$u_{0/L}$, the the fluid particle velocity (4.29), (4.30) satisfy

$$-v_{\mathrm{T}}^{0}(L_{\mathrm{T}}) = \frac{\upsilon_1 A_{\mathrm{T}}^{0}}{2\rho c k^2 (L_{\mathrm{T}}+l_{\mathrm{T}})^2} + \frac{\upsilon_2 B_{\mathrm{T}}^{0}}{2\rho c k^2 (L_{\mathrm{T}}+l_{\mathrm{T}})^2} = i\omega u_0 \,, \tag{4.64}$$

$$v_{\mathrm{T}}^{L}(2L_{\mathrm{T}}+L_{\mathrm{C}}) = \frac{e^{ik(2L_{\mathrm{T}}+L_{\mathrm{C}})}\upsilon_2 A_{\mathrm{T}}^{L}}{2\rho c k^2 (L_{\mathrm{T}}+l_{\mathrm{T}})^2} + \frac{e^{-ik(2L_{\mathrm{T}}+L_{\mathrm{C}})}\upsilon_1 B_{\mathrm{T}}^{L}}{2\rho c k^2 (L_{\mathrm{T}}+l_{\mathrm{T}})^2} = i\omega u_L \,, \tag{4.65}$$

$$\upsilon_1 = -1 - ik(L_T + l_{\mathrm{T}}), \qquad \upsilon_2 = -1 + ik(L_T + l_{\mathrm{T}}). \tag{4.66}$$

As in the case of the lizards (2.76), directions into the cavity are positive and those out of the cavity are negative. The above equations can be used together with expressions for the internal pressure, Eqs. (4.58) and (4.59), and the matrix M^{xen} (4.60) to eliminate the coefficients $A_{\mathrm{T}}^{0/L}$ and $B_{\mathrm{T}}^{0/L}$ to express the internal pressure in terms of the eardrum displacement $u_{0/L}$. We now define sum and difference expressions analogous to Eqs. (2.87) to (2.90) such that,

$$u_{\pm} = u_L \pm u_0, \quad p_{\pm}^{\mathrm{in}} = p_L^{\mathrm{in}} \pm p_0^{\mathrm{in}} \,, \tag{4.67}$$

$$p_{\pm}^{\mathrm{in}} = \Gamma_{\pm}^{\mathrm{xen}} u_{\pm} \,, \tag{4.68}$$

resulting, as before, in coefficients $\Gamma_{\pm}^{\mathrm{xen}}$ (2.98) that quantify the internal pressure generated by the motion of the eardrums and are given in terms of the transformation matrix M^{xen} as

$$\Gamma_{\pm}^{\mathrm{xen}} = -ik\frac{\rho c^2}{2}(\upsilon_2 - \upsilon_1)\frac{\pm 2 + \mathrm{Tr}\left[\left(\begin{smallmatrix} -\upsilon_2 & -\upsilon_1 \\ \upsilon_2 & \upsilon_1 \end{smallmatrix}\right) M^{\mathrm{xen}}\right]}{\left(\begin{smallmatrix} \upsilon_2 & \upsilon_1 \end{smallmatrix}\right) M^{\mathrm{xen}} \left(\begin{smallmatrix} \upsilon_2 \\ -\upsilon_1 \end{smallmatrix}\right)} \,, \tag{4.69}$$

where Tr denotes the trace of a matrix, and $\mathbb{1}$ the identity matrix. For the barn owl, the boundary conditions are equivalent to the piston approximation of Chapter 2 (cf. Eqs. (2.75) and (2.76)) and, now in terms of the average displacements $u_{0/L}^{\mathrm{ave}}$, read

$$-v_{\mathrm{T}}^{0}(L_{\mathrm{T}}) = A_{\mathrm{T}}^{0} + B_{\mathrm{T}}^{0} = i\rho c\omega u_0^{\mathrm{ave}} \,, \tag{4.70}$$

$$v_{\mathrm{T}}^{L}(2L_{\mathrm{T}}+L_{\mathrm{C}}) = e^{ik(2L_{\mathrm{T}}+L_{\mathrm{C}})}A_{\mathrm{T}}^{L} + e^{-ik(2L_{\mathrm{T}}+L_{\mathrm{C}})}B_{\mathrm{T}}^{L} = i\rho c\omega u_L^{\mathrm{ave}} \,, \tag{4.71}$$

Similar to *Xenopus*, the matrix M^{owl} (4.63) be used to calculate the coefficients,

$$\Gamma_{\pm}^{\mathrm{owl}} = -ik\frac{\rho c^2}{S_{\mathrm{T}}}\frac{\pm 2 + \mathrm{Tr}\, M^{\mathrm{owl}}}{\left(\begin{smallmatrix} 1 & -1 \end{smallmatrix}\right) M^{\mathrm{owl}} \left(\begin{smallmatrix} 1 \\ 1 \end{smallmatrix}\right)} \,, \tag{4.72}$$

Using the matrix from Eq. (4.57) in the above expression results in the familiar $\Gamma_{\pm}$ coefficients from Chapter 2; cf. Eq. (2.98).

4.3 Sound input

The sound input to the eardrum for *Xenopus* is of a similar form to the one described for the lizards in Section 2.1.3. However, we must account for the fact that the underwater speed of sound c_w and, consequently, the wavelength are 4.3 times higher. At 4 kHz, the upper limit of *Xenopus*'s hearing range [107], the underwater sound wavelength is around 37 cm, while the animal's interaural distance is approximately 2 cm [57]. As a result, the diffraction of sound by the head and acoustic shadowing can be neglected for *Xenopus*'s entire hearing range. In other words, the small head model of Figure 2.7 for the lizards holds in the present case as well. Correspondingly, the sound inputs, which only differ in phase and not in amplitude, are given by

$$p_0^{\text{ex}} = p\exp(i\omega t)\exp(-ik_w\Delta/2), \qquad p_L^{\text{ex}} = p\exp(i\omega t)\exp(-ik_w\Delta/2), \tag{4.73}$$
$$\text{where} \qquad \Delta = L_{\text{xen}}\sin\ \theta$$

is the additional distance traveled by the sound wave to reach the opposite ear (see Fig. 4.9a) and $k_w = \omega/c_w$ is the now the wavenumber in water. The speed of sound in water is c_w is approximately 4.3 times the speed of sound in air c. For an interaural separation L_{xen}, $\Delta = L_{\text{xen}}\sin\ \theta$ is the additional distance traveled by a sound wave to reach the opposite ear; cf. Fig. 4.9a.

Barn owls, on the other hand, are larger than *Xenopus* and are entirely terrestrial. The eardrums themselves are positioned at the end of canals, whose openings are asymmetric with respect to a horizontal plane passing through the eyes [108, 109]. The interaural distance, which in this case is between the openings of the ear canals, is approximately 5 cm (based on Knudsen and Konishi [110]). As a result, the effective interaural distance L_{owl} is greater than the horizontal separation between the eardrums; cf. Fig. 4.9b. In our model, we ignore the vertical asymmetry as it does not contribute to the generation of azimuthal sound localization cues. The inputs to the barn owl ear are thus given by

$$p_0^{\text{ex}} = p\exp(i\omega t)\exp(-ik\Delta/2), \qquad p_L^{\text{ex}} = p\exp(i\omega t)\exp(-ik\Delta/2), \tag{4.74}$$
$$\text{where} \qquad \Delta = L_{\text{owl}}\sin\theta$$

is the additional distance traveled by the sound wave to reach the opposite ear (see Fig. 4.9b) and $k = \omega/c$ is now the wave number in air. At frequencies above 5 kHz ($\lambda \approx 6.8$ cm), the amplitude difference generated by the facial ruff would become significant [111–113]. However, we can safely neglect the amplitude difference between p_0^{ex} and p_L^{ex} up to 3 kHz, as hearing cues in this range are no longer generated by ICE, but by the inputs through the ears

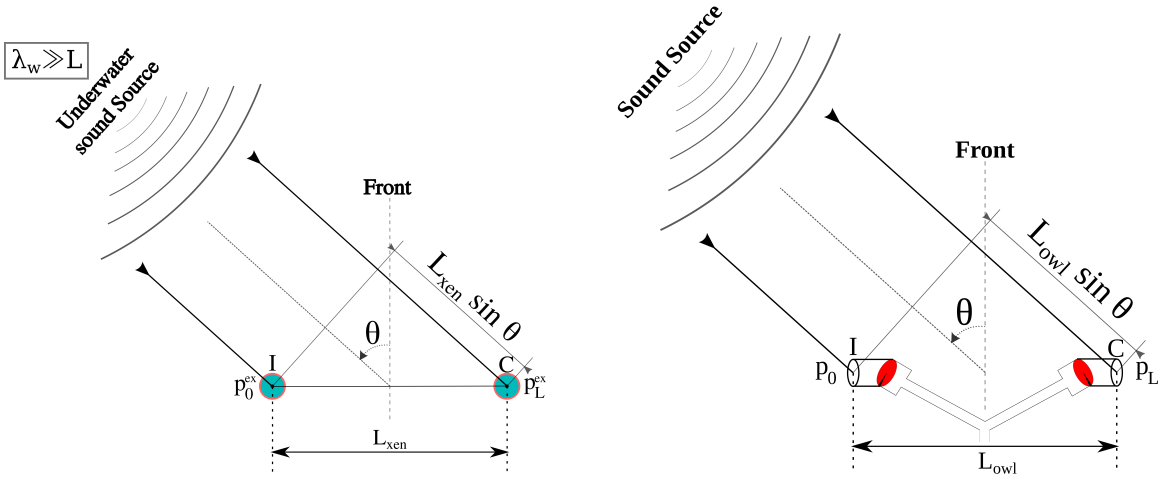

(a) *Xenopus* (b) Barn owl

Fig. 4.9 The acoustic head model for ICE in *Xenopus* (a) and the barn owl (b). For *Xenopus*, the small head size approximation, i.e. $L_{\text{xen}} \ll \lambda_w$ approximation of Section 2.1.3 is still valid (cf. Fig. 2.7), as underwater sound wavelengths are 4.3 times larger than in air for the same frequency. As a result, sound travels extra distance $\Delta = L_{\text{xen}} \sin\theta$ to reach the contralateral ear, which gives rise to a phase difference $k_w\Delta$. For the barn owl, as the eardrums are located at the end of an external canal, the effective interaural distance L_{owl} is greater than the physical separation between the eardrums. As a result, the extra distance traveled is now $\Delta = L_{\text{owl}} \sin\theta$, with a phase difference of $k\Delta$ in *air*.

themselves in the form of interaural time and level differences. As a result, at frequencies above 3 kHz, we are more interested in the frequency behavior of the interaural cavity than in the generation of iTD and iLD cues through ICE.

As a consequence of the chosen forms of the sound input, while the interaural level difference (ILD) are zero for both animals (4.73), the interaural time difference (ITD) depends on the medium such that for a direction θ

$$\text{ITD}_{\text{xen}} = L_{\text{xen}} \sin\theta / c_w \qquad \text{ITD}_{\text{owl}} = L_{\text{owl}} \sin\theta / c \,. \tag{4.75}$$

$$\text{ILD}_{\text{xen}} = \text{ILD}_{\text{owl}} = 0 \,. \tag{4.76}$$

4.4 Coupled eardrum vibrations

Xenopus

Using the expressions for the radiative force (4.17), internal pressure (4.68) in terms of the $\Gamma_{\pm}^{\text{xen}}$ coefficients (4.69) and the external underwater sound input (4.73), we can rewrite the

equations of motion for the eardrums (4.13) for quasi-steady-state solutions of the form $u_{0/L}\exp(i\omega t)$ such that

$$-m_{\rm p}\omega^2 u_\pm = S_{\rm p}p_\pm^{\rm ex} - \left(S_{\rm p}\Gamma_\pm^{\rm xen} - \omega\Gamma_r + \kappa + ib\omega\right)u_\pm \ . \tag{4.77}$$

The eardrum vibrations can be compactly expressed in terms of the "spring" constant generated by the tympanic annulus κ (4.12) and damping b as

$$2u_{0/L} = \frac{S_{\rm p}\left(p_L^{\rm ex} + p_0^{\rm ex}\right)}{1/\Lambda^{\rm xen} + S_{\rm p}\Gamma_+^{\rm xen} - \omega\Gamma_r} \mp \frac{S_{\rm p}\left(p_L^{\rm ex} - p_0^{\rm ex}\right)}{1/\Lambda^{\rm xen} + S_{\rm p}\Gamma_-^{\rm xen} - \omega\Gamma_r} \ , \tag{4.78}$$

$$\Lambda^{\rm xen}(\omega) = \left[-m_{\rm p}\omega^2 + \kappa + i\omega b\right]^{-1} \ , \tag{4.79}$$

where $\Lambda^{\rm xen}$ is the frequency response for an independent *Xenopus* eardrum in the absence of acoustic radiation and an internal pressure. In other words, for an external pressure of form $p\exp(i\omega t)$, the displacement of the eardrum is given by $S_{\rm p}\Lambda \times p\exp(i\omega t)$; compare with Eq. (2.97).

Barn owl

For the barn owl, as the eardrums are instead driven by an external sound pressure in air (4.74), the expressions for the average membrane displacements $u_{0/L}^{\rm ave}$ are almost identical to those for the lizard eardrum (2.100), except for the cavity $\Gamma_\pm$ coefficients (4.72). In terms of the membrane frequency response $\Lambda^{\rm tot}$ (4.19), the average displacements $u_{0/L}^{\rm ave}$ are given by

$$S_{\rm T}\ u_{0/L}^{\rm ave}(r,\phi) = \frac{1}{2}\left(\frac{p_L^{\rm ex} + p_0^{\rm ex}}{1 + \Lambda_{\rm tot}\Gamma_+^{\rm owl}} \mp \frac{p_L^{\rm ex} - p_0^{\rm ex}}{1 + \Lambda_{\rm tot}\Gamma_-^{\rm owl}}\right)\Lambda_{\rm tot} \ . \tag{4.80}$$

Hearing cues: The vibration amplitudes thus derived for both animals can now be used to define the hearing cues of Chapter 3, i.e., the internal time (3.2) and level (3.7) differences between the eardrum vibrations

$$\text{iTD} = \text{Arg}(u_L^{\rm ave}/u_0^{\rm ave})/\omega \qquad \text{iLD} = 20\,\text{Log}_{10}|u_L^{\rm ave}/u_0^{\rm ave}| \ . \tag{4.81}$$

4.5 Results

The material parameters for *Xenopus* and the barn owl are given in Table 4.1. For *Xenopus*, the cavity volumes were chosen in accordance with typical adult values which range between .04 and .07 cm^3 [114], while the eardrum area agrees with anatomical measurements [95].

The Young's modulus of the tympanic annulus was taken to be similar to values for typical hyaline cartilage [115]. For the barn owl, the values corresponding to cavity volume are based partially on data from Kettler et al. [56] and the density and thickness of the eardrum are based on typical avian eardrum values measured for a duck [81]. We again note that the distance between the internal surfaces of the barn owl eardrums via the interaural canal is $L_C + 2L_T = 40$ mm, which is lesser than the effective interaural distance L_{owl}, but greater than the physical "external" separation between the eardrums. The volume V_H of the Helmholtz resonator is variable in the case of *Xenopus*, as it is formed by the lungs and can be inflated and deflated. Under normal conditions in nature, the volume of the lungs is between 1.0–2.0 cm^3 while diving. In the barn owl however, as the resonator is formed by the cavity of the sphenoid bone, it has a fixed value.

Table 4.1 Material and geometrical parameters used for *Xenopus* and the barn owl.

Parameter	*Xenopus*	Barn owl
Interaural distance	$L_{xen} = 20$ mm	$L_{owl} = 50$ mm
TC Depth L_T	1.5 mm	2.0 mm
InC Length L_C	17 mm	36 mm
Cavity Volume V_{cav}	53 mm^3	1660 mm^3
Eardrum area	$S_p = 35$ mm^2	$S_{mem} = 38.5$ mm^2
Eardrum mass	$m_p = 5$ mg	–
Eardrum density	–	$\rho_M = 1.2$ mg/mm^3
Eardrum resonance	–	$f_0 = 3.0$ kHz
Eardrum thickness	–	$d_M = 20$ μm
Annulus width	$a_{ann} = .4$ mm	–
Annulus thickness	$h = .11$ mm	–
Young's Modulus	$E = 39.2$ MPa	–
Damping α_p	6 ms^{-1}	18.8 ms^{-1}
Resonator neck length L_H	4.3 mm	0.5 mm
Neck cross section S_H	0.3 mm^2	3.0 mm^2

4.5.1 *Xenopus*

Eardrum vibration amplitude

In Figs. 4.10a and 4.10b we compare experimentally measured eardrum vibration amplitudes with those obtained from our model for two cases, viz., when the lungs have a typical volume of $V_H = 1.5$ cm^3 and when they are completely deflated, i.e., $V_H = 0$ cc. Given the analytical simplicity of our model, we see a much better agreement with experimentally determined values for our chosen value of lung inflation, than with deflated lungs. Inflating the lungs

increases the amplitude of vibrations in the lower frequency range (0.8-1.2 kHz). In the 1.5-2.0 kHz range, there is an increase in the directionality as the contralateral amplitude has a markedly lower amplitude, although this happens at the cost of an overall reduced vibration amplitude.

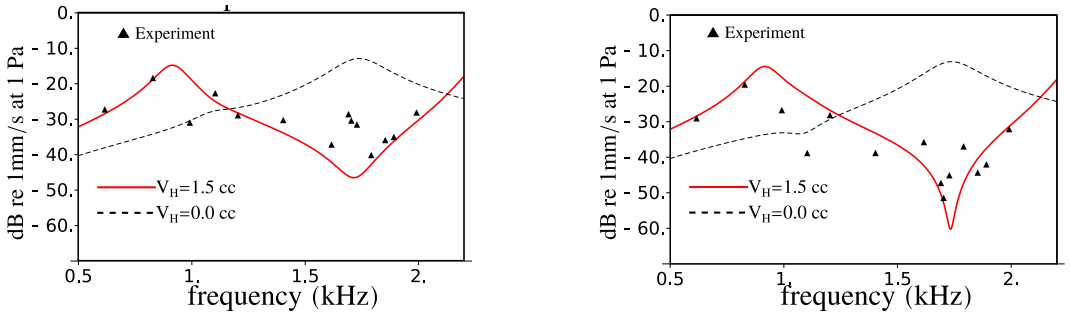

(a) Ipsilateral (b) Contralateral

Fig. 4.10 Experimentally measured (filled triangles) and model vibration velocities of the *Xenopus* (a) ipsilateral and (b) contralateral eardrum underwater. The eardrum vibration velocities have been measured [57] by using laser vibrometry and have been normalized w.r.t. the input pressure. The solid (red) line corresponds to inflated lungs with a total volume $V_{\mathrm{H}} = 1.5$ cm^3 and the dashed (black) line corresponds to the case $V_{\mathrm{H}} = 0$ cc, i.e., absent or fully deflated lungs. The sound-source direction is $\theta = 90^\circ$. The contralateral amplitude is significantly lower than the ipsilateral amplitude. As both plots show, the experimental results can be explained only with inflated lungs, whose Helmholtz-resonator function has been discussed in Section 4.2.2.

The influence of the lung volume on the eardrum vibration amplitude is further illustrated for the underwater and air cases in Figs. 4.11a and 4.11b, respectively. On the whole, the eardrum response is shifted to lower frequencies underwater relative to air. This is due to the radiation of acoustic energy into the medium and is related to the reduction in pitch of a plate vibrating in contact with water [116, 117], due to the increased effective mass of the eardrum (4.18). In both cases, however, the inflation of the lungs results in higher vibration amplitudes in the 0.8-1.2 kHz range, with the first peak corresponding to the Helmholtz resonance of the lungs.

The second peak is a function of both the cavity geometry and the eardrum resonance subject to the surrounding medium. Because of the difference in the surroundings, the second peak occurs at a higher frequency in air than under water. The two-peaked spectrum as well as its dependence upon lung volume is consistent with experimentally observed values [57, 118]. The increased eardrum amplitude between 0.8-1.2 kHz agrees with peak frequencies in adult-frog hearing [114]. The frequency region around 1 kHz is behaviorally

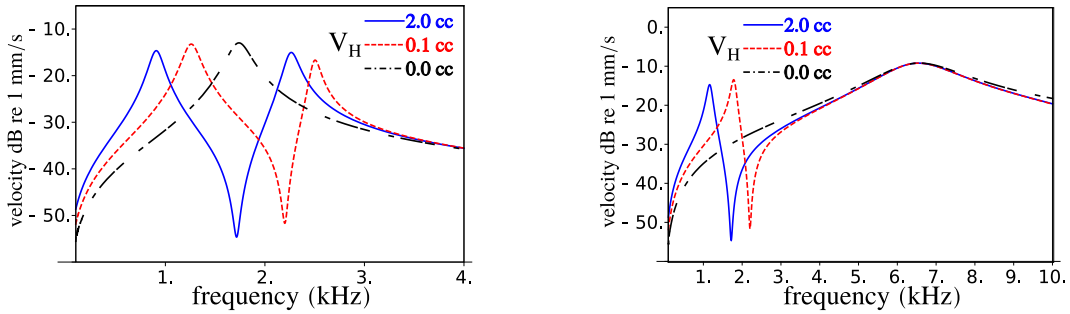

(a) Underwater (b) In air

Fig. 4.11 Vibration velocity of the *Xenopus* eardrum (a) underwater and (b) in air for different lung volumes. The pronounced underwater peaks and their shifts to lower frequencies as compared to those in air are to be noted. The solid (blue) line corresponds to a volume of 2 cm^3 and the dashed (red) line corresponds to deflated lungs, of total volume 0.1 cc. The dot-dashed (black) line corresponds to absent lungs. In all cases the sound source is directly in front of the animal, i.e., $\theta = 0^\circ$ and iLD=0 as both ears thus receive the same input. The units are decibel values with respect to a velocity of 1 mm/s with a sound input amplitude of 1 Pa. A significant portion of the *Xenopus* male advertisement call is concentrated around 1 kHz, which is consistent with the lower frequency peaks in (a) and (b) with inflated lungs.

relevant to *Xenopus* as a significant portion of the energy of the male advertisement call is centered around 1 kHz [86].

Internal level difference

Figures 4.12a and 4.12b show the frequency dependence of the internal level difference or iLD (4.81) between eardrum vibrations underwater and in air, respectively. In both cases, the iLD is generated solely by the coupling through the interaural cavity, even though the inputs to both ears have the same amplitude; cf. (4.73). The volume of the Helmholtz resonator V_H, which represents the air-filled lungs, was fixed at 1.5 cm^3 in all cases, based on typical lung volumes in a submerged *Xenopus* [57]. Underwater, we see a pronounced, albeit narrow, peak at around 1.7 kHz for all three sound source directions with a maximum value for $\theta = 90^\circ$. A peak iLD at 1.7 kHz is consistent with the spectrum of the mating calls of a male *Xenopus*, where the majority of the energy is concentrated in a band between 1.7kHz and 2.2 kHz [86]. Furthermore, by varying the lung volume the female can tune into the 'mating' frequency of different males. The interaural level difference between the inputs to the ears, as in the case of the lizards, is effectively zero (4.76).

Shallow water acts as a high-pass filter for underwater sound, i.e., below a certain cut-off frequency, the sound pressure amplitude decreases exponentially with distance. For instance,

in a pond of depth 0.5 m with a mud bottom – natural conditions for *Xenopus* [119] – the cut-off frequency would be at least 1.0 kHz [120]. As a result, the enhanced hearing cues around 1.7 kHz would be advantageous to *Xenopus* for long-range communication in shallow water. In air, we see that the iLD is negative around 1.5 kHz and positive around 2.3 kHz. A negative iLD physically means that the contralateral ear has a higher amplitude than the ipsilateral ear and suggests that, at least in air, the iLD is a better hearing cue at frequencies above 2 kHz.

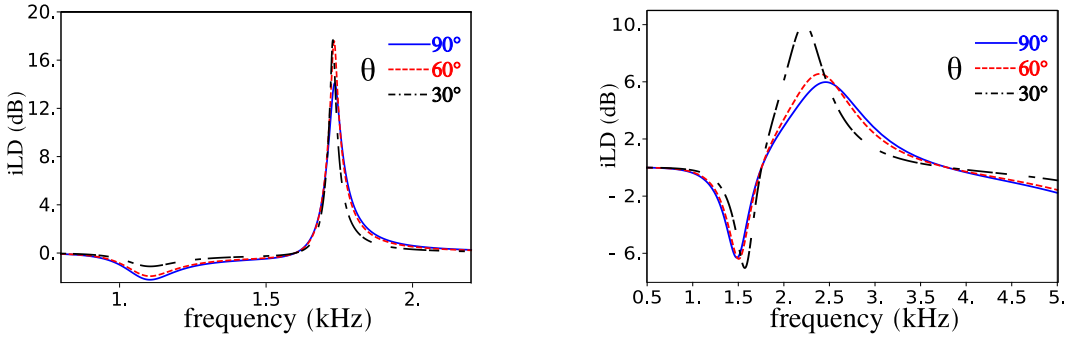

(a) Underwater (b) In air

Fig. 4.12 Frequency dependence of the decibel internal level difference (iLD) of the *Xenopus* eardrum (a) underwater and (b) in air. The directions shown are with respect to the ipsilateral ear, where the positive angle corresponds to a sound source on the same side as the ear; cf. Fig. 2.7. The solid (blue) line and the dashed (red) line correspond to $\theta = 90°$ and $\theta = 60°$, respectively, while the dot-dashed (black) line corresponds to $\theta = 30°$; cf. Fig. 2.7. The volume of the lung-related Helmholtz resonator is $V_{\mathrm{H}} = 1.5$ cm^3 in all cases. In (a) the iLD peak is concentrated in a narrow range around 1.7 corresponding to the dominant portion of the underwater mating call spectrum of the male *Xenopus*.

Figures 4.13a and 4.13b exhibit the variation of the iLD spectrum with lung volume for a sound source direction of $\theta = 90°$. Underwater, decreasing the lung volume increases the peak iLD frequency, thereby providing a means to tune the animal's hearing. In air, the variation in the iLD spectrum upon decreasing the lung volume from 2.0 cm^3 to 1.0 cm^3 is negligible, with peak positive values at around 2.5 kHz. The iLDs for absent lungs corresponding to a Helmholtz resonator volume of $V_{\mathrm{H}} = 0.0$ cm^3 is also given. We see that in air, the iLD performance is best in the absence of the lungs, whereas underwater the lungs are essential to generating large (maximal) iLDs around 1.7 kHz. As Fig. 4.13a indicates, reduction of the fully inflated volume even allows a fine tuning of the maximum. These two facts strongly suggest that the lungs are essential to underwater sound localization.

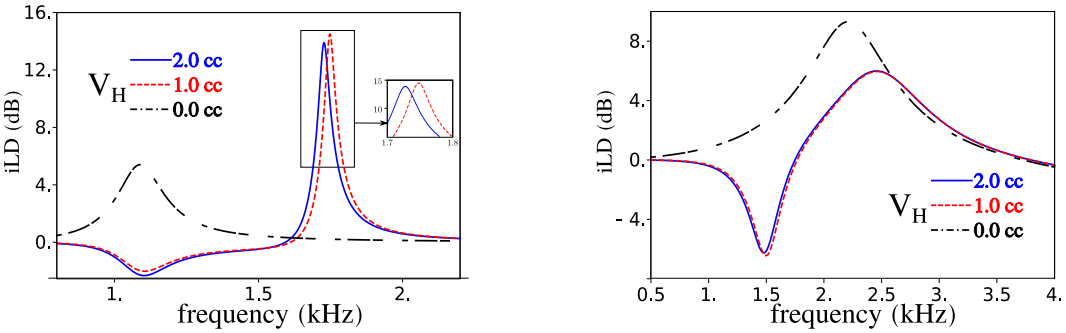

(a) Underwater (b) In air

Fig. 4.13 Frequency dependence of the interaural level difference (iLD) between the eardrums for varying lung volumes V_H (a) underwater and (b) in air. The sound source direction in all cases is taken to be $\theta = 90°$. The inset in (a) shows the variation of the iLD peak with lung volume where the maximum shifts in a window of around 100 Hz. As Fig. 4.13a shows, the female can tune in to the male calls at about 1.7 kHz by varying the lung volume. However, the influence of the lungs is negligible in air, suggesting that their influence on hearing is primarily an underwater adaptation.

Using iLD for sound-source localization: The direction dependence of the iLDs for different frequencies is illustrated in Figs. 4.14a and 4.14b. In general, ipsilateral ($\theta > 0°$) iLDs are positive, whereas contralateral ($\theta < 0°$) iLDs are negative. The steep increase in iLD around 0° is conducive to localizing sound sources directly in front of the animal. A maximal iLD nearly always occurs at $\theta = 90°$ and the animal can localize a sound source by rotating its head to perceive the steep transition at $\theta = 0°$. Furthermore, as opposed to predator or prey behavior, where a fast reaction is essential, mating behavior is in general not characterized by a narrow time window. Thus, the localization of the mating call through a rotation of the head is feasible.

Internal time difference

The frequency-dependent iTD gain or time-dilation factor (TDF), defined as in Chapter 3 as the ratio of internal and interaural time difference (iTD/ITD) (4.81) has been plotted in Figs. 4.15a and 4.15b for the underwater and air cases, respectively. Unlike in the case of terrestrial animals with ICE, specifically, geckos where the iTD gain can be higher than 3 [12], *Xenopus* does not experience any significant iTD gain either underwater or in air. This is due to the rigid-plate construction of the eardrum and the higher mass of the attached middle-ear system, i.e. extracolumella & columella; see Section 4.1.1.

Figures 4.16a and 4.16b show that varying the lung volume does not improve the iTD gain significantly either. Compared to interaural time differences (ITD) of around 58 μs in

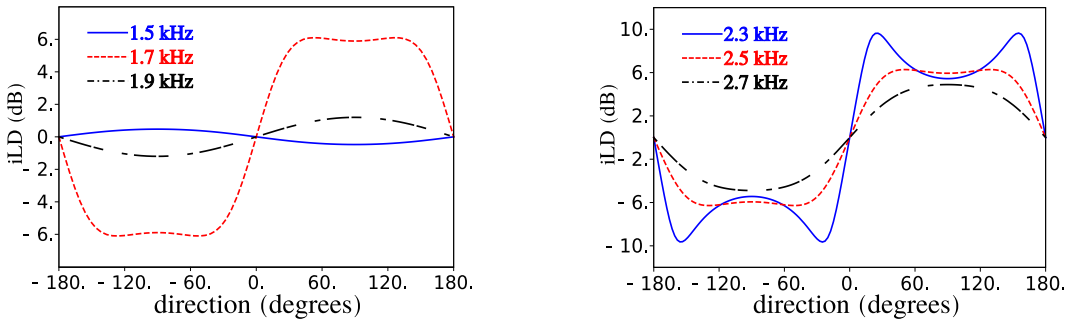

(a) Underwater (b) In air

Fig. 4.14 Direction dependence of the interaural level difference (iLD) between the eardrums for for different frequencies (a) underwater and (b) in air. The lung volume V_{H} is 1.5 cm^3 in all cases. By rotating its head, the animal can exploit the steep iLD increase around $\theta = 0°$ to localize the sound source. This is of particular relevance to mating behavior, as it is not characterized by a narrow time window.

air and and 13 μs underwater, a moderate gain of around 1.5, corresponding to a maximum iTD of 87 μs in air and 20 μs underwater, for nearly completely deflated lungs of volume 0.1 cm^3 is also obtained. This is in stark contrast to the lizards, where we see a time dilation factor of around 3.5 for Tokay and over 10 for a young *Varanus*; cf. Figs. 3.6a and 3.6b. Note that realistic lungs volumes for *Xenopus*, however, are between 1.0-2.0 cm^3 [57]. Our results therefore suggest that, *Xenopus* cannot rely on time difference cues both underwater, and in air and must solely rely on internal level differences for mating and their lateral line system [121] for time-sensitive activities like predation.

Terrestrial vs. aquatic eardrums: *Xenopus* vs *Xenopus*2

In order to understand the specialization of the *Xenopus* eardrum in its aquatic environment, we compare its behavior with the one of an eardrum belonging to a typical terrestrial animal with ICE, as described for the Tokay gecko and *Varanus* in Chapter 2 (cf. Section 2.1.1) as well as for the barn owl in the present chapter (cf. Section 4.1.2). In other words, we consider a model of the eardrum as a thin, circular and linear-elastic membrane asymmetrically loaded by an extracolumella. Subject to underwater sound, each eardrum – one at at $x = 0$ and the other at $x = L$ – feels a radiative pressure proportional to the average displacement $u^{\mathrm{ave}}_{0/L}$ of its surface quantified by the coefficient Γ_r (4.17), such that $u^{\mathrm{ave}}_{0/L}$ is given by an expression similar to Eq. (4.78),

$$2u^{\mathrm{ave}}_{0/L} = \frac{S_{\mathrm{tymp}}\,(p_L + p_0)}{S^2_{\mathrm{tymp}}/\Lambda_{\mathrm{tot}} + S_{\mathrm{tymp}}\Gamma^{\mathrm{xen}}_{+} - \omega\Gamma_r} \mp \frac{S_{\mathrm{tymp}}\,(p_L - p_0)}{S^2_{\mathrm{tymp}}/\Lambda_{\mathrm{tot}} + S_{\mathrm{tymp}}\Gamma^{\mathrm{xen}}_{-} - \omega\Gamma_r}\,. \tag{4.82}$$

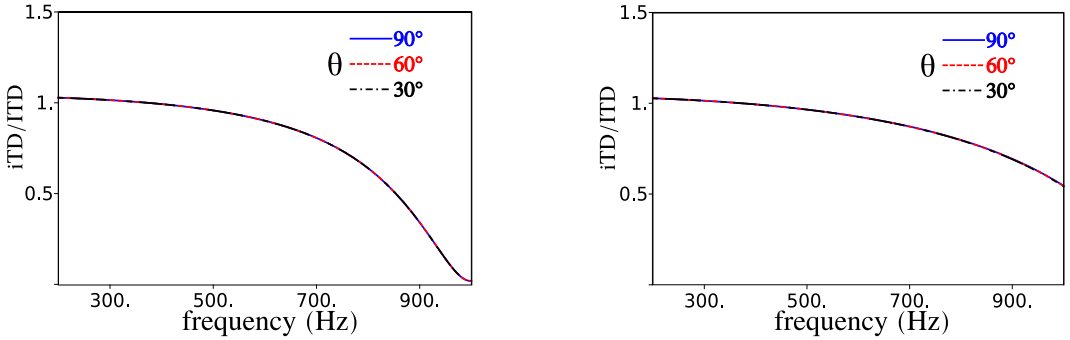

(a) Underwater (b) In air

Fig. 4.15 Frequency dependence of the time-dilation factor or iTD gain (= iTD/ITD) of the *Xenopus* eardrum (A) underwater and (B) in air. The directions shown are with respect to the ipsilateral ear, where the positive angle corresponds to a sound source on the same side as the ear. In all cases the volume of the Helmholtz resonator originating from the lungs is taken to be $V_{\rm H} = 1.5$ cc. In both media there is no significant amplification of iTDs, suggesting that it is not a realistic hearing cue for the animal.

where $\Lambda_{\rm tot}$ is the membrane frequency response of the lizard eardrum of area $S_{\rm tymp}$ defined in Eq. (2.97).

In order to compare the behavior of the two eardrums, we postulate a hypothetical animal *Xenopus*2 that has the same interaural cavity described in Sec. 4.2, albeit with flexible gecko-like eardrums, as opposed to the actual rigid-plate construction of the natural *Xenopus*. The instantaneous sound power absorbed by the eardrums in both cases is given by

$$P_{\rm X1} = p_0^{\rm ex}\dot{u}_0 + p_L^{\rm ex}\dot{u}_L\,, \quad P_{\rm X2} = p_0^{\rm ex}\dot{u}_0^{\rm ave} \;+\; p_L^{\rm ex}\dot{u}_L^{\rm ave} \tag{4.83}$$

where "X1" refers to our model of *Xenopus* as it occurs in nature, whereas "X2" refers to the fictitious *Xenopus*2 with a flexible eardrum.

Figures 4.17a and 4.17b show the absolute values (in dB re 1 nW) of the instantaneous sound power absorption $|P_{\rm X1}|$ & $|P_{\rm X2}|$ with respect to frequency underwater and in air, respectively. In Fig. 4.17a, we see peaks in the 2-2.5 kHz region in both cases, which is driven by the Helmholtz resonance of the lungs. The rigid-plate construction, however, absorbs more power than the flexible eardrum in the behaviorally relevant 1 kHz region under water as well as in air; see Fig. 4.17b. The power absorption of the flexible-membrane construction, however, only peaks below 400 Hz both under water and in air. This suggests that the *Xenopus* eardrum is adapted to improve hearing in the 1 kHz frequency region in both media. In passing, it is good to remember that *Xenopus* can tune the resonances of Figs. 4.17a and 4.17b by varying its lung volume; Figs. 4.13a and 4.13b.

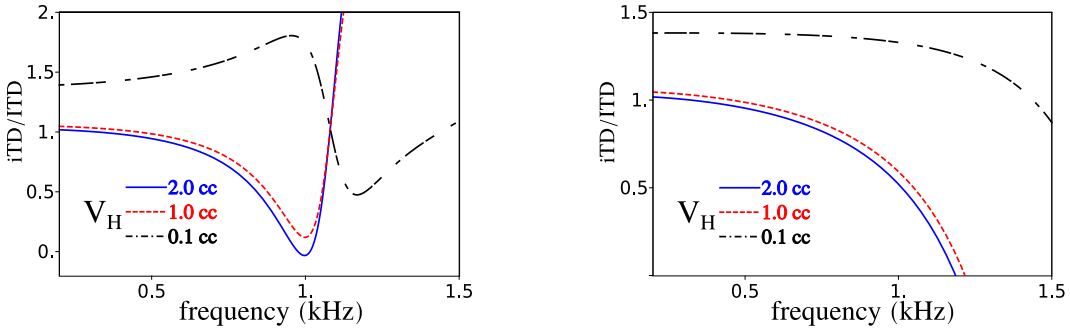

(a) Underwater (b) In air

Fig. 4.16 Frequency dependence of the time-dilation factor (TDF) or iTD gain (=iTD/ITD) of the *Xenopus* eardrums for varying lung volumes V_H (A) underwater and (B) in air. Reducing the lung volume leads to a marginal improvement on the TDF in both media, suggesting that the animal cannot realistically use time-difference cues to localize sound sources. The sound-source direction is $\theta = 90^\circ$ in all cases.

4.5.2 Barn owl

Cavity resonance

Given the high hearing frequency range of the barn owl, it is likely that the acoustic resonance of its interaural cavity plays a significant role in its hearing. An internal separation of 40 mm ($(L_C + 2L_T)$, cf. Table 4.1) between the barn owl's eardrums of Fig. 4.5b give an estimated first and second resonance frequencies of about 4.3 kHz and 8.6 kHz ($f_1 = c/2(L_C + 2L_T)$ & $f_2 = c/(L_C + 2L_T)$) for a sound speed of $c = 343$ m/s at 20°C, respectively. These frequencies are certainly within the hearing range, in which the animal is capable of azimuthal sound localization. Although the exact resonance frequency deviates slightly from this rough estimate, we will subsequently see that the value still lies within the barn owl's hearing range. In previous treatments of ICE [49, 50], as well as in our description of ICE for lizards (see Chapters 2 and 3), the interaural coupling was achieved through cylindrical acoustic cavities. The resonances of cylindrical acoustic ducts, however, deviate from those of realistic interaural cavities. For example, the resonance frequency of the interaural cavity of a Tokay gecko skull with an interaural separation of 2.2 cm [25] was numerically estimated by Vossen [49] to be around 3.2 kHz. On the other hand, the resonance frequency of a closed cylinder of length $L = 2.2$ cm is around 7.7 kHz. As the barn owl interaural cavity narrows down to around 3 mm in diameter at its center [56], there will likely be a similar deviation of its resonance from that of a cylindrical cavity.

The resonance behavior of the interaural cavity can be seen most clearly through the $\Gamma_\pm$ coefficients defined for the barn owl in Eq. (4.72). Using the definition of ς_{owl} from

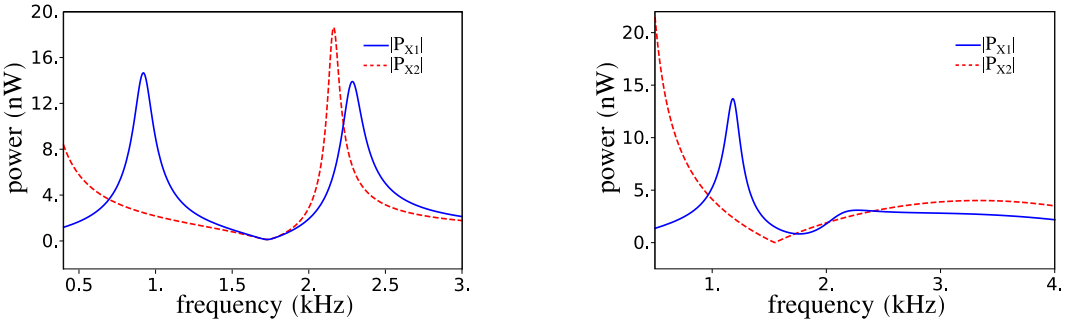

(a) Underwater (b) In air

Fig. 4.17 Frequency dependence of the power absorption by *Xenopus*' ICE system (dB re nW) for a lung volume $V_H = 1.5$ cm^3 (A) underwater and (B) in air. The solid (blue) line corresponds to *Xenopus* as it exists in nature with rigid-plate eardrums, whereas the dashed (red) line corresponds to the fictitious *Xenopus*2 with thin, flexible, eardrums. In all cases the sound-source direction is $\theta = 90°$. Compared to flexible "lizard-like" eardrums, the rigid-plate eardrums absorb more sound power both underwater and in air in the behaviorally relevant 1 kHz region, suggesting that the *Xenopus* eardrum is adapted to hearing underwater.

Eq. (4.56), the expressions for $\Gamma_{\pm}^{\text{owl}}$ can be simplified into the form

$$\Gamma_{+}^{\text{owl}} = -\frac{\rho c^2 k}{S_T} \frac{(S_T - S_C \tan kL_T \tan kL_C/2) + i\chi_H (S_C \tan kL_T + S_T \tan kL_C/2)}{(S_T \tan kL_T + S_C \tan kL_C/2) - i\chi_H (S_C - S_T \tan kL_T \tan kL_C/2)} , \tag{4.84}$$

$$\Gamma_{-}^{\text{owl}} = \frac{\rho c^2 k}{S_T} \frac{S_C \tan kL_T + S_T \tan kL_C/2}{S_C - S_T \tan kL_T \tan kL_C/2} . \tag{4.85}$$

In the absence of the Helmholtz resonator, we have $\chi_H \to 0$. Further setting $S_C \to S_T$ in Eqs. (4.84) and (4.85) reduces the $\Gamma_{\pm}^{\text{owl}}$ coefficients to

$$\Gamma_{+}^{\text{cyl}} = -\frac{\rho c^2 k}{S_T} \cot k(L_T + L_C/2) \quad \text{and} \quad \Gamma_{-}^{\text{cyl}} = \frac{\rho c^2 k}{S_T} \tan k(L_T + L_C/2) ,$$

which are equivalent to the $\Gamma_{\pm}$ coefficients for the lizard defined in Eqs. (2.8) and (2.9), but now for a cylinder of length $2L_T + L_C$ and cross section S_T. It should be immediately apparent, that our naive estimate for the resonance frequency, i.e. $f = c/2(L_C + 2L_T)$ and its odd multiples correspond to $\Gamma_{-}^{\text{cyl}} \to \infty$, whereas its even multiples correspond to $\Gamma_{+}^{\text{cyl}} \to \infty$. Moreover, as the $\Gamma_{\pm}$ coefficients result from Neumann boundary conditions Eqs. (4.70) and (4.71) the eardrum, their divergences correspond to the resonances of a *closed* cavity.

Estimating the resonances of the cavity: In order to exactly calculate the resonances of the interaural cavity, we therefore seek the divergences of $\Gamma_{\pm}^{\text{owl}}$ in the absence of the Helmholtz

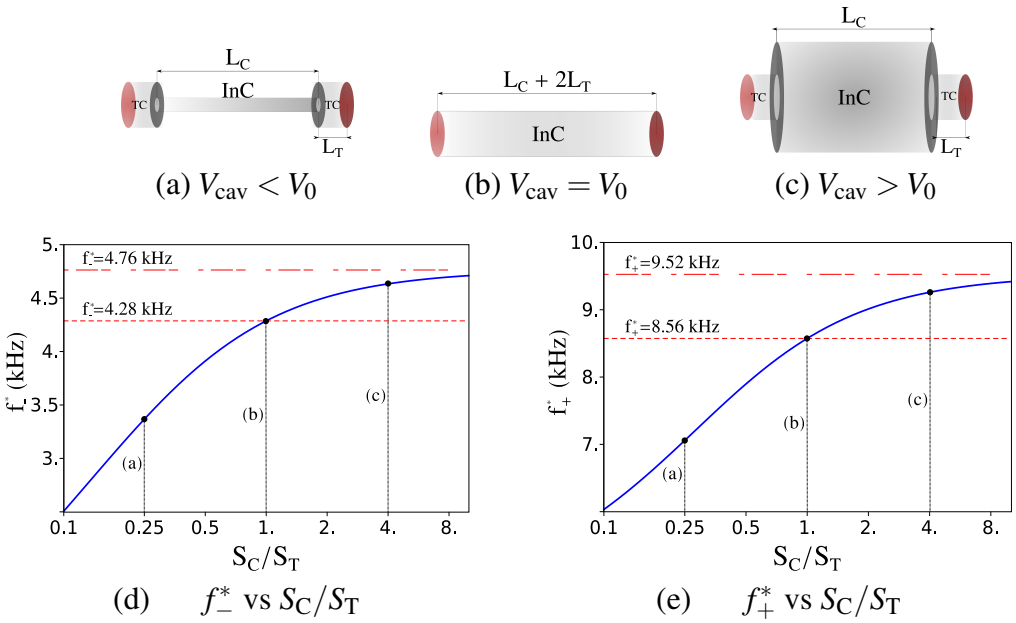

(a) $V_{\text{cav}} < V_0$ (b) $V_{\text{cav}} = V_0$ (c) $V_{\text{cav}} > V_0$

(d) f_-^* vs S_C/S_T (e) f_+^* vs S_C/S_T

Fig. 4.18 Interaural cavity shapes when the internal canal (InC) is narrower than (a), equal in cross section to (b) and wider than (c) the tympanic cavities (TC); cf. Fig. 4.5b. (b) corresponds to the interaural cavity used in a previous treatment of ICE [49, 50] and has a volume V_0 equal to a cylinder with a radius equal to that of the eardrum and a length equal to the interaural distance. (a) and (c) correspond to volumes lesser and greater than V_0, respectively. In (d)&(e) we plot the continuous variation of the resonance frequencies $f_\mp^*$ (corresponding to the poles of $\Gamma_\mp$; cf. Eqs. (4.86) and (4.87)) of the interaural cavity with the ratio of the cross section of the internal canal and tympanic cavity, i.e. S_C/S_T. The resonance frequencies of the configurations in (a), (b) & (c) are indicated via vertical dotted black lines, whereas the (horizontal) dashed red line denotes the resonance frequency of a cylinder of length $2L_T = L_C$ =40 mm. From (d) and (e) we also see that the resonance frequencies increase with S_C/S_T, and are bounded above by the resonances of the cylinder of length $L_C = 36$ mm.

resonator, i.e., $V_H = 0$. To do so, we set the denominators in Eqs. (4.84) and (4.85) as well as χ_H to zero, which results in the following transcendental equations for the resonance frequencies $f_\pm^*$

$$\Gamma_- \longrightarrow \tan k_\pm^* L_T \tan k_\pm^* L_C/2 = S_C/S_T \,, \tag{4.86}$$

$$\Gamma_+ \longrightarrow \tan k_\pm^* L_T + \frac{S_C}{S_T} \tan k_\pm^* L_C/2 = 0 \,, \tag{4.87}$$

$$\text{where} \quad k_\pm^* = \frac{2\pi f_\pm^*}{c} \,.$$

In Figs. 4.18a to 4.18c, we illustrate three different configurations for analyzing the dependence of the cavity resonance of *closed* cavities on their volume. Fig. 4.18b corresponds to a standard cylindrical interaural cavity of length L, similar to the one used by to model the interaural cavity in the common house gecko and Tokay in an earlier treatment of ICE [49, 50]; cf. Fig. 2.6a. Figure 4.18a corresponds to the interaural cavity of the barn owl, where the internal canal is narrower than the tympanic cavities, whereas in Figure 4.18c, the converse is true, i.e the internal canal is wider than the tympanic cavities. In Figs. 4.18d and 4.18e, we graph the variation of the resonance frequencies $f_{\pm}^{*}$ with the ratio of the cross sections of the internal canal and tympanic cavities, $S_{\mathrm{C}}/S_{\mathrm{T}}$. We see that the resonance frequency increases with a wider internal canal, implying that, the resonance frequency of the barn owl interaural cavity occurs *below* that of a cylinder of the same length. For a configuration based on the parameters from Table 4.1, the first two resonance frequencies calculated from Eqs. (4.86) and (4.87) are

$$f_{-}^{*} = 3.37 \text{ kHz} \qquad \text{and} \qquad f_{+}^{*} = 7.06 \text{ kHz}, \tag{4.88}$$

which are considerably lower than our initial naive estimates of 4.3 kHz and 8.6 kHz. Furthermore, our results are consistent with the numerical estimates of Vossen [49], where a widening of the interaural cavity around its center led to an increase in the fundamental frequency.

Setting the $\Gamma_{\pm}$ coefficients to infinity in Eq. (4.80) results in membrane vibrations that are either fully out-of or in phase, respectively. Moreover, they do so with equal amplitude regardless of the sound source direction. A consequence of this is that all directional information contained in $p_{0/L}^{\mathrm{ex}}$ is lost. Such a complete loss of directional information, would put a nocturnal predator like the barn owl at a great disadvantage in terms of prey localization. However, the barn owl hears without any apparent difficulty at least up to 9 kHz [87], even though both interaural cavity resonances are seemingly below this frequency. This apparent discrepancy is resolved by requiring a finite volume of the Helmholtz resonator V_{H}, which results in a non-zero value for χ_{H} and, consequently, a non-zero denominator in Eq. (4.84). The presence of the Helmholtz resonator thus immediately eliminates the "even" resonances associated with Γ_{+}. As a result, a medially attached Helmholtz resonator could be of great advantage to the barn owl with regard to its hearing and sound localization. As we will subsequently see, tuning the Helmholtz resonator such that $f_{\mathrm{H}} = f_{-}^{*}$, will also significantly improve the generation of both iTD and iLD cues, as well as the hearing sensitivity close to f_{-}^{*}.

Eardrum vibration amplitude

Given the high hearing frequency range of the barn owl, both the resonances of the interaural cavity $f_{\pm}^{*}$ calculated previously can influence hearing in the animal. As the Helmholtz resonator represents the cavity of the sphenoid bone, its volume cannot be voluntarily or involuntarily varied by the animal, unlike in the case of *Xenopus*. However, as the choice of the volume V_{H} and thus the resonance frequency f_{H} of the Helmholtz resonator as well as its relation to the cavity resonances $f_{\pm}^{*}$ has important consequences for the frequency and directional behavior of the system, we will be treating it as a variable parameter in the following. In Figs. 4.19a to 4.19c the frequency dependence average vibration velocities $i\omega u_{0/L}^{\mathrm{ave}}$ of the eardrum for different directions are plotted for three cases:

1. without a medially attached Helmholtz resonator, i.e. $V_{\mathrm{H}} = 0$ or $f_{\mathrm{H}} \to \infty$,
2. with a resonator such that $f_{\mathrm{H}} = f_{-}^{*}$, or $V_{\mathrm{H}} \approx 1.65$ cc and,
3. with a "large" resonator such that $f_{\mathrm{H}} = 0.7 f_{-}^{*}$, or $V_{\mathrm{H}} \approx 3.4$ cc.

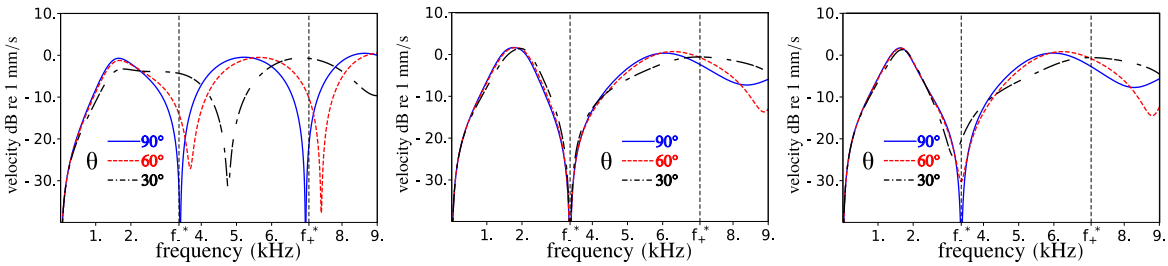

(a) $f_{\mathrm{H}} \to \infty$ (b) $f_{\mathrm{H}} = f_{-}^{*}$ (c) $f_{\mathrm{H}} = 0.7 f_{-}^{*}$

Fig. 4.19 Vibration velocity of the barn owl eardrum for different sound source directions θ (a) without, (b) with a medially attached Helmholtz resonator of resonance f_{H} frequency equal to the cavity resonance f_{-}^{*}, and (c) with a large attached resonator such that, $f_{\mathrm{H}} = 0.7 f_{-}^{*}$. In all three cases, we see "dips" in the velocity corresponding to the resonance f_{-}^{*} of the interaural cavity. However, when $f_{\mathrm{H}} = f_{-}^{*}$, the drops in velocity are limited to a narrower frequency region, independent of the source direction. The second dip at f_{+}^{*} is only present when the Helmholtz resonator is absent and is eliminated by its presence, thereby improving the animal's hearing sensitivity around f_{+}^{*}. The solid (blue) line and the dashed (red) line correspond to $\theta = 90^{\circ}$ and $\theta = 60^{\circ}$, respectively, whereas the dot-dashed (black) line corresponds to $\theta = 30^{\circ}$ The units are decibel values with respect to a velocity of 1 mm/s with a sound input amplitude of 1 Pa.

In all three figures, we see pronounced drops in the vibration velocity of the eardrum in the vicinity of the first resonance frequency of the interaural cavity f_{-}^{*}. However, in

Fig. 4.19b, the frequency at which the drop in velocity occurs is independent of direction, unlike in the other two cases. The reason for this is that, by setting $f_{\mathrm{H}} = f_{-}^{*}$, we have made both Γ_{+} and Γ_{-} diverge at $f = f_{-}^{*}$; cf. Eqs. (4.84) and (4.85). As a result, by effectively "tuning" the volume of the resonator, the frequency region in which the hearing sensitivity can be impaired has been reduced to a narrower band. The second drop in velocity in, which corresponds to the second resonance of the interaural cavity f_{+}^{*}, is only present in the absence of a medially attached resonator. A Helmholtz resonator with a finite volume constrains Γ_{+} to take a non-zero value, thereby effectively eliminating the second resonance; cf. Eq. (4.84). The influence of the Helmholtz resonator can, however, be seen more clearly by analyzing the resulting directional hearing cues, i.e., the internal time and level differences (iTD & iLD).

Internal level difference

In a similar fashion to the eardrum vibration amplitude, the frequency dependence of the internal level difference (iLD) between the eardrum vibrations (4.81) is plotted for a cavity with Helmholtz resonance frequency $f_{\mathrm{H}} \to \infty$ or, equivalently, volume zero in in Fig. 4.20a, for a resonance frequency $f_{\mathrm{H}} = f_{-}^{*}$ in Fig. 4.20b, and for a large cavity of volume $V_{\mathrm{H}} \approx 3.4$ cm^3 or $f_{\mathrm{H}} = 0.7 f_{-}^{*}$ in Fig. 4.20c. As in the case of the vibration velocity, we see that the choice of the Helmholtz resonator volume V_{H} has important consequences for the generation of sound localization cues. As in the case of the lizards, the *interaural* level difference between the inputs to the ears is effectively zero; cf. Eq. (4.76).

In contrast to the case of the lizards Section 3.3, the peak iLD occurs well below the chosen membrane resonance frequency $f_0 = 3.0$ kHz. This is a consequence of the fact that, due the geometry of the system, the cavity resonance is considerably lower than that of a cylindrical interaural cavity. From Figs. 4.20b and 4.20c, we see that the presence of a resonator generates considerable iLD cues between 1 & 2 kHz, which is consistent with the observed low-frequency behavior of the interaural cavity [56], as well as with the range of interspecific calls in the barn owl [89]. However, the case with a smaller cavity volume of around 1.65 cc, such that $f_{\mathrm{H}} = f_{-}^{*}$ generates much higher (≈ 12 dB) iLD cues, as compared to the case with a cavity of volume of around 3.4 cc, such that $f_{\mathrm{H}} = 0.7 f_{-}^{*}$, suggesting that the Helmholtz resonator volume can be optimized with respect to the interaural cavity volume. As in the case of *Xenopus*, a smaller resonator volume results in a higher frequency peak for the iLD. The presence of a tuned resonator also eliminates the sharp drop in the iLD at the first cavity resonance f_{-}^{*} , as compared to the other two cases.

From Fig. 4.20a it can be discerned that, without a medially attached resonator, the iLD for a source at 30° is higher than for those at 60° and 90°. This can be seen more clearly in

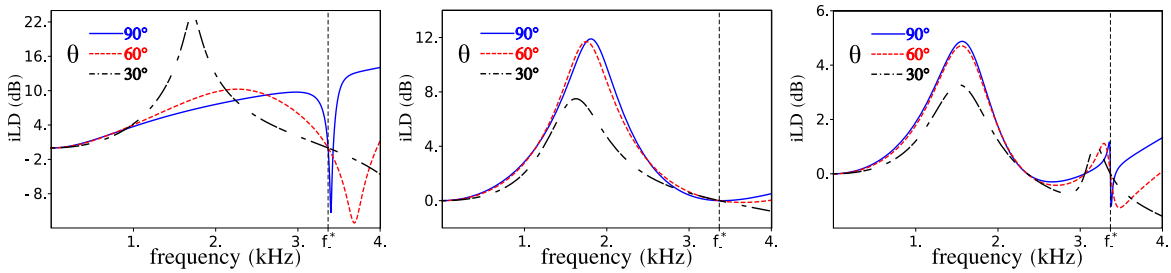

(a) $f_{\mathrm{H}} \to \infty$ (b) $f_{\mathrm{H}} = f_{-}^{*}$ (c) $f_{\mathrm{H}} = 0.7 f_{-}^{*}$

Fig. 4.20 Frequency dependence of the decibel internal level difference (iLD) between the barn owl eardrums for different sound source directions θ (a) without, (b) with a medially attached Helmholtz resonator of resonance f_{H} frequency equal to the cavity resonance f_{-}^{*}, and (c) with a "large" attached resonator such that, $f_{\mathrm{H}} = 0.7 f_{-}^{*}$. The directions shown are with respect to the ipsilateral ear, where the positive angle corresponds to a sound source on the same side as the ear; cf. Fig. 4.9b. The solid (blue) line and the dashed (red) line correspond to $\theta = 90^{\circ}$ and $\theta = 60^{\circ}$, respectively, whereas the dot-dashed (black) line corresponds to $\theta = 30^{\circ}$. The resonance frequencies of the cavity are denoted by $f_{\pm}^{*}$. The presence of a resonator results in considerable iLD cues between 1 & 2 kHz corresponding to the range of the barn owl's interspecific calls [56]. Furthermore, the "tuned" resonator in (b) removes the sharp drop in the iLD at $f = f_{-}^{*}$ as compared to (a)&(c) and thus improves the quality of iLD cues.

Fig. 4.21a, where we plot the direction dependence of the interaural level difference between the eardrum vibrations for different input frequencies, in the absence of a resonator. For comparison, we also plot the direction dependence of the iLDs for the case with a cavity with Helmholtz resonance at $f_{\mathrm{H}} = f_{-}^{*}$ in Fig. 4.21b as well as for the case with a larger resonator with a resonance frequency $f_{\mathrm{H}} = 0.7 f_{-}^{*}$ in Fig. 4.21c. In all three cases we see a sharp increase across 0°, which becomes less pronounced with an increase in the resonator volume. The presence of the resonator, however, generates iLD cues that are maximal at 90°, i.e., with the source closest to the ipsilateral ear, similar to that for the Tokay gecko; cf. Fig. 3.7a.

Internal time difference

In contrast to the lizards, barn owls are capable of neuronally processing time difference cues to localize sound at frequencies up to 10 kHz [122]. Given their relatively large interaural distance and the fact that they live in air, barn owls would have a maximal ITD of around 145 μs between their ears. On the one hand, we cannot expect a significant time dilation factor or TDF (iTD/ITD) in our model for the entire hearing range, given that the fundamental frequency of the tympanic membrane is 3 kHz; cf. Table 4.1. On the other hand, as shown

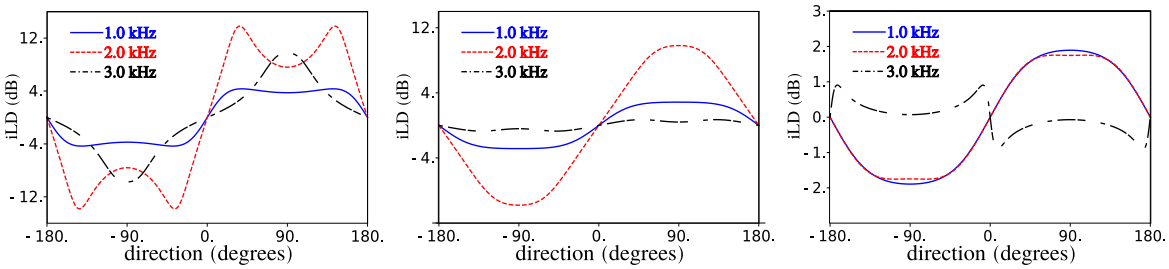

(a) $f_{\mathrm{H}} \to \infty$ (b) $f_{\mathrm{H}} = f_{-}^{*}$ (c) $f_{\mathrm{H}} = f_{-}^{*}$

Fig. 4.21 Direction dependence of the decibel internal level difference (iLD) between the barn owl eardrums for different sound source directions θ (a) without, (b) with a medially attached Helmholtz resonator of resonance f_{H} frequency equal to the cavity resonance f_{-}^{*}, and (c) with a large attached resonator such that, $f_{\mathrm{H}} = 0.7 f_{-}^{*}$. The directions shown are with respect to the ipsilateral ear, where the positive angle corresponds to a sound source on the same side as the ear; cf. Fig. 4.9b. The solid (blue) line and the dashed (red) line correspond to a frequency $f = 1.0$ kHz and $f = 2.0$ kHz, respectively, whereas the dot-dashed (black) line corresponds to $f = 3.0$ kHz. In all cases there is a sharp increase across $\theta = 0^{\circ}$, which becomes less pronounced with an increase in V_{H}. The directional behavior of the case $f_{\mathrm{H}} = f_{-}^{*}$ (b), with its maximum at $\theta = 90^{\circ}$ makes it most conducive to sound localization.

earlier in this chapter, both the first and second resonances of the interaural cavity $f_{\mp}^{*}$ lie within this range; cf. Section 4.5.2. As a result, unlike in the case of the lizards, the influence of the cavity resonance is bound to play a role in generation of iTD cues in the barn owl. As in the case of the vibration amplitude and iLD, the TDF is plotted against input frequency for different sound source directions in the absence of a Helmholtz resonator in Fig. 4.22a, for a "tuned" Helmholtz resonator with frequency $f_{\mathrm{H}} = f_{-}^{*}$ in Fig. 4.20b, and for a large cavity of volume $V_{\mathrm{H}} \approx 3.4$ cm^3 or $f_{\mathrm{H}} = 0.7 f_{-}^{*}$ in Fig. 4.20c.

In Figs. 4.22a and 4.22c, we see abrupt increases in the TDF in the vicinity of f_{-}^{*} which, however, are absent in the presence of a "tuned" Helmholtz resonator with frequency $f_{\mathrm{H}} = f_{-}^{*}$ in Fig. 4.22b. The abrupt decrease in the TDF in the vicinity of f_{+}^{*} is only present in the absence of a resonator with finite volume, and is removed by the resonator as Γ_{+} (4.84) no longer diverges at f_{+}^{*} with a finite resonator volume. In addition, the TDF between f_{-}^{*} and f_{+}^{*} is no longer flat, but rather varies with both direction and frequency and is therefore disadvantageous with respect to neuronal processing. Although the system does not generate an amplification of time difference cues over the relevant hearing range, the presence of a tuned Helmholtz resonator ensures a flat frequency dependence of the iTD independent of the sound source direction, similar to the lizards at low frequencies (see Figs. 3.6a and 3.6b).

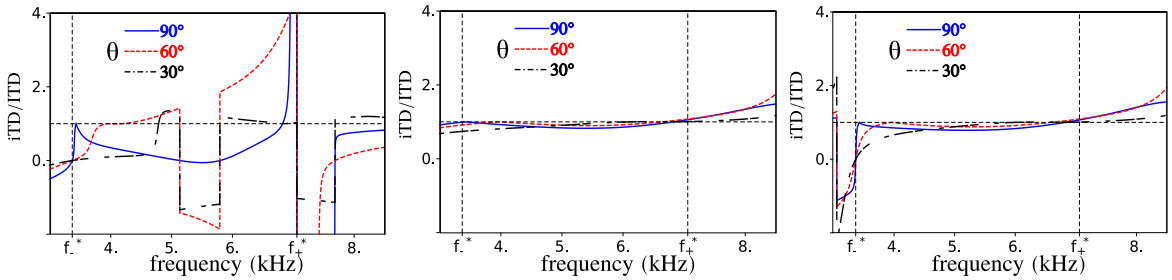

(a) $f_{\mathrm{H}} \to \infty$ (b) $f_{\mathrm{H}} = f_{-}^{*}$ (c) $f_{\mathrm{H}} = 0.7 f_{-}^{*}$

Fig. 4.22 Frequency dependence of the time dilation factor (iTD/ITD) between the barn owl eardrums for different sound source directions θ (a) without, (b) with a medially attached Helmholtz resonator of resonance f_{H} frequency equal to the cavity resonance f_{-}^{*}, and (c) with a large attached resonator such that, $f_{\mathrm{H}} = 0.7 f_{-}^{*}$. With the resonator, there is an increase in the iTD with respect to the interaural time difference (ITD). Unlike the case without a resonator, however, the frequency dependence is flat, which is far more conducive to neuronal processing. Moreover, the presence of the resonator eliminates the "jumps" associated with the higher resonance f_{+}^{*} of the interaural cavity, while a tuned resonator also improves the iTD around the lower resonance f_{-}^{*}. The artifact between 5.0 and 6.0 kHz for $\theta = 30^{\circ}$ & 60° in (a) corresponds to a change in phase from $+\pi$ to $-\pi$ and has no bearing on the iTD cues.

4.6 Conclusion

In the present chapter, a modified version of the ICE model from Chapter 2 has been developed to explain the sound localization ability of the African clawed frog *Xenopus* and the barn owl *Tyto alba*. Although the animals live in vastly different habitats and are anatomically very different, they share one significant similarity. In addition to having an interaural coupling between their eardrums, both animals have an air-filled cavity medially attached to their interaural cavity. In *Xenopus*, the lungs are attached to the interaural cavity, whereas in the barn owl the cavity of the sphenoid bone plays a similar role. In Section 4.1.1 we introduced the modified eardrum model for *Xenopus*, consisting of a rigid cartilaginous plate suspended in a flexible ring. By treating the ring as a homogeneous Kirchoff-Love plate, we were able to calculate the restoring force acting on the tympanic plate given a small deflection (4.12). As *Xenopus* is primarily an aquatic animal, the influence of the surrounding water was treated as an external force generated by the acoustic radiation resulting from its own vibration; cf. Section 4.1.1 and Eq. (4.17). For the barn owl, we relied on the anatomical similarities between the eardrums of most reptiles and birds and modeled its eardrum as flexible and lizard-like, albeit with distinct material parameters; cf. Section 4.1.2 and Table 4.1. The interaural cavities modeled for both animals in Section 4.2 share marked similarities. In both animals the interaural cavity is narrower in the middle than at the ears;

cf. Figs. 4.4a and 4.4b. The interaural cavity was thus modeled in both animals as two tympanic cavities (TC) connected via a narrower internal canal (InC); Figs. 4.5a and 4.5b. In contrast to the barn owl tympanic cavity, which could be modeled as having a cylindrical shape (see Figs. 4.6a and 4.6b), the *Xenopus* tympanic cavity has a distinct taper. As a result, it was modeled as having a conical structure; Figs. 4.6c and 4.6d. The pressure inside the *Xenopus* tympanic cavity was derived using Webster's horn equation (see Eqs. (4.25), (4.27) and (4.28)), whereas the pressure inside the barn owl tympanic cavity, as well as in the internal canal for both animals was modeled as a plane wave in a cylindrical cavity; Eqs. (4.23) and (4.24). The medially attached air-filled cavity was modeled in both cases as a Helmholtz resonator of volume V_{H}, attached to the internal canal via a duct of length L_{H} and cross section S_{H}. By requiring the conservation of pressure and volume flow rate at the junctions between the tympanic cavities and internal canals (Eqs. (4.32) to (4.39)), as well as at the junction between the internal canal and the Helmholtz resonator (Eqs. (4.40) and (4.41)) pressure at the internal surface of one eardrum was compactly expressed in terms of the pressure at the internal surface of the opposite eardrum by means of 2×2 matrices denoted by M (4.48), one for each animal. The properties of the matrices Eqs. (4.49) to (4.51) and (4.53) to (4.55), were then used along with the boundary conditions for the pressure at the eardrum surfaces to derive $\Gamma_{\pm}$ coefficients analogous to those derived for the lizards in Chapter 2. By modeling the sound inputs for both animals based on their size and medium of sound localization Eqs. (4.73) and (4.74), complete expressions for the directional coupled eardrum vibration amplitudes as a function of frequency were obtained for both *Xenopus* (4.78) and the barn owl (4.80).

Given external inputs to the ear with a small phase difference and no amplitude difference, the model agreed with eardrum vibration velocities measured by using laser vibrometry; cf. Figs. 4.10a and 4.10b. As shown in Fig. 4.12a, the model also generates significant internal level differences (iLDs) between the eardrum vibrations. Underwater, the lung inflation is essential to generating iLDs in the $1.7 - 2.0$ kHz region, corresponding to the advertisement calls of the male *Xenopus*. The peak iLD frequency also varied with lung volume, which suggests that *Xenopus* could inflate its lungs to tune its hearing; Fig. 4.13a. Enhanced hearing cues above 1.7 kHz would also be of advantage with regards to long-range communication in shallow water, as the medium itself behaves as a high-pass filter with a cut-off frequency of around 1.0 kHz at a depth of 0.5 m. On the other hand, lung inflation between $1.0 - 2.0$ cm^3 does not lead to significant iLD generation in air; cf. Fig. 4.13b. The presence of the lungs also significantly increases vibration velocity at lower frequencies ($0.8 - 1.2$ kHz) in both media and could thus improve hearing sensitivity at these frequencies, as illustrated by Figs. 4.11a and 4.11b. On the other hand, even accounting for lung inflation, there were

no significant internal time differences (iTDs) in both environments; see Figs. 4.15a, 4.15b, 4.16a and 4.16b. This suggests that the animal cannot use time difference cues to localize sound, but is bound instead to use internal level differences (iLDs) as sound localization cues. Finally, in Sec. 4.5.1, we compared the response of a *Xenopus* eardrum to that of a Tokay gecko eardrum, a typical terrestrial animal with ICE; cf. Chapters 2 and 3. To this end, we constructed a fictitious animal *Xenopus*2 with gecko-like eardrums coupled through the *Xenopus* interaural cavity described in Section 2.2.2 and compared the instantaneous sound power (4.83) absorbed in both cases. The rigid-plate eardrums absorbed more sound energy from the medium, both under water and in air in the behaviorally relevant 1 kHz region; cf. Figs. 4.17a and 4.17b. This suggests that *Xenopus*' eardrum and the connection of its lungs to the interaural cavity are adaptations to improve underwater hearing in the 1 kHz region and to improve underwater sound localization in the 1.7 kHz range, respectively.

The presence of a medially attached Helmholtz resonator was also shown to have significant effects in the generation of iTD and iLD cues in the barn owl as well. Given its larger size and high frequency range of hearing (up to 10 kHz), the resonances of the interaural cavity are bound to affect the animal's hearing and sound localization. The resonance frequencies $f_-^* = 3.37$ kHz and $f_+^* = 7.06$ kHz, estimated, respectively, from the divergence of the $\Gamma_\mp$ coefficients were both found to be within the animal's hearing range. Moreover, the variation of the resonance frequencies with the width of the internal canal was consistent with numerically determined values [49]. The presence of a medially attached resonator suppressed the effect of the higher resonance f_+^*, irrespective of the resonator volume; Figs. 4.19a to 4.19c. Moreover, by "tuning" the volume of the Helmholtz resonator such that its resonance frequency f_H was equal to the first cavity resonance f_-^*, the influence of f_-^* was limited to a much narrower frequency range, thereby improving hearing sensitivity in the vicinity of the resonance frequency. For the iLDs, it was shown that, the presence of a *tuned* resonator generates significant decibel level differences between eardrum vibrations in the 1-3 kHz range, corresponding to the range of interspecific calls in the barn owl [56]; Figs. 4.20a to 4.20c. Moreover, tuning the resonator ensures that maximal iLDs are present at 90°, while generating iLDs of up to 12 dB at the same time; Figs. 4.20b and 4.21b. Unlike lizards, which use iTDs as low frequency hearing cues, barn owls are capable of neuronally processing iTDs at frequencies up to 9 kHz [122]. Although the interaural coupling cannot generate a significant TDF beyond the fundamental frequency ($f_0 = 3$ kHz) of the eardrum (see Section 3.3), the cavity resonances $f_\pm^*$ can influence the iTDs. In the absence of the Helmholtz resonator, there were abrupt increases and decreases of the iTD in the vicinity of the resonances, corresponding to the eardrums vibrating either fully out-of- or in-phase with each other; Fig. 4.22a. As in the case of the vibration amplitude, the presence of a res-

onator nullified the effect of the second resonance f_+^*, irrespective of its volume; Figs. 4.22b and 4.22c. From Fig. 4.22b, it can also be seen that a tuned resonator with $f_{\mathrm{H}} = f_-^*$ also improves the iTD around the first resonance of the cavity. Finally, a Helmholtz resonator medially attached to the interaural cavity ensured a flat frequency dependence of the iTDs, thereby making it more conducive to neuronal processing, similar to the case of the lizards at low frequencies; cf. Figs. 3.6a and 3.6b. We conclude the chapter by stressing the subtle difference between *Xenopus* and the barn owl, with respect to the notion of "tuning" the Helmholtz resonator. In *Xenopus*, the tuning is an active process, as the lung volume can be voluntarily varied by a live frog. For the barn owl, however, the volume of the sphenoid cavity is only determined by the interaural cavity volume and cannot be actively controlled by the animal. In contrast to the previous two chapters, the present chapter is thus an extension of ICE to underwater and high-frequency hearing.

Chapter 5

Summary and Outlook

In this dissertation, a generalization of the mathematical theory of internally coupled ears or ICE, first developed by Vossen [49, 50] for lizards, was presented with regard to a better understanding of the material and geometrical parameters involved. In Chapter 2, complete expressions for the coupled vibrations of the eardrums in response to an external sound stimulus were derived, such that the influence of the material properties of the eardrums, as well as the geometry of the interaural cavity were immediately apparent; Eqs. (2.99) and (2.100). The derived expressions were then used in Chapter 3 to demonstrate the emergence of directionality in the vibrations of the individual eardrums (see Section 3.2), as well as the enhancement of directional hearing cues in the form of internal time and level differences (iTD and iLD); see Section 3.3. The iTD and iLD were enhanced in comparison to the small interaural time difference (ITD), and practically absent interaural level difference (ILD) between the sound inputs to the ears given the small head size of the animals. The role played by the fundamental frequency of the eardrum f_0 in segregating the hearing cues into a low-frequency iTD dominant region and a high-frequency iLD dominant region was also established; see Section 3.3.3. Moreover, the dependence of both hearing cues on the cavity volume was established in Section 3.5. The expressions derived in Chapter 2 and the results of Chapter 3 were then used to develop a numerical procedure to estimate the eardrum material parameters from an alive animal; see Section 3.6. Chapters 2 and 3 constitute a "definitive" ICE model for a typical animal which uses internally coupled ears as an adaptation for terrestrial low-frequency hearing.

The results of Chapters 2 and 3 were then extended to explain the unique hearing and sound localization abilities of the clawed frog *Xenopus* and barn owl *Tyto alba* in Chapter 4. The narrow interaural cavities of both animals are medially connected to an additional air-filled chamber which was modeled as a Helmholtz resonator; see Section 4.2. In *Xenopus*, this chamber corresponds to the lungs, while in the barn owl it is the cavity of the sphenoid

bone. It was demonstrated in Section 4.5.1 that the inflated lungs improve hearing in the behaviorally relevant 1 kHz range and increase iLDs around 1.7 kHz, corresponding to the male advertisement calls; cf. Figs. 4.11a and 4.12a. In contrast, the system offered neither any advantage to hearing in air, nor any to iTDs in air and water; Figs. 4.11b, 4.12b, 4.15a and 4.15b. The results indicate that, the lungs, in conjunction with the unique plate-like construction of the *Xenopus* eardrum (see Section 4.1.1) are adaptations to its underwater environment; also see Figs. 4.17a and 4.17b. In the barn owl, the Helmholtz resonator was found to improve hearing and sound localization by negating the effects of its interaural cavity resonances on both its eardrum vibrations and its iTDs at high frequencies; Figs. 4.19a to 4.19c and 4.22a to 4.22c. In addition, the presence of a medially attached cavity also enhanced the iLDs between 1.0 and 2.5 kHz, corresponding to its interspecific calls; Figs. 4.20a to 4.20c. Thus an entirely new application of ICE to sound localization has also been presented, as a contrast to the low-frequency terrestrial theme of Chapters 2 and 3.

Given the current state of research in ICE, and with regard to the terrestrial-underwater distinction between the chapters of this dissertation, it is interesting to ask if an animal, say, an alligator can have the best of both worlds, i.e., it is able to localize sound both underwater and in air. As the speed of sound is different in both media, and as localization using time differences is carried out through maps of the kind discussed in Section 1.1.1, the animal *cannot*, in general, use the same map both in air and underwater. However, given the large amount of time that alligators and other crocodilians spend hunting both underwater, and in air, an iTD-map based sound localization system equally well adapted to both environments would be highly advantageous. It was mentioned in passing in the introductory chapter of the present work that crocodilians also have an air-filled interaural connection between their ears; see Section 1.2. In contrast to the animals discussed so far, however, the interaural cavity of crocodilians is composed to two parallel, i.e., one dorsal and one ventral canal with an fleshy opening into the mouth cavity at the bottom of the ventral canal [32, 33]. Evidence of directionality in the eardrum vibrations has been observed in the American alligator in air [123, 124]. Taking these factors into account and, given their high amphibious hearing sensitivity [125], it is tempting to speculate that crocodilians can localize sound in both media, such that their underwater localization is governed by ICE, while in air they can rely on the interaural time and level differences generated by their considerable size. Studying the possible mechanisms that could to such a “hybrid” localization is therefore a natural next step in the understanding of ICE.

Chapter 6

Frequently Used Abbreviations

Table 6.1 List of Abbreviations

ICE	Internally coupled ears
TDF	Time dilation factor
IAC	Interaural cavity
TC	Tympanic cavity
InC	Internal canal
TM	Tympanic membrane
ITD	Interaural time difference
ILD	Interaural level difference
iTD	Internal time difference
iLD	Internal level difference
cc	Cubic centimeters

References

[1] L. Chittka and A. Brockmann. "Perception space—the final frontier". *PLoS Biol.*, 3 (4), 04 2005.

[2] J. Christensen-Dalsgaard, Y. Tang, and C. E. Carr. "Binaural processing by the gecko auditory periphery". *J. Neurophysiol.*, 105(5):1992–2004, May 2011.

[3] N. Anthwal, L. Joshi, and A. S. Tucker. "Evolution of the mammalian middle ear and jaw: adaptations and novel structures". *J. Anat.*, 222(1):147–160, Jan 2013.

[4] J. C. Saunders, K. R. Duncan, D. E. Doan, and Y. L. Werner. "The middle ear of reptiles and birds". In Robert J. Dooling, Richard R. Fay, and Arthur N. Popper, editors, *Comparative Hearing: Birds and Reptiles*, pages 13–69. Springer New York, New York, NY, 2000.

[5] J. W. Schnupp and C. E. Carr. "On hearing with more than one ear: lessons from evolution". *Nat. Neurosci.*, 12(6):692–697, jun 2009.

[6] J. A. Clack and E. Allin. "The evolution of single- and multiple-ossicle ears in fishes and tetrapods". In Geoffrey A. Manley, Richard R. Fay, and Arthur N. Popper, editors, *Evolution of the Vertebrate Auditory System*, pages 128–163. Springer New York, New York, NY, 2004.

[7] G. A. Manley and Jennifer A. Clack. "An outline of the evolution of vertebrate hearing organs". In G. A. Manley, Richard R. Fay, and Arthur N. Popper, editors, *Evolution of the Vertebrate Auditory System*, pages 1–26. Springer New York, New York, NY, 2004.

[8] J. A. Clack. "The evolution of tetrapod ears and the fossil record". *Brain Behav. Evol.*, 50(4):198–212, 1997.

[9] M. J. Mason. "Internally coupled ears in living mammals". *Biological Cybernetics*, 110(4):345–358, Oct 2016.

[10] P. Friedel, B. A. Young, and J. L. van Hemmen. "Auditory localization of ground-borne vibrations in snakes". *Phys. Rev. Lett.*, 100:048701, Jan 2008.

[11] J. Christensen-Dalsgaard, C. Brandt, K. L. Willis, C. B. Christensen, D. Ketten, P. Edds-Walton, R. R. Fay, P. T. Madsen, and C. E. Carr. "Specialization for underwater hearing by the tympanic middle ear of the turtle, *Trachemys scripta elegans*". *Proc. Royal Soc. Lond. B*, 279(1739):2816–2824, 2012.

[12] A. P. Vedurmudi, J. Goulet, J. Christensen-Dalsgaard, B. A. Young, R. Williams, and J. L. van Hemmen. "How internally coupled ears generate temporal and amplitude cues for sound localization". *Phys. Rev. Lett.*, 116:028101, Jan 2016.

[13] D. W. Batteau. "The role of the pinna in human localization". *Proc. Royal Soc. Lond. B*, 168(1011):158–180, 1967.

[14] K. Koka, H. G. Jones, J. L. Thornton, J. E. Lupo, and D. J. Tollin. "Sound pressure transformations by the head and pinnae of the adult Chinchilla (*Chinchilla lanigera*)". *Hear. Res.*, 272(1-2):135–147, Feb 2011.

[15] J. Blauert and J. S. Allen. *Spatial Hearing: The Psychophysics of Human Sound Localization*. MIT Press, 1997.

[16] J. W. Strutt. "On our perception of the direction of a source of sound". *Proceedings of the Musical Association*, 2:75–84, 1875.

[17] J. W. Strutt. "On our perception of sound direction". *Philos. Mag.*, 13(74):214–232, 1907.

[18] J. Schnupp, I. Nelken, and A. King. *Auditory Neuroscience: Making Sense of Sound*. MIT Press, 2011.

[19] A. Coffin, M. Kelley, G. A. Manley, and A. N. Popper. "Evolution of sensory hair cells". In Geoffrey A. Manley, Richard R. Fay, and Arthur N. Popper, editors, *Evolution of the Vertebrate Auditory System*, pages 55–94. Springer New York, New York, NY, 2004.

[20] D. J. Tollin and T. C. Yin. "Interaural phase and level difference sensitivity in low-frequency neurons in the lateral superior olive". *J. Neurosci.*, 25(46):10648–10657, Nov 2005.

[21] L. A. Jeffress. "A place theory of sound localization". *J. Comp. Physiol. Psychol.*, 41 (1):35–39, feb 1948.

[22] C. E. Carr and M. Konishi. "Axonal delay lines for time measurement in the owl's brainstem". *Proc. Natl. Acad. Sci. U.S.A.*, 85(21):8311–8315, Nov 1988.

[23] T. N. Parks and E. W. Rubel. "Organization and development of brain stem auditory nuclei of the chicken: organization of projections from n. magnocellularis to n. laminaris". *J. Comp. Neurol.*, 164(4):435–448, Dec 1975.

[24] J. M. Goldberg and P. B. Brown. "Response of binaural neurons of dog superior olivary complex to dichotic tonal stimuli: some physiological mechanisms of sound localization.". *J. Neurophysiol.*, 32(4):613–636, 1969. PMID: 5810617.

[25] J. Christensen-Dalsgaard and G. A. Manley. "Directionality of the lizard ear". *J. Exp. Biol.*, 208(6):1209–1217, 2005.

[26] J. Christensen-Dalsgaard and G. A. Manley. "Acoustical coupling of lizard eardrums". *J. Assoc. Res. Otolaryngol.*, 9(4):407–416, 2008.

[27] G. A. Manley. "A review of the auditory physiology of the reptiles". *Prog. Sens. Physiol.*, 2:49–134, 1981.

[28] A. Michelsen. "Hearing and sound communication in small animals: Evolutionary adaptations to the laws of physics". In Douglas B. Webster, Arthur N. Popper, and Richard R. Fay, editors, *The Evolutionary Biology of Hearing*, pages 61–77. Springer New York, 1992.

[29] S. H. Chung, A. Pettigrew, and M. Anson. "Dynamics of the amphibian middle ear". *Nature*, 272:142–147, Mar 1978.

[30] A. S. Feng and W. P. Shofner. "Peripheral basis of sound localization in anurans. acoustic properties of the frog's ear". *Hear. Res.*, 5(2):201 – 216, 1981.

[31] M. B. Jørgensen, B. Schmitz, and J. Christensen-Dalsgaard. "Biophysics of directional hearing in the frog eleutherodactylus coqui". *J. Comp. Physiol. A*, 168(2):223–232, 1991.

[32] R. Owen. "On the communications between the cavity of the tympanum and the palate in the crocodilia (gavials, alligators and crocodiles)". *Philos. Trans. R. Soc. Lond.*, 140:521–527, 1850.

[33] E. H. Colbert. "The eustachian tubes in the crocodilia". *Copeia*, 1946(1):12–14, 1946.

[34] Lawrence M. Witmer, Ryan C. Ridgely, David L. Dufeau, and Molly C. Semones. "Using CT to peer into the past: 3d visualization of the brain and ear regions of birds, crocodiles, and nonavian dinosaurs". In Hideki Endo and Roland Frey, editors, *Anatomical Imaging: Towards a New Morphology*, pages 67–87. Springer Japan, Tokyo, 2008.

[35] Michael B. Calford and Robert W. Piddington. "Avian interaural canal enhances interaural delay". *J. Comp. Physiol. A*, 162(4):503–510, Jul 1988.

[36] R. L. Hyson, E. M. Overholt, and W. R. Lippe. "Cochlear microphonic measurements of interaural time differences in the chick". *Hear. Res.*, 81(1-2):109–118, Dec 1994.

[37] O. N. Larsen, R. J. Dooling, and A. Michelsen. "The role of pressure difference reception in the directional hearing of budgerigars (melopsittacus undulatus)". *J. Comp. Physiol. A*, 192:1063–1072, 2006.

[38] K. G. Hill, D. B. Lewis, M. E. Hutchings, and R. B. Coles. "Directional hearing in the Japanese quail (*Coturnix Coturnix Japonica*): I. Acoustic properties of the auditory system". *J. Exp. Biol.*, 86(1):135–151, 1980.

[39] M. J. Lankheet, U. Cerkvenik, O. N. Larsen, and J. L. van Leeuwen. "Frequency tuning and directional sensitivity of tympanal vibrations in the field cricket Gryllus bimaculatus". *J. Royal Soc. Interface*, 14(128), Mar 2017.

[40] D. Robert, R.N. Miles, and R.R. Hoy. "Directional hearing by mechanical coupling in the parasitoid fly ormia ochracea". *J. Comp. Physiol. A*, 179(1):29–44, 1996.

[41] J. L. van Hemmen, J. Christensen-Dalsgaard, C. E. Carr, and Peter M. Narins. "Animals and ice: meaning, origin, and diversity". *Biol. Cybern.*, 110(4):237–246, Oct 2016.

[42] Hansjochem Autrum. "Über lautäußerungen und Schallwahrnehmung bei Arthropoden II. Das Richtungshören von Locusta und Versuch einer Hörtheorie für Tympanalorgane vom Locustidentyp". *Z. Vergl. Physiol.*, 28:326–352, 1940.

[43] H. Autrum. "Schallempfang bei Tier und Mensch". *Naturwissenschaften*, 30:69–85, January 1942.

[44] A. Michelsen. "The physiology of the locust ear". *J. Comp. Physiol.*, 71(1):102–128, Mar 1971.

[45] H. F. Olson. "Gradient microphones". *J. Acoust. Soc. Am.*, 17(3):192–198, 1946.

[46] J. Christensen-Dalsgaard and C.E. Carr. "Evolution of a sensory novelty: tympanic ears and the associated neural processing.". *Brain. Res. Bull.*, 75(2-4):365–70, 2008.

[47] C. E. Carr and J. Christensen-Dalsgaard. "Evolution of the auditory system". In E. Bruce Goldstein, editor, *Encyclopedia of Perception*. SAGE Publications, Inc., Thousand Oaks, 2010.

[48] A. P. Vedurmudi, B. A. Young, and J. L. van Hemmen. "Internally coupled ears: mathematical structures and mechanisms underlying ICE". *Biol. Cybern.*, 110(4-5): 359–382, October 2016.

[49] C. Vossen. *Auditory Information Processing in Systems with Internally Coupled Ears*. PhD thesis, Technische Universität München, 2010.

[50] C. Vossen, J. Christensen-Dalsgaard, and J. L. van Hemmen. "Analytical model of internally coupled ears.". *J. Acoust. Soc. Am.*, 128:909–918, 2010.

[51] G. A. Manley. "The middle ear of the tokay gecko". *J. Comp. Physiol.*, 81(3):239–250, 1972.

[52] E. G. Wever. *The reptile ear: Its structure and function*. Princeton University Press, Princeton, NJ, 1978.

[53] G. A. Manley. "The hearing organs of lizards". In Robert J. Dooling, Richard R. Fay, and Arthur N. Popper, editors, *Comparative Hearing: Birds and Reptiles*, pages 139–196. Springer New York, New York, NY, 2000.

[54] G. A. Manley. "Frequency response of the middle ear of geckos". *J. Comp. Physiol.*, 81(3):251–258, 1972.

[55] E. G. Wever. "The evolution of vertebrate hearing". In W. D. Keidel and W. D. Neff, editors, *Auditory System: Anatomy Physiology (Ear)*, pages 423–454. Springer Berlin Heidelberg, Berlin, Heidelberg, 1974.

[56] L. Kettler, J. Christensen-Dalsgaard, O. N. Larsen, and H. Wagner. "Low frequency eardrum directionality in the barn owl induced by sound transmission through the interaural canal". *Biol. Cybern.*, 110(4-5):333–343, Oct 2016.

[57] J. Christensen-Dalsgaard and A. Elepfandt. "Biophysics of underwater hearing in the clawed frog, *Xenopus laevis*". *J. Comp. Physiol. A*, 176(3):317–324, May 1995.

[58] C. Köppl and C. E. Carr. "Maps of interaural time difference in the chicken's brainstem nucleus laminaris". *Biol. Cybern.*, 98(6):541–559, 2008.

[59] D. Han and B. A. Young. "Biophysical heterogeneity in the tympanic membrane of the asian water monitor lizard, varanus salvator". *Zoomorphology*, Feb 2018.

[60] A. Michelsen and O. N. Larsen. "Pressure difference receiving ears". *Bioinspiration Biomim.*, 3(1):011001, 2008.

[61] N. H. Fletcher. *Acoustic Systems in Biology*. Oxford University Press, Oxford, 1992.

[62] E. Ventsel and T. Krauthammer. *Thin Plates and Shells: Theory: Analysis, and Applications*. Taylor & Francis, 2001.

[63] E. Kreyszig. *Advanced Engineering Mathematics*. John Wiley & Sons, 2010.

[64] N. H. Asmar. *Partial Differential Equations with Fourier Series and Boundary Value Problems*. Pearson Education, Limited, 2005.

[65] E. T. Copson. *Introduction to the Theory of Functions of a Complex Variable*. Clarendon Press, Oxford, 1973.

[66] M. Abramowitz and I. A. Stegun. *Handbook of Mathematical Functions with Formulas, Graphs, and Mathematical Tables*. Dover, New York, 1964.

[67] M. B. Jørgensen. "Vibrational patterns of the anuran eardrum". In Norbert Elsner and Martin Heisenberg, editors, *Gene-Brain-Behaviour. Proceedings of the 21st Göttingen Neurobiology Conference*, page 231, Stuttgart, 1993. Georg Thieme Verlag.

[68] M. B. Jørgensen and M. Kanneworff. "Middle ear transmission in the grass frog, Rana temporaria". *J. Comp. Physiol. A*, 182(1):59–64, Jan 1998.

[69] D. T. Heider and J. L. van Hemmen. "Geometric Perturbation Theory for a Class of Fiber Bundles". *ArXiv e-prints*, December 2018.

[70] S. N. Rschevkin, O. M. Blunn, and P. E. Doak. *A Course of Lectures on the Theory of Sound.* Pergamon, 1963.

[71] S. Temkin. *Elements of Acoustics*. Wiley, 1981.

[72] W. J. Duncan, A. S. Thom, and A. D. Young. *Mechanics of Fluids*. Arnold, 1970.

[73] C. Pozrikidis. *Fluid Dynamics: Theory, Computation, and Numerical Simulation*. Springer, 2009.

[74] C. Rajalingham, R.B. Bhat, and G.D. Xistris. "Vibration of circular membrane backed by cylindrical cavity". *Int. J. Mech. Sci.*, 40(8):723 – 734, 1998.

[75] L. Zhang, J. Hallam, and J. Christensen-Dalsgaard. "Modelling the peripheral auditory system of lizards". In Stefano Nolfi, Gianluca Baldassarre, Raffaele Calabretta, John C.T. Hallam, Davide Marocco, Jean-Arcady Meyer, Orazio Miglino, and Domenico Parisi, editors, *From Animals to Animats 9*, volume 4095 of *Lecture Notes in Computer Science*, pages 65–76. Springer Berlin Heidelberg, 2006.

[76] J. Zwislocki. "Analysis of the middle-ear function. Part I: Input impedance". *J. Acoust. Soc. Am.*, 34(9B):1514–1523, 1962.

[77] R. Fitzpatrick. *Oscillations and Waves: An Introduction*. Oscillations and Waves: An Introduction. Taylor & Francis, 2013.

[78] G. A. Manley. "Cochlear mechanisms from a phylogenetic viewpoint". *Proceedings of the National Academy of Sciences*, 97(22):11736–11743, 2000.

[79] M. R. Szpir, S. Sento, and D. K. Ryugo. "Central projections of cochlear nerve fibers in the alligator lizard". *J. Comp. Neurol.*, 295(4):530–547, May 1990.

[80] M. B. Calford. "Constraints on the coding of sound frequency imposed by the avian interaural canal". *J. Comp. Physiol. A*, 162(4):491–502, 1988.

[81] P. G. G. Muyshondt, J. A. M. Soons, D. de Greef, F. Pires, P. Aerts, and J. J. J. Dirckx. "A single-ossicle ear: Acoustic response and mechanical properties measured in duck". *Hearing Research*, 340:35 – 42, 2016. MEMRO 2015 – Basic Science meets Clinical Otology.

[82] J. Stoer and R. Bulirsch. *Introduction to numerical analysis*. Texts in applied mathematics. Springer, 2002.

[83] J. Christensen-Dalsgaard and T. M. Elliott. "Amphibian underwater hearing: Biophysics and neurophysiology". *Bioacoustics*, 17(1-3):60–62, 2008.

[84] R. Müller and U. Scheer. "Klangspektrographische untersuchung der lautäusserung beim krallenfrosch,xenopus laevis". *Experientia*, 26(4):435–436, Apr 1970.

[85] M. L. Tobias, B. J. Evans, and D. B. Kelley. "Evolution of advertisement calls in African clawed frogs". *Behaviour*, 148(4):519–549, 2011.

[86] M. D. Picker. "Hormonal induction of the aquatic phonotactic response of xenopus by". *Behaviour*, 84(1):74–90, 1983.

[87] M. Konishi. "How the owl tracks its prey: Experiments with trained barn owls reveal how their acute sense of hearing enables them to catch prey in the dark". *Am. Sci.*, 61 (4):414–424, 1973.

[88] E. I. Knudsen, G. G. Blasdel, and M. Konishi. "Sound localization by the barn owl (tyto alba) measured with the search coil technique". *Journal of comparative physiology*, 133(1):1–11, Mar 1979.

[89] P. Bühler and W. Epple. "Die Lautäußerungen der Schleiereule (tyto alba)". *J. Ornithol.*, 121(1):36–70, Jan 1980.

[90] A. Moiseff and M. Konishi. “The owl’s interaural pathway is not involved in sound localization”. *J. Comp. Physiol.*, 144(3):299–304, Sep 1981.

[91] E. Stellbogen. “Über das äußere und mittlere Ohr des Waldkauzes (*Syrnium aluco L.*)”. *Z. Morphol. Oekol. Tiere*, 19(4):686–731, 1930.

[92] S. H. Chung, A. Pettigrew, and M. Anson. “Hearing in the frog: dynamics of the middle ear”. *Proc. Royal Soc. Lond. B*, 212(1189):459–485, 1981.

[93] C. G. S. de Villiers. “Über das Gehörskellet der aglossen Anuren”. *Anat. Anz.*, 74: 33–55, 1932.

[94] E. G. Wever. *The Amphibian Ear*. Princeton University Press, Princeton, NJ, 1985.

[95] M. Mason, M. Wang, and P. Narins. “Structure and function of the middle ear apparatus of the aquatic frog, *Xenopus laevis*”. *Proc. Inst. Acoust.*, 31:13–21, Jan 2009.

[96] S. Timoshenko and S. Woinowsky-Krieger. *Theory of Plates and Shells*. McGraw-Hill Book Company, New York, 1959. .

[97] L. E. Kinsler. *Fundamentals of acoustics*. Wiley, 2000.

[98] K. Homma, Y. Du, Y. Shimizu, and S. Puria. “Ossicular resonance modes of the human middle ear for bone and air conduction”. *J. Acoust. Soc. Am.*, 125(2):968–979, 2009.

[99] G. A. Manley and O. Gleich. “Evolution and specialization of function in the avian auditory periphery”. In Douglas B. Webster, Arthur N. Popper, and Richard R. Fay, editors, *The Evolutionary Biology of Hearing*, pages 561–580. Springer New York, New York, NY, 1992.

[100] A. Chaigne and J. Kergomard. *Acoustics of Musical Instruments*. Modern Acoustics and Signal Processing. Springer New York, 2016.

[101] J. Blauert. “Horns and stepped ducts”. In *Acoustics for Engineers: Troy Lectures*, pages 103–115. Springer Berlin Heidelberg, Berlin, Heidelberg, 2008.

[102] A. G. Webster. “Acoustical Impedance and the Theory of Horns and of the Phonograph”. *Proc. Natl. Acad. Sci. U.S.A.*, 5(7):275–282, Jul 1919.

[103] G. K. Batchelor. *An Introduction to Fluid Dynamics*. Cambridge University Press, Cambridge, 2000. .

[104] D. Marx, H. Bailliet, and J.-C. Valiére. “Analysis of the acoustic flow at an abrupt change in section of an acoustic waveguide using particle image velocimetry and proper orthogonal decomposition”. *Acta Acustica united with Acustica*, 94(1), 2008.

[105] A. Hirschberg and S. W. Rienstra. *An Introduction to Acoustics*. IWDE-Report. 2015.

[106] H. von Helmholtz and A. J. Ellis. *On the Sensations of Tone as a Physiological Basis for the Theory of Music*. Longmans, Green, 1885.

[107] A. Elepfandt, I. Eistetter, A. Fleig, E. Gunther, M. Hainich, S. Hepperle, and B. Traub. "Hearing threshold and frequency discrimination in the purely aquatic frog xenopus laevis (pipidae): measurement by means of conditioning". *J. Exp. Biol.*, 203(23): 3621–3629, 2000.

[108] R. A. Norberg. "Ocurrence and independent evolution of bilateral ear asymmetry in owls and implications on owl taxonomy". *Philos. Trans. Royal Soc. B*, 280(973): 375–408, 1977.

[109] R. S. Payne. "Acoustic location of prey by barn owls (tyto alba)". *J. Exp. Biol.*, 54(3): 535–573, 1971.

[110] E. I. Knudsen and M. Konishi. "Mechanisms of sound localization in the barn owl (tyto alba)". *J. Comp. Physiol.*, 133(1):13–21, Mar 1979.

[111] R. B. Coles and A. Guppy. "Directional hearing in the barn owl (Tyto alba)". *J. Comp. Physiol. A*, 163(1):117–133, May 1988.

[112] L. Hausmann, M. von Campenhausen, F. Endler, M. Singheiser, and H. Wagner. "Improvements of sound localization abilities by the facial ruff of the barn owl (tyto alba) as demonstrated by virtual ruff removal". *PLoS One*, 4(11):1–13, 11 2009.

[113] M. von Campenhausen and H. Wagner. "Influence of the facial ruff on the sound-receiving characteristics of the barn owl's ears". *J. Comp. Physiol. A Neuroethol. Sens. Neural. Behav. Physiol.*, 192(10):1073–1082, Oct 2006.

[114] B. Katbamna, J. A. Brown, M. Collard, and C. F. Ide. "Auditory brainstem responses to airborne sounds in the aquatic frog xenopus laevis: correlation with middle ear characteristics". *J. Comp. Physiol. A*, 192(4):381–387, Apr 2006.

[115] G. Spahn and R. Wittig. "Biomechanical properties (compressive strength and compressive pressure at break) of hyaline cartilage under axial load". *Zentralbl. Chir.*, 128 (1):78–82, Jan 2003.

[116] H. Lamb. "On the vibrations of an elastic plate in contact with water". 98(690): 205–216, 1920.

[117] M. K. Kwak. "Vibration of circular membranes in contact with water". *J. Sound Vib.*, 178(5):688 – 690, 1994.

[118] J. Christensen-Dalsgaard, T. Breithaupt, and A. Elepfandt. "Underwater hearing in the clawed frog, Xenopus laevis. Tympanic motion studied with laser vibrometry". *Naturwissenschaften*, 77(3):135–137, Mar 1990.

[119] D. D. Yager. "A unique sound production mechanism in the pipid anuran *Xenopus borealis*". *Zool. J. Linnean Soc.*, 104(4):351–375, 1992.

[120] P. H. Rogers and M. Cox. "Underwater sound as a biological stimulus". In Jelle Atema, Richard R. Fay, Arthur N. Popper, and William N. Tavolga, editors, *Sensory Biology of Aquatic Animals*, pages 131–149, New York, NY, 1988. Springer New York.

[121] P. M. J. Shelton. “The structure and function of the lateral line system in larval xenopus laevis”. *J. Exp. Zool.*, 178(2):211–231, 1971.

[122] C. Köppl. “Phase locking to high frequencies in the auditory nerve and cochlear nucleus magnocellularis of the barn owl, tyto alba”. *J. Neurosci.*, 17(9):3312–3321, 1997.

[123] H. S. Bierman, J. L. Thornton, H. G. Jones, K. Koka, B. A. Young, C. Brandt, J. Christensen-Dalsgaard, C. E. Carr, and D. J. Tollin. “Biophysics of directional hearing in the American alligator (Alligator mississippiensis)”. *J. Exp. Biol.*, 217(Pt 7):1094–1107, Apr 2014.

[124] H. S. Bierman and C. E. Carr. “Sound localization in the alligator”. *Hear. Res.*, 329: 11–20, Nov 2015.

[125] D. M. Higgs, E. F. Brittan-Powell, D. Soares, M. J. Souza, C. E. Carr, R. J. Dooling, and A. N. Popper. “Amphibious auditory responses of the American alligator (Alligator mississipiensis)”. *J. Comp. Physiol. A Neuroethol. Sens. Neural. Behav. Physiol.*, 188 (3):217–223, Apr 2002.

Acknowledgements

I would first and especially like to my advisor, Prof. *Leo van Hemmen*, without whose guidance this project would not have been possible. He has always been a source of great support and encouragement, whose enthusiasm for research, and patience for those conducting it is enviable.

I would also like to thank the Bernstein Center for Computational Neuroscience and FRM II for agreeing to fund my project.

I am very grateful to the collaborators in our projects: *Julie Goulet, Bruce Young, Jakob Christensen-Dalsgaard* and *David Heider* for their insights with regard to biology and physics of hearing. *Julie Goulet* deserves a special mention for her guidance during my Master's project, which was my introduction into the topic of Internally Coupled Ears. A special thanks also goes to David Heider for his invaluable insights, mathematical and otherwise, and for his help with the proof-reading and translating. I'm also very grateful to Elke Fehsenfeld and Susanne Tillich for readily helping me navigate the administrative jungle from time to time.

My many friends in Munich and those back home for keeping my spirits up and my sanity intact through the years. *Aditi, Arun, Harsha, Hrishik, Marcel, Lucas, Taoufik, Manu, Johann, Bruno, Julian, Lisa and Sasha* in Munich and *Kartik, Abhishek, Ganesh, Karthik, Mayank, Sumedh, Atul, Rahul* and *Hrishi* who are now scattered all over the world, to name a few.

I am also very grateful to my parents and my sister for their unconditional support throughout the years and for the sacrifices they made on my behalf.

And Eberhard for being there.

List of Publications

Peer-Reviewed

- Vedurmudi, A. P., Goulet, J., Christensen-Dalsgaard, J., Young, B. A., Williams, R., and van Hemmen, J. L. (2016). How internally coupled ears generate temporal and amplitude cues for sound localization. *Physical Review Letters*, 116:028101.

- Vedurmudi, A. P., Young, B. A., and van Hemmen, J. L. (2016). Internally coupled ears: Mathematical structures and mechanisms underlying ICE. *Biological Cybernetics*, 110(4):237–246.

In Preparation

- Vedurmudi, A. P., Christensen-Dalsgaard, J., and van Hemmen, J. L. (2018). Modeling underwater hearing and sound localization in the frog *Xenopus laevis*. To be submitted to the *Journal of the Acoustical Society of America* (2018).